UNIVERSITÀ
DEGLI STUDI
DI PADOVA

UNIVERSITY OF PADUA

Department of Pharmaceutical and Pharmacological Sciences

DOCTORAL SCHOOL IN MOLECULAR SCIENCES

PHARMACEUTICAL SCIENCES CURRICULUM

XXIX CYCLE

Development of nanocarriers with responsive interfacial properties for site-specific drug delivery

School Director: Prof. Antonino Polimeno

Curriculum Coordinator: Prof. Stefano Moro

Supervisor: Prof.Stefano Salmaso

Ph.D Student: Michela Barattin

Alla mia famiglia

Success consistes of going from failure to failure without loss of enthusiasm.

W. Churchill

Index

Abbreviations

^{1}H NMR	Nuclear Magnetic Resonance
ACN	Acetonitrile
Arg	Arginine
BIB	2-bromo-isobutyryl bromide
Boc	Tert-butyl carbonate
$CDCl_3$	d-chloroform
CH_2Cl_2	Dichloromethane
Chol	Cholesterol
^{13}C NMR	Carbon Nuclear Magnetic Resonance
CPE	Cell Penetrating Enhancer
CPP	Cell Penetrating Peptides
Da	Dalton
DAG	Di-acyl-glicerole
DAG-Arg_4	TetraArg-[G-2]-distearoyl glycerol
DAPI	2-(4-Amidinophenyl)-6-indolecarbamidine dihydrochloride
DCC	N,N-dicyclohexylcarboimmide
DCM	Dichloromethane
DCU	Dicyclohexylurea
DDS	Drug delivery system
DLS	Dynamic Light Scattering
DMAP	4-(dimethylamino)pyridine
DMF	Dimethylformamide
DMSO	d_6-dimethil sulfoxide
DP	Degree of Polymerisation

EDC	*N*Ethyl-*N*′(3-dimethylaminopropyl)carbodimide hydrochloride
EPR	Enhanced Permeability and Retention
Et_2O	Diethyl ether
EtOAc	Ethyl acetate
FBS	Fetal Bovine Serum
Gly-Gly	Glycyl-glycine
HBSS	Hank's Balanced Salt solution
HBTU	N′-tetramethyluronium hexafluorophosphate
HCl	Hydrochloric acid
HEPES	4-(2-hydroxyethyl)-1-piperazine ethanesulfonic acid
HoBt	1-Hydroxybenzotriazole hydrate
HSPC	Soy Hydrogenated Phosphatidyl Choline
MeOH	Methanol
mPEG-NH_2	Methoxy PEG Amine
MS	Mass Spectrometry
MW	Molecular Weight
N_2	Nitrogen
NaCl	Sodium Chloride
NaH	Sodium hydride
NaOH	Sodium hydroxide
NHS	N-Hydroxysuccinimide
Pbf	2,2,4,5,7-Pentametilbenzofuril-6-solfonile
PBS	Phosphate Saline Buffer
PDI	Poly Dispersity Index
PEG	Polyethylene glycol
pKa	Acid dissociation constant

RAFT	Reversible addition−fragmentation chain-transfer polymeri-zation
RP-HPLC	Reverse Phase – High Pressure Liquid Chromatography
SD	Sulfadimethoxine
SDM	Methacryloyl sulfadimethoxine
t –Boc	Di-tert-butyl dicarbonate
TFA	Trifluoroacetic acid
THF	Tetrahydrofuran
TLC	Thin Layer Chromatography
UV	Ultraviolet
VIS	Visible

Abstract

The functional and morphological alterations of the vascular endothelium of the lymphatic system, the micro-environmental alterations such as the amplification of the enzyme kit, the overexpression of specific receptors, the increase in the redox potential, temperature and the lowering of the pH, are typical characteristics of tumor tissues. These features can be exploited successfully for the development of suitable supramolecular and colloidal systems with passivelly and actively guided delivery of anticancer drugs at the site of action. Here we aimed at investigating anovel pH responsive liposomal platform to achive selective tumor targeting to ensure the accumulation of the drug in adequate therapeutic concentration. Liposomes were decorated with a novel non-peptidic cell penetrating enhancer (CPE) that simulates the action of the natural peptides known from the literature studies. A synthetic procedure was developed to obtain a oligoarginyl-dendron derivative to be included in the lipid bilayer of the liposomes. The derivative TetraBoc-Arg(pbf)-[G-2]-distearoyl glycerol (Arg4-DAG) consists of a central polyester core to which arginines were conjugated on one side and that was terminated with a distearoyl glycerol chain on the other. The resulting macromolecule possesses a amphiphilic character in virtue of its two combined moieties: 1) the hydrophobic distearoyl tail acting as lipidic anchor for lipid bilayer association , 2) the positively charged peripheral arginines, which provides for high cationic density and mimic the basic aminoacid residues of TAT peptide, thus conferring the biological activity to the system. The intermediates and the final product were characterized by ^{1}H, ^{13}C NMR and mass spectrometries.

Liposomes obtained with a 2:1 HSPC/cholesterol molar ratio were generated with increasing ratio of the CPE with respect to lipids using the post insertion technique which provided for the increase of liposome zeta potential from +8 mV to +24 mV as the ratio of CPE increased from 1% to 4%, then reaching a plateau.

The biological properties of fluorescently labelled CPE coated liposomes were investigated on HeLa cancer cells. Flow cytometry analysis and confocal microscopy study confirmed the high capacity of the liposomes to associate with

cells. A 30 times higher efficiency of cancer cell association was found with respect to naked liposomes. The CPE coated liposomes demonstrated a remarkable ability to deliver in the cytosol albumin and calcein. BSA was chosen as protein model, whereas calcein was selected because it is a strongly hydrophilic molecule, so as to mimic the behavior of water soluble drugs. Both molecules were incorporated into the hydrophilic core of liposomes. The calcein was not release from the liposomes for at least 16 days, whereas BSA was completely released in 7 days.

In order to confer to liposomes sensitivity to pH alterations for controlled access to cancer cells, a pH sensitive polymer of mPEG-oligosulphadimethoxine ($mPEG_{5kDa}$-SDM_8) was synthesized by radical polymerization of sulfadimethoxine methacrylate from 2-bromo-isobutyryl-methoxyPEG (mPEG-Br) 5kDa. $mPEG_{5kDa}$-SDM_8 possesses a pKa of 7.12 which ensures a deprotonated state with negative charge at physiological pH (7.4) and a protonated neutral state at pH 6.5, which corresponds to the tumor environment.

Zeta potential analysis performed on Arg4-DAG coated liposomes decorated with the $mPEG_{5kDa}$-SDM_8 polymer confirmed that the most finely regulated shielding/unshielding capacity is obtained when the two modules are equimolar, both at 4% in moles with respect to lipids. This formulation was found to be stable even in the presence of serum proteins, which does not alter the charge-to-charge interaction between the oligo-sulfadimethoxine of the pH responsive polymer and oligo-arginines of the CPE as observed by zeta potential analysis. The SPR study also confirmed this result, proving the polymer association with the CPE coated liposomes at pH 7.4 and the release at pH 6.5 mimicking the tumor, which corresponds to a sheddable physical PEGylating under controllable conditions.

Finally, the biological studies confirmed the ability of the pH responsive polymer to shield the CPE on the liposomal surface under physiological conditions (pH 7.4), which prevents the internalization of both the unloaded pH responsive vesicles, and the calcein loaded vesicles, whereas revealing it when exposed to tumor mimicking acid environment, allowing for liposome cell entry and payload intracellular delivery.

AIM OF THE PROJECT

Nanomedicines and nanocarriers are valuable tools to improve the unsatisfactory therapeutic responses of anticancer drugs. Inadequate drug pharmacokinetic profiles and biodistribution yield poor therapeutic responses and side effects. Thus, the encapsulation of the drug in nanocarriers can overcome a variety of these issues encountered when a free drug is administered. The drug is protected within the nanocarrier and its degradation is slowed down. In addition, its site-specificity can be optimized, the accumulation in off-target sites is reduced while increasing the dose ratio accumulating in tissue affected by diseases such as the tumour. Furthermore, the drug toxicity is reduced and the release, and thus bioavailability, can be controlled by programming the local sensitivity of the carrier or by external stimuli.[1]

In this scenario, it is possible to design and implement macromolecular and colloidal 'smart' systems by providing them with suitable stability and reduced clearance by the reticulo-endothelial system (RES) at systemic level. The assembly of the carriers with responsive materials allow to instruct these systems to accumulate prevalently in the tumor tissue and to selectively carry out their pharmacological activity only where the sensing of pathophysiological conditions promote the accumulation, cell uptake and release of the loaded drug. Notably, the pH gradient that is established between the healthy and the tumor tissues can be exploited to guide the internalization of smart drug nanocarriers by tumor cells when sensing the local peculiar feature of the cancer tissue that prompt the alteration of morphology and/or surface properties. [2, 3]

The aim of this PhD project was to develop pH-sensitive liposomes for site-selective intracellular delivery and to extensively investigate the control of cell penetration under weakly acid pH conditions, such as that of solid tumors or tissue affected by acute/cronic inflammation. In order to prepare acid sensitive liposomes, whose cellular association is triggered only under conditions of lower pH than the physiological one, a non-peptidic oligo-arginyl derivative has been synthetized as novel cell penetrating enhancer. This module was incorporated into the bilayer of the liposomes to promote their cellular uptake, and then shielded with a pH

responsive polyanionic oligo-sulfadimethoxine-polyethylene glycol copolymer (mPEG-oligo-sulfadimethoxine) that is the functional component that ensure the cellular uptake of the liposomes in acid conditions. The sulfadimethoxine was used as pH molecular sensor here since it is a weak acid that, under physiological conditions, undergoes deprotonation and appears in the anionic form. The negative charge of the oligo-sulfadimethoxyl residues of the copolymer allows a charge-to-charge complexation with the oligo-arginine derivative on the surface of the liposome. The derivative of mPEG-oligo-sulfadimethoxine undergoes protonation at pH below its apparent pKa (7.12) typical of the tumoral interstitium, and consequently loses the charge-to-charge interaction with the oligo-arginines derivative on the liposome surface. This event triggers the exposure of the oligo-arginines components and permit the interaction of the liposomes with the cell surface, thus promoting the internalization of the liposomes with a mechanism that is comparable to that promoted by TAT peptide that was extensively discussed in the literature.

In this work, BSA and calcein were used as model hydrophilic macromolecules and small drugs, respectively. The use of liposomal systems in fact is intriguing because they allow the delivery to the tumor tissue of both water-soluble molecules by carrying them in the aqueous core and water insoluble molecules in the lipidic bilayer. The use of drug nano-vehicles that are able to deliver to the tumor a sufficient dose ratio of drug to achieve the desired pharmacological effect is therefore crucial for the therapeutic effect of the treatment and for the minimization of side effects.

Figure 1 summarizes the proposed mechanism of controlled cell internalization of the nanocarrier: after passive accumulation in the tumour interstitium according to the EPR effect[4].

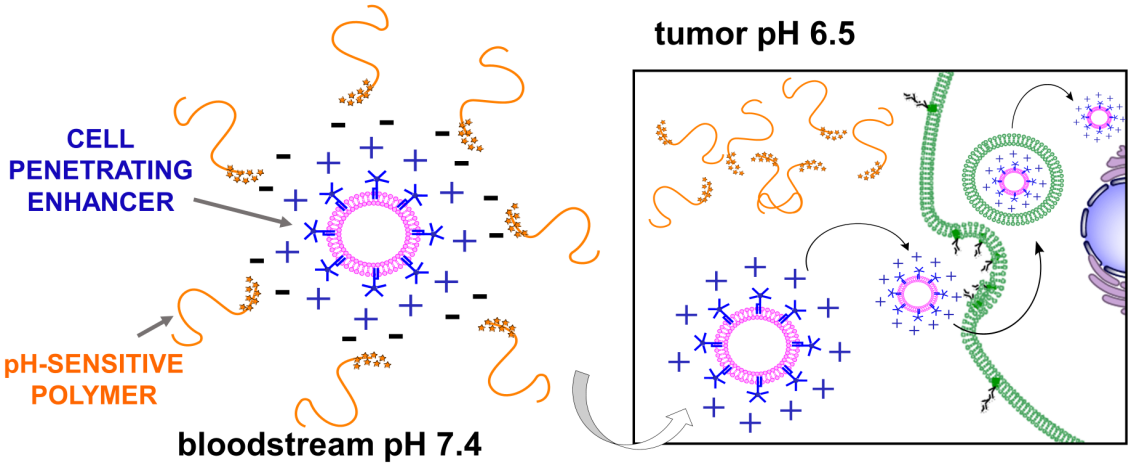

Figure 1. Mechanism of pH controlled cell uptake of responsive liposomes coated with the synthetic cell penetration enhancer and pH responsive polymer.

1. INTRODUCTION

1.1 NANOMEDICINES

The clinical use of many biologically active molecules is often limited by their inadequate physico-chemical and pharmacokinetic characteristics such as low solubility and stability, biodistribution and inadequate absorption and rapid elimination from the body. The science of drug delivery is the field of advanced pharmaceutical technology that allows to formulate innovative release systems able to convey drugs to a specific site of the organism and to release them according to predetermined kinetics. The aim is the optimization of therapeutic effect and the minimization of side effects. To obtain these results, various supramolecular systems have been developed, "polymer therapeutics" or "nanomedicines"[5-8], obtained by chemical conjugation or physical assembly of biologically active molecules with the polymer macromolecules. Such polymeric colloidal systems allow for the improvement of the pharmacokinetic profile of the drug, as a consequence of the enhanced stability and solubility and thus increasing the therapeutic index (ratio between therapeutic dose and toxic dose). The use of chemical and physical polymer bioconjugates for drug delivery has opened new therapeutic perspectives through the development of systems applicable to a wide spectrum of diseases. In particular, those systems have been investigated for anti-tumoral therapy, since most of the chemotherapeutic drugs are highly toxic and act at the level of all tissues with limited selectivity, causing severe side effects. Many different kinds of colloidal systems for drug delivery have been developed over the last decades, such as liposomes, micelles, dendrimers, nanoparticles and nanocapsules, and more recently, polymer based vesicles, namely polymersomes (Figure 2).

The search for suitable formulations for the administration of protein drugs (e.g. antibodies, hormones, enzymes, cytokines, growth factors and other biomodulator) is another interesting challenge in the technological-pharmaceutical field.[9-11] The therapeutic importance of these molecules is mainly attributable to their high activity and specificity of action, and they often represent the only option for a variety of pathologies.

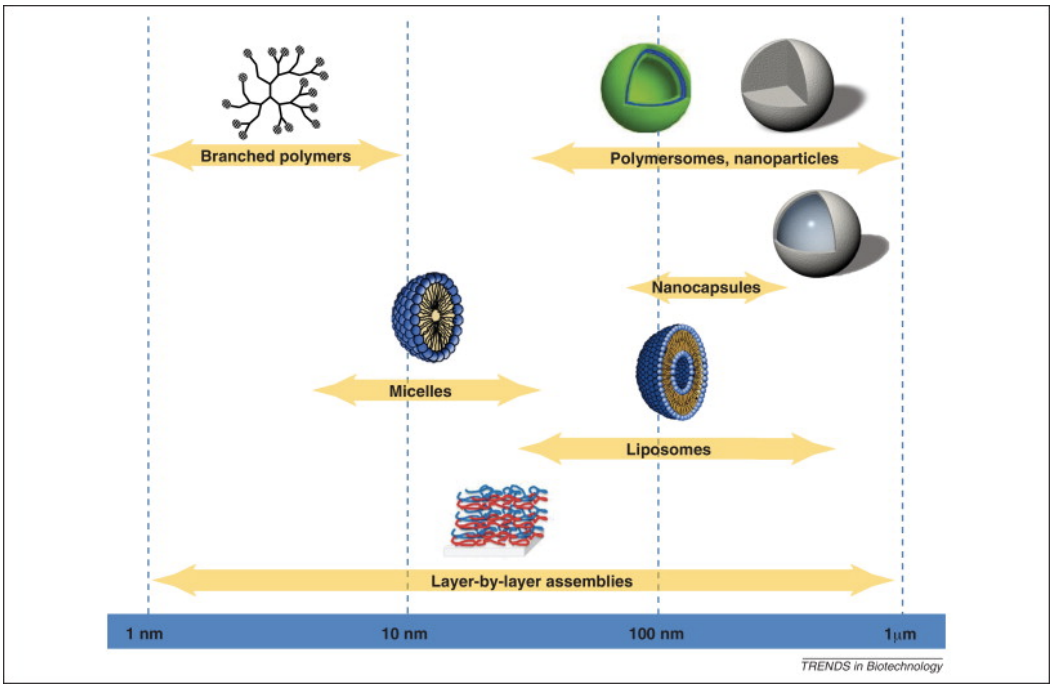

Figure 2. Representative nanovectors under development the last decades.[9]

The use of biotegnological drugs in the clinical setting, however, meets major limitations because of their particular molecular structure and features. The main reasons for the difficulty with the use of these drugs are: the rapid elimination from the circulation, the high chemical and physical instability, the rapid degradation by proteolytic enzymes, immunogenicity, the difficulty of passing through the membranes.[12]

In order to improve the therapeutic profile of protein drugs, two different strategies are pursued: generate new protein derivatives with better biopharmaceutical and immunologic features and generate new formulations able to allow an adequate supply of medication to the body. Among the proposed strategies of this family, the most studied are nanoparticulate systems such as liposomes micelles, polymeric nanoparticles and lipid.[13-15]

1.2 OVERVIEW ON CANCER

The tumor tissue is characterized by structural peculiarities of vascular endothelium, microenvironmental conditions (pH, temperature, redox potential and enzymatic kit) and by the overexpression of specific receptors that can be

successfully used for the development of new and selective anti-tumor therapeutic strategies. For these reasons, the studies to generate more efficient nanosystems for drug delivery are becoming increasingly important in the research for efficient anti-cancer therapies.

1.2.1 Tumor tissue features

The tumor tissues have peculiar properties compared to healthy ones. Among these, the most important are amplification of the enzymatic pool, the increase in the oxidation-reduction potential and cellular metabolism, which causes an increase of the temperature and a lowering of the pH in the extracellular matrix. There are also changes of the vasculature and the lymphatic system, with an increase of blood vessels permeability and a decrease of lipid drainage.[16, 17]

Lowering of the pH: the mechanisms involved in the lowering of pH in the tumor tissue mainly involve the production of lactic acid, resulting in the hydrolysis of ATP and hypoxia and abnormal activity of the Na^+/H^+ pump. This antiporter system seems to be of particular importance: it has been shown, in fact, that mutant cells lacking the activity of Na^+/H^+ pump are not able, or have reduced ability to generate solid tumors because they are unable to generate the acidic conditions during the proliferation of malignant cells. The pH gradient that is established between the healthy and the tumor tissues may have various effects on the response of cells to conventional anticancer drugs and represents, therefore, a possible way to optimize the selectivity of therapy. For example, if a drug is a relatively lipophilic weak acid, at a pH as acidic as that of the tumor site it will be in its non-ionized state and may easily cross the cell membrane. Once entered in the neutral intracellular compartment, the drug is deprotonated and will remain trapped within the cell, resulting in a substantial gradient in the intracellular/extracellular drug distribution between healthy and tumor tissues.

Innovative, polymer based drug delivery nano-systems, have also been developed, which exploit the acidity of the extracellular matrix of cancer cells to enhance the drug accumulation in the tumor.[3]

Vascular system: the tumors arise from a single stem cell and are able to reach, by taking oxygen and nutrients from the adjacent vessels, masses of not more than 150-200 μm, after which the central core of the tumor undergoes an hypoxic condition and decrease of nutrients. The further development of the tumor requires new blood vessels that are generated from existing ones with a mechanism called angiogenesis (Figure 3).[18-21]

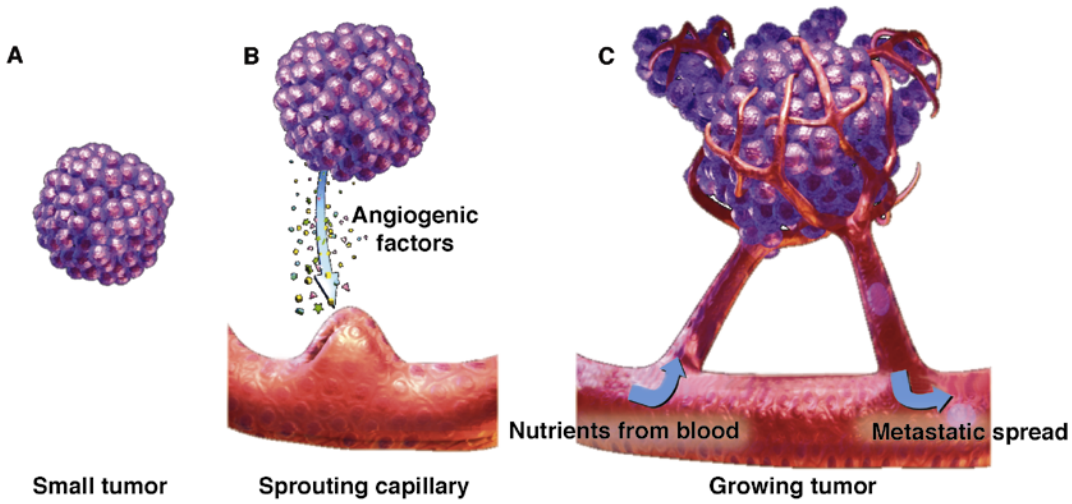

Figure 3. Representation of tumor mass development and relationship with the neo-vasculature. From: *Siemann DW., Vascular targeting agents. Horizons in Cancer Therapeutics: From Bench to Bedside. 2002;3(2):4-15*

The neo-vasculature characteristics are highly variable and different from those of healthy tissue. The neo-vessels possess peculiar endothelial composition, structure of the basement membrane and size of the fenestration and they are devoid of pericytes (regulators of maturation and differentiation of capillaries). Their permeability is extremely high, not only in virtue of the higher section of the fenestrations and for the incompleteness of the basal membrane, but also of the presence of abundant permeation enhancers.

Lymphatic drainage: the lymphatic vessels originate in tissues as capillary endings, and are supported by a single layer of endothelium. They possess widely fenestrated endothelial junctions and are easily permeable to macromolecules of the interstitial fluid.

The lymphatic fluid is drained by a series of lymph vessels to the lymph nodes, pouring in the venous circulation. The tumor tissues lack an organized system of lymphatic drainage.

Macromolecules can easily extravasate and penetrate the tumor across the wide fenestrae, but cannot be drained and accumulate in depth into the tumor mass. This hindrance to the diffusion of fluids in the tissue generates a back pressure that can lead to collapse of the blood capillaries in the core of the tumor mass, with the formation of hypoxic and anoxic areas and consequent onset of necrosis within the tumor. On the basis of these characteristics of tumor tissue, the design of new macromolecular and colloidal systems can be rationalized in order to selectively respond to peculiar pathophysiological characteristics of this tissue.[4, 22]

1.2.2 Cancer therapies and limitations

The main issue of tumor chemotherapy is that the majority of anticancer drugs acts on all types of cells, both healthy and diseased, causing dramatic side effects. Side effects related to cancer treatments lead to a drastic worsening of the patient's quality of life and, in worst cases, even death.[23-25] This is a consequence of the fact that the tumor cells have a physiology mostly similar to that of healthy cells. In fact, if on one side it is relatively easy to develop antibiotics with a selectively direct toxicity against prokaryotic cells that have different biochemical machineries from the eukaryotic one, on the other hand it is much more difficult to find molecules with selective toxicity for cancer cells, since they essentially undergo the same biological events of healthy cells and the differences in the biological and molecular mechanisms are minimal.[26] Consequently, the drug can also reach high concentrations in different healthy organs, causing cellular and tissue damage.

Carcinogenicity studies have identified differences between healthy and cancer cells in the genetic constitution, enzyme activation and growth kinetics. Unfortunately, none of these differences is exclusive of tumor cells and the drugs currently on the market are not, however, able to fully exploit these differences.

There are a variety of fast proliferating cells that can be very sensitive to chemotherapy such as those of the hair, the red blood cells bulbs, white blood cells and intestinal epithelial cells. Side effects of chemotherapy that occur more frequently are cytostatic action on the cells of the bone marrow generating myelosuppression, leukopenia, neutropenia, thrombocytopenia, anaemia and damage to the immune system, causing the patient's exposure to disease-induced microorganisms. Other side effects include ulceration of the mouth and bowel mucosa with susceptibility to bacterial sepsis of the intestinal tract (in case of immunosuppression), pulmonary fibrosis, venous occlusive disease of the liver, neurotoxicity and ototoxicity, alopecia, nausea, vomiting, diarrhoea or constipation, cardiotoxicity, hepatotoxicity and nephrotoxicity. Rash, loss of appetite may result in malnutrition and weight decrease and, in some cases, memory loss and dizziness, dehydration, fluid retention, xerostomia and bleeding.[27-29]

Most anticancer drugs are formulated to be administered intravenously, which ensure the immediate availability of the drug and its rapid access to the tumor. The control of the bioavailability of the administered molecule represents a critical issue in the case of chemotherapeutic agents that have a very narrow therapeutic window. The intravenous administration of the drug, as well as determining a lower access to therapeutic treatment by the patient and increased cost of treatment, requires the development of dedicated drug formulations aimed at improving the physico-chemical features of the drug, in particular solubility and stability, and the PK profile to modulate the bioavable fraction and reduce administration frequencies.[30-32]

The chemotherapeutic protocols have been recently set up by the combination of multiple drugs to limit the onset of resistance. Another limitation of the anticancer therapy is the fact that each treatment can only kill a cellular pool (fractional kill) with peculiar genotypic profile, which requires for continuous dosing and multiple cycles to avoid regrowth of the tumor.[33, 34] To date, however, a therapeutic protocol of proven effectiveness for each different type of neoplasm is still missing. Also, dosage must be tailored to each patient so that the dose is as close as possible to the maximum individual dose and the maximum possible frequency of administration to prevent regrowth of the tumor.

1.2.3 Anti-cancer therapy

The classical therapeutic approach for the treatment of solid and localized tumors involves the surgical removal of the tumor mass that is usually combined with radiotherapy and/or chemotherapy protocols to decrease the risk of possible recurrence. In general, it can be stated that radiotherapy efficacy can be increased by co-administration of radio-sensitizing drugs. Chemotherapy, on the other hand, in virtue of its systemic administration, is more suitable in the case of metastatic tumors in order to prolong patient life by reducing disease progression. These two approaches can, however, be combined together according to two different therapeutic strategies:

- adjuvant therapy (postoperative chemotherapeutic treatment): in the case of localized solid tumors, surgical resection of the tumor is first applied, followed by chemotherapeutic and radiotherapeutic treatments, to eliminate micrometastases and thereby avoid recurrences;

- neoadjuvant (preoperative chemotherapeutic treatment) is applied to reduce the volume of the tumor and facilitate subsequent resection or radiation therapy, which are still needed for solid tumors, because chemotherapeutic agents often cannot reach the deeper areas of the solid tumors.

Currently, research in the pharmaceutical field has evolved and anticancer drugs include alkylating agents, anti-metabolites, molecules of natural origin, and the more recent “gene therapy”, vaccines and other strategies to stimulate the immune and endocrine systems. The strategies for the development of new therapeutic approaches in the treatment of cancer are:

1. search for low molecular weight molecules with antiproliferative activity mainly obtained by means of combinatorial chemistry and pharmacology activity screening of natural products and semisynthetic leads[23, 35];

2. identification of new biological targets for chemotherapy, such as receptors, antigens, angiogenesis activators, biochemical mediators that are involved in the tumor growth and that can be inhibited with specific drugs[36];

3. development of antisense nucleotides (siRNA) to silence intracellular proteins participating to tumor evolution[37];

4. development of nanocarriers that can be directed to the site of disease and can release drugs yielding site specific and targeted therapy of the tumor tissue.

Categories of chemotherapeutic agents currently on the market or under development are inhibitors of cell replication and DNA synthesis (alkylating agents, DNA-intercalators, antimetabolites and precursors), topoisomerase inhibitors and antibiotic/anticancers, microtubules stabilizing or destabilizing agents, enzyme inhibitors, receptor antagonists.[38, 39] Some newer drugs, such as few monoclonal antibodies and tyrosine kinase inhibitors (Gleevec), do not directly interfere with the DNA as the majority of classical anticancer drugs, but have been designed to hit specific targets on peculiar cancer cells types. In addition, some drugs modulate the cell cycle by acting on growth activators: within this category, some of the hormone inhibitors are included.

Ideal antineoplastic drugs should be capable of selectively affect cancer cells without harming the healthy tissue cells. Only a few drugs among those currently available comply with this request, and the clinical use of these drugs should be preceded by a thorough evaluation of the relationship between beneficial effects and toxicity in order to achieve the best possible therapeutic index. Chemotherapeutic agents used to treat cancer are among the drugs with lower therapeutic index. The serious side effects they cause restrict their use both in time, and dose. In addition to side effects related to systemic toxicity of anticancer drugs, their effectiveness is strongly dependent on their bioavailability. It is not uncommon that, due to a poor bioavailability, drugs under clinical study have high pharmacodynamic activity while showing a negligible therapeutic activity, which makes them unusable for therapeutic purposes. The pharmacologically active molecules that possess limited bioavailability, show, in general, one or more of the following characteristics: high lipophilicity and consequent poor solubility in aqueous body fluids; low permeability to biobarriers or biological membranes; absorption through biological barriers that is regulated by a transport process facilitated or active and saturable; enzymatic or hydrolytic instability especially for drugs administered orally due to sensitiveness to the gastric environment.

1.3 DRUG DELIVERY

"Drug delivery technology" is a research field participating to the preclinical development of drugs. It refers to approaches, formulations, technologies, and systems aimed at guaranteeing the transport of a pharmaceutical molecule within the body in order to achieve its intended therapeutic activity at a precise site, thus minimizing undesired off target effects. To this aim, drug delivery technology is focused on the development of innovative systems, namely drug carriers, which are able to ameliorate the physico-chemical features of the drug, protect it while circulating in the bloodstream and efficiently target the tissue affected by a specific disease and control the release of the drug. These strategies allow to improve the biopharmaceutical performance of drugs and the therapeutic outcome. Moreover, formulations designed for prolonged or controlled drug release can enhance the compliance of patients affected by chronic pathologies who need time extended treatments by decreasing the frequency of administration.[1, 40, 41]

Biotechnological drugs[42], such as proteins[11, 43-45], siRNA[46, 47], miRNA[48, 49] and DNA, require efficient formulative strategies to prevent their in vivo degradation.[50] These macromolecules possess in fact intrinsic poor stability and undergo, in few cases, immediate inactivation upon administration.

In the past decades, many carriers have been developed and investigated as drug delivery systems (DDSs) for parenteral, oral, transdermal, transmucosal and ocular administration[40]: either inorganic or organometallic nanoparticles (including gold[51], iron oxide[52] or silica core/shell nanoparticles[53]), polymeric bioconjugates (polymer-protein[54], polymer-drug), and self-assembling systems (micelles[55-58], liposomes[59, 60] or polymeric vesicles[61-63]). In the future, the progress in the discovery of physio-pathological processes underlining the development of many diseases will allow the generation of new highly performing biotechnological medicines whose formulation with the more advanced delivery technologies will be mandatory to win the challenges of accessing physiologic barriers such as the blood brain barrier, and act selectively by targeting intracellular pathways.

1.3.1 Nanomedicine in cancer therapy

Nanoparticulate systems can be generated with a variety of materials including proteins, peptides, lipids, metals, metal oxides and organic polymers. So far, the most investigated types of nanomedicine to target cancer cells include drug conjugates, lipid-based nanocarriers, polymer-based nanocarriers, viral vectors and inorganic nanoparticles (Figure 4). All these nanosystems can be functionalized with targeting molecules and loaded with drugs and contrast agents.[7, 64]

- *Chemical conjugates* (antibody-drug, polymer-drug, polymer-protein conjugates) can be generated with releasable chemical bonds for controlled release of drug. They are defined as “nanotherapeutics” or “nanomedicines” because of their size scale in the lower nanometer range and their conjugation to active pharmaceutical ingredients[65]

- *Lipid-based nanocarriers* include liposomes (naked or stealth)[66], micelles and solid-lipid nanoparticles. Lipid nanocarriers provide a carrying capacity three to four orders of magnitude greater than chemical conjugates. Few liposome formulations have been approved for clinical use; among these is the Doxil®[67, 68], in which the encapsulation of doxorubicin in a lipid bilayer coated with PEG prolongs the residence time of the molecule into the systemic circulation, increases its safety and the therapeutic index compared to free drug that suffers from a variety of side effects not limited to cardiotoxicity.

- *Synthetic polymer-based nanocarriers* are promisinig tools to generate nanocarriers because of their chemical versatility. They include dendrimers, polymeric micelles[55], polymersomes[61] and polymeric nanoparticles. *Dendrimers* are hyperbranched nanostructures whose size can be controlled through specific polymerization techniques, conventionally small planar molecules, or can be synthetized as 3D spherical nanostructure. They possess hollow area in their core where drugs and contrast agents can be inserted with a good loading efficiency. The synthesis of dendrimers can be controlled in order to achieve a defined molecular weight and chemical composition. *Micelles* are colloidal systems used as carriers of drugs and contrast agents since they can be formulated with relatively uniform size, and they can be prepared from a variety of amphiphilic

materials. Micelles are exploited to increase the solubility of hydrophobic molecules encapsulated in the hydrophobic core or anchored to the hydrophilic polymer of the unimers used to assemble micelles.

- *Inorganic nanoparticles* are used for a variety of applications, including tumor imaging (in particular iron oxide nanoparticles), enhancement of radiotherapy, or drug delivery. No inorganic nanoparticles for drug delivery has reached marketing approval as yet although paclitaxel-loaded gold nanoparticles are under clinical investigation.[69-71]

- *Viral nanoparticles* are obtained using tumor-homing viruses engineered to express therapeutic proteins. These viruses preferentially replicate in tumor cells. Specific features of cancer cells (such as lack of apoptotic pathways, deregulation of cell replication, immune system evasion) have been beneficially exploited to design therapeutic viruses. Several oncolytic viruses have been tested in clinical trials over the last years, but none of these has reached the market as yet.[72-74]

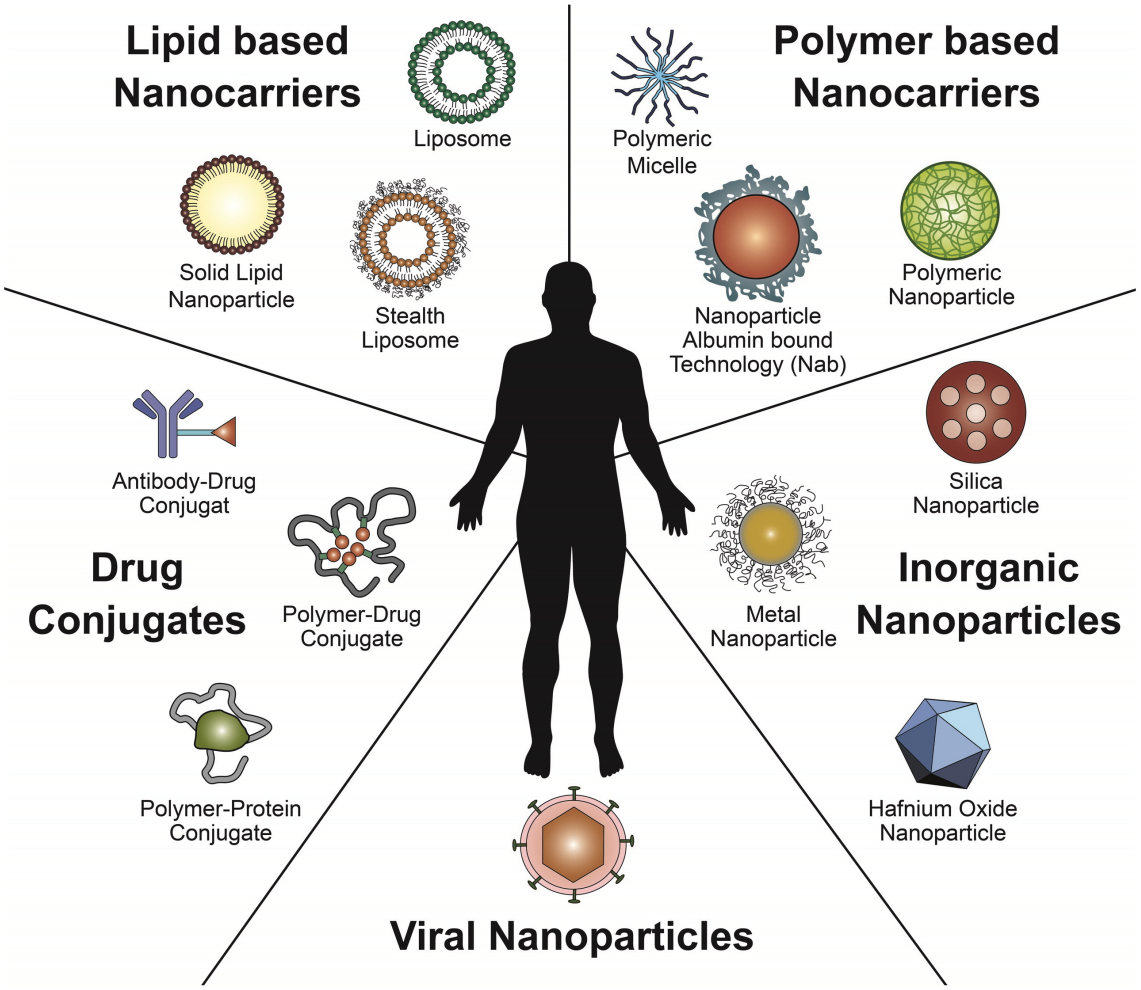

Figure 4. Examples of nanoparticulate systems used for anticancer drug delivery.[7]

1.3.2 Passive and active targeting

The EPR effect (enhanced permeability retention effect)[4, 22, 75, 76] characterizes the tissues of all solid tumors, with the exception of those hypervascularised localized at levels of prostate and pancreas. This phenomenon causes greater extravasation of the macromolecules in the cancer tissue and their permanence up to several weeks. It has been shown that there is a positive correlation between the increase in AUC (area under the concentration curve) plasma of macromolecular and a colloidal systems and their tumor biodistribution, while decreasing renal clearance. The peculiarities of the neoplastic tissue determining the EPR effect are ascribable to the fact that the rapid replication of malignant cells requires plenty of oxygen and nutrients that are guaranteed by a

rich, extensive and very permeable vascular system.[19] It is for this reason that tumor angiogenesis is particularly active and extensive which generate, thus, a dense vascularization network of vessels with incomplete endothelium, large fenestrations and, therefore, high permeability. The inhibition of the vessel growth with specific molecules (e.g. endostatin and angiostatin), induces tissue necrosis and inhibits the development of metastases. Besides the hyper-vascularization, irregularity of endothelium and increased vascular permeability, tumor tissues possess erratic blood flow and a slow venous drainage that dictates, together with the reduced lymphatic clearance, accumulation of macromolecular drugs and nanoparticles in the tumor interstitium. Vasal smooth muscles have also been found atrered in the tumor with consequent alteration of the regulation of the flow and blood pressure. Therefore, the abundant but abnormal vascularity favours the accumulation of macromolecules in cancer tissues as plasma proteins, macromolecular drugs and nanoparticles, while the reduced lymphatic drainage causes such colloidal systems to be retained in the tumor site for a longer time if compared to normal tissues. Consequently, the EPR effect related to the specific architecture of the tumor vessels appears to be key for the selective delivery of macromolecular anticancer drugs.[4]

Tissue targeting can be another valuable strategy to optimize the selectivity of the drug to the site of action, reducing the off-site disposition into the body and thus lowering the minimum effective dose and toxicity. These factors favour the clinical application of anti-cancer drugs that possess generally reduced therapeutic index. In order to optimize the biopharmaceutical performance of the drug delivery system, the carrier can be modified with targeting molecules that recognize specific cell receptors. Folic acid, galactose and small peptides have been extensively studied for the realization of the active targeting.[77, 78] The high affinity of these ligands for biological receptors, mainly of the cell membrane, allows to enhance the cytosolic access of the drug carrier. In addition, such systems can also lead to an improvement of the therapeutic effect, since the drug can undergo an intracellular localization different from the one which would follow the free drug. This will ensure that it can circumvent the intrinsic resistance or acquired multidrug-resistance.[79-81]

The development of resistance to chemotherapeutic agents due to the heterogeneity of cancer cells and the selective pressure is one of the main limitations of anticancer treatments and explains the failure of the cures that do not involve a combined therapy.[34] Active targeting can significantly support the overcoming of the appearance of cellular resistance to chemotherapeutic treatment. Drug resistance can appear as consequence of a variety of cellular modifications. Generally, the reduced effectiveness of a drug when resistance appears can be attributed to its reduced intracellular concentration, the ability of tumor cells to repair the damage induced by the drug or to mutations that alter the drug target. These events occur due to the overexpression of energy-dependent pumps such as P-glycoprotein[82, 83], which allow the exocytosis of the active molecule, the onset of biochemical processes that increase the conversion of the active drug into inactive metabolite, the faster DNA repair systems, the reduction of the intracellular concentration of the molecular target of the drug. All these processes lead to the development of increasingly different clones from the original cell, that are not only resistant to the drug with which they come into contact, but also to others of different therapeutic families. The major strategy to overcome the resistance issue is the use of non-cytotoxic inhibitors of the extrusion pump systems. However, other mechanisms remain active leading to the onset of cross-resistance. One valuable strategy to overcome drug resistance is targeting drug loaded nanocarriers with suitable agents. This allows to deliver intracellularly the anticancer drug by eluding the extrusion systems. The development of new carriers for the active targeting is closely related to the distribution and overexpression of specific receptors and the cellular mechanisms of internalization and uptake.

Figure 5 represents a cartoon of passively targeted nanocarriers (EPR effect) *vs* actively targeted nanocarriers. The EPR effect (A) allows the extravasation from tumor blood vessels of nanoparticels that remain trapped in the tumor stroma due to higher interstitial pressure, which is a consequence of lack of effective lymphatic drainage coupled with lower intravascular pressure. However, aside to the well perfused and rapidly growing regions, a non-uniform tissue oxygenation due to the vascular heterogeneity led to the presence of poorly perfused and necrotic areas in which the efficacy of the treatment is hampered. (B) Actively targeted nanoparticles can be functionalized with specific ligands that

specifically bind receptors expressed primarily on malignant cells. This approach improves the intracellular delivery of the drug, leading to receptor-mediated internalization, which is often necessary to deliver macromolecules and drugs with low cell membrane permeability inside the cells.

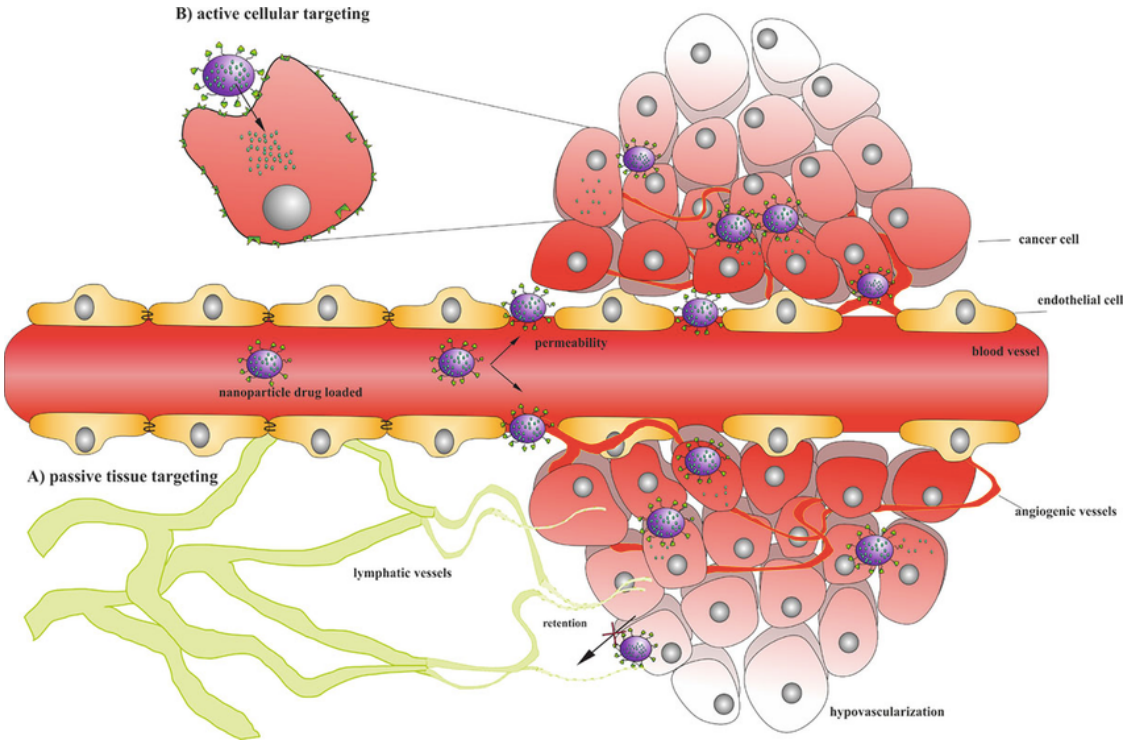

Figure 5. A) Passive targeting (EPR effect). The macromolecular systems and nanocarriers do not cross vessel endothelium of healthy tissue, but can extravasate into tumor tissues. B) Active targeting can be achieved by coating nanocarriers with targeting ligands. After the colloidal system accumulates in the tumor tissue through EPR effect, its ligand is selectively bound by the tumour cell and may be internalized.

In most cases cellular receptors (trans-membrane proteins) or cell membrane epitopes are involved for active targeting, which modulate the receptor-mediated endocytosis (RME) of the drug carrier. Upon internalization by receptor-mediated mechanism, the ligand-receptor system is directed to an acid compartment (endosome) through a maturation and fusion mechanism.[84] Within the endosome, a number of processes takes place that determines the final fate of the endosome content: ligand receptor and targeting agent dissociate and are

transported selectively to the Golgi apparatus and plasma membrane, respectively. Some endosomal processes can be induced by the slightly acidic pH (5-6) that characterizes these intracellular vesicles. The following step of release of the therapeutic molecules is crucial to ensure that the DDS (drug delivery system) provide the activity for which it has been administered.

In metastatic cell, many receptors implicated in the RME are overexpressed. This feature can be exploited for the active anti-cancer targeting. Carriers can be prepared taking into account the expression at the tumor site of specific receptors for endogenous ligands such as transferrin, folate, glucose, mannose and lipoproteins.

1.4 LIPOSOMES

Liposomes (from the Greek *lipos*, fat, and *soma*, body) were discovered in 1961 by Alec D. Bangham while observing the behavior of the phospholipids in water.[85]

Phospholipids are amphiphilic molecules dispersed in water; they are oriented in such a way as to form a double layer (phospholipid bilayer) in which the hydrophilic portions of the molecule are directed toward the aqueous environment, while the non-polar portions, namely the alkyl chains, remain in contact with each other inside the bilayer. The term *liposomes* indicates vesicular closed systems, consisting in phospholipid bilayers arranged in a concentric manner, highly ordered and enclosing an aqueous compartment.

Liposomes are able to incorporate pharmacologically active molecules. Hydrophilic drugs may be included in their aqueous, while lipophilic drugs are distributed in the lipid phase of the phospholipid bilayer (Figure 6). Molecules with amphiphilic characteristics will dispose within the hydrophobic portion between the tails of the phospholipids while the hydrophilic molecules will dispose in the aqueous core. Molecules can be adsorbed on the surface of the liposomes through charge/charge interactions, hydrophobic interactions, hydrogen bridges, etc. Liposomes can be used as carriers of drugs[59, 66, 68, 86] and offer considerable protection of the active molecule from any chemical or enzymatic degradation

process before they reach the target tissue. Liposomes are very versatile in term of characteristics, which make them appropriate for various therapeutic and formulative purposes.[87-91]

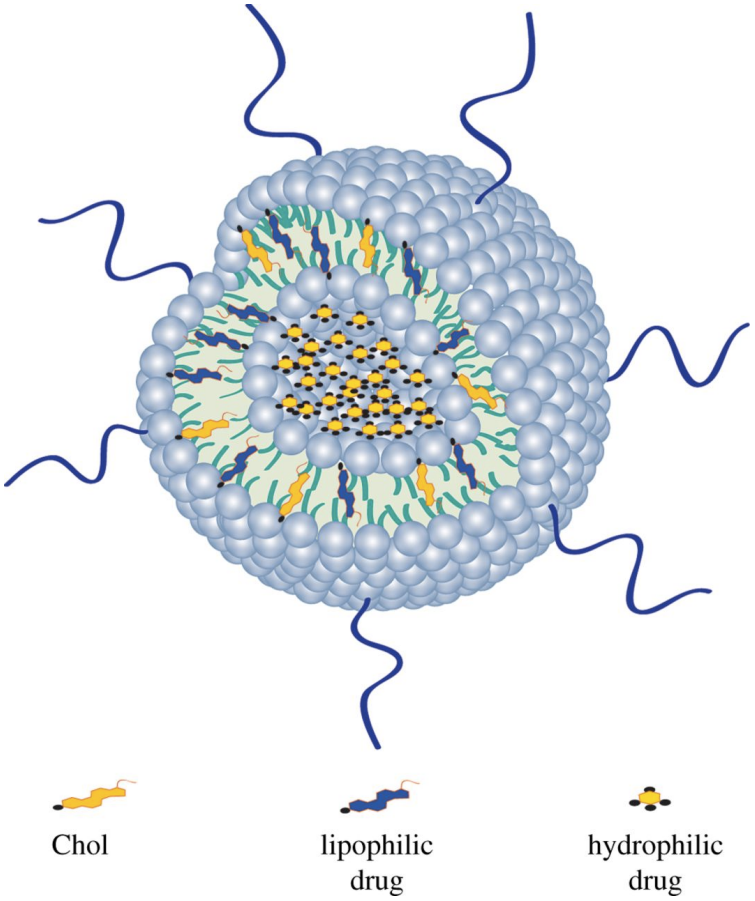

Figure 6. Representation of hydrophilic and lipophilic drug encapsulation into the liposome.[92]

1.4.1 Stealth liposomes

Although liposomes are made of lipidic components and they resemble biomembranes, they are still exogenous nano-objects to the body. Therefore, liposomes may be phagocited by the mononuclear phagocytic system (MPS) after opsonisation by plasma proteins that favour their binding to MPS receptors. Accordingly, they are cleared from the bloodstream.

Coating liposomes with PEG reduces the uptake by macrophages and lead to a prolonged presence of the lipidic veisicles in the blood circulation and, therefore, provides extended time for these liposomes to leak out from the

circulation through leaky endothelium mostly in tissues where the vessel endothelium possess wide fenestrations. PEGylated liposomes showed half-life of 15-24 hours in rodents and 45 hours in humans. Actually, the PEG coating inhibits specific and non-specific interactions with proteins on the liposome surface, which usually promote liposome removal from the blood stream through the RES system.[41, 93, 94]

In virtue of the flexibility of the PEG, linear PEG chains on the liposome surface have been shown to confer adequate surface stabilization and stealth properties, in particular a 5% molar ratio of PEG-phospholipid with respect to the lipid components has been selected to generate commercial products.[88, 95, 96] In order to decorate liposomes, the polymers are converted into their lipopolymer counterparts by conjugation with a lipidic moiety, conventionally a phospholipid but also an acyl group can provide anchoring to the bilayer of the liposome. PEG can be selected with different length and architecture. The PEG chain can be attached to an acyl group through a linker, which can be an ester, an ester carboxylate, an amide, a di-sulfide or an ether. The choice of the linker used to conjugate the PEG to the lipophilic moiety has a significant impact on the behaviour of the liposome; in particular, few chemical groups such as ester, vinyl ether and acetal are highly susceptible to hydrolysis, which can promote the controlled release of the PEG coating in acidic environments (such as the tumor), thus locally and selectively promoting the interaction of the liposomes with cancer cell membrane. On the other hand, a phosphate group integrated in the PEG-lipid component confers negative charge to the liposomes, which can lead to complement activation (see chapter 1.4.2).[95]

According to the chemical structure of the lipophilic anchor, two classes of PEG derivatives can be generated:

• PEG-Phospholipid: in this group the linear chain of methoxy-PEG is covalently linked to the phospholipid, in general a distearoil-, dipalmoil- and dimyristoyl-phosphatidylethanolamine (DSPE, DPPE and DMPE, respectively). The increased persistence in the bloodstream of liposomes coated with this lipo-polymer depends on both the length of the PEG chain and the grafting density. The PEG generates on the surface of the liposome an aqueous ”cloud”, which

increases the stealthiness of the liposomes and reduces their interaction with biological surfaces and molecules such as the opsonines. In general, the PEG with long-chain promotes a better barrier than that which would be created with shorter chains.

• PEG-lipid: in this case a lipid anchor with chemical structure different from a phospholipid is used. The family of lipo-polymers thus generated represents a new class of materials. The purpose of using lipid different from phospholipids is to eliminate potential issues related to charged head group of the phospholipid. In fact, the phosphate group possesses a negative charge that can generate a negative zeta potential on the liposome surface which is associated to phenomena of hypersensitivity. Furthermore, the phospholipids are relatively unstable and they are particularly susceptible to enzymatic degradation. Consequently, there is a growing interest in the use of lipids that are devoid of the phosphate group.

The use of cholesterol as components of liposomal formulations is very relevant. The cholesterol improves the hydration of the lipid head groups, stabilizes the membrane and increases the retention of hydrophilic drugs in the liposome core. Various studies have shown that the use of cholesterol may reduce the fluidity of the lipid bilayer of liposomes, increase its stability and control the permeability of the drug across the liposomal bilayer. [97] PEG-Cholesterol conjugate can also be used as PEGylating agent. The polymer chain is conjugated to the lipid by an ester bond or ether bond involving the OH group in position 3 of cholesterol. In virtue of the lipophilicity and structural compatibility of cholesterol with the phospholipids of the liposomes, PEG-cholesterol conjugate is easily embedded in the bilayer of the liposome.[88]

1.4.2 Liposome composition

The main advantage of liposomes as drug carriers is represented by the fact that the lipids that are selected to assemble these vesicles, phospholipids and cholesterol commonly used for their preparation, are natural components of all cell membranes, and therefore biologically safe. This allows the use of liposomal formulations for potential administration through various routes of administration.

Liposomes are generally made of natural or synthetic lipids, but they typically include other functional components such as amphiphilic polymers to enhance their colloidal stability.

Table 1. Liposome-based drug formulation on market

Product name	Route of injection	Drug	Particle type/size	Drug form/Storage time	Lipid composition	Approved indication
Ambisome	Intravenous	Amphotericin B	Liposome	Powder/36 months	HSPC, DSPG, cholesterol, and amphoteracin B (2:0.8:1:0.4 molar ratio)	Sever fungal infections
Abelcet	Intravenous	Amphotericin B	Lipid complex	Suspension/24 months	DMPC and DMPG (7:3 molar ratio)	Sever fungal infections
Amphotec	Intravenous	Amphotericin B	Lipid complex	Powder/24 months	Cholesteryl sulfate	Sever fungal infections
DaunoXome	Intravenous	Daunorubicin	Liposome	Emulsion/12 months	DSPC and cholesterol (2:1 molar ratio)	Blood tumors
Doxil	Intravenous	Doxorubicin	PEGylated liposome	Suspension/20 months	HSPC, cholesterol, and PEG 2000-DSPE (56:39:5 molar ratio)	Kaposi's sarcoma, Ovarian/breast cancer
Lipo-dox	Intravenous	Doxorubicin	PEGylated liposome	Suspension/36 months	DSPC, cholesterol, and PEG 2000-DSPE (56:39:5 molar ratio)	Kaposi's sarcoma, ovarian/breast cancer
Myocet	Intravenous	Doxorubicin	Liposome	Powder/18 months	EPC and cholesterol (55:45 molar ratio)	Combination therapy with cyclophosphamide in metastatic breast cancer
Visudyne	Intravenous	Verteporfin	Liposome	Powder/48 months	EPG and DMPC (3:5 molar ratio)	Age-related molecular degerneration, pathologic myopia, ocular histoplasmosis
Depocyt	Spinal	Cytarabine	Liposome	Suspension/18 months	Cholesterol, Triolein, DOPC, and DPPG (11:1:7:1 molar ratio)	Neoplastic meningitis and lymphomatous meningitis
DepoDur	Epidural	Morphine sulfate	Liposome	Suspension/24 months	Cholesterol, Triolein, DOPC, and DPPG (11:1:7:1 molar ratio)	Pain management
Epaxal	Intramuscular	Inactivated hepatitis A virus (strain RG-SB)	Liposome	Suspension/36 months	DOPC and DOPE	Hepatitis A
Inflexal V	Intramuscular	Inactivated hemaglutinine of Influenza virus strains A and B	Liposome	Suspension/12 months	DOPC and DOPE	Influenza

To date, a variety of liposomal commercial products (Table 1)[59] with different composition are present in the market. In the literature many examples are reported showing how the lipidic mixture used to assemble liposomes can affect their in vivo stability, pharmacokinetic profile[98], and complement system activation. Koynova et al. demonstrated that phospholipids physico-chemical features affect the bilayer permeability in a manner that is somewhat predictable from their phase transition temperature.[99] Thus, liposomes prepared with phospholipids with short acyl chains (C14:0, namely 1,2-dimyristoyl-sn-glycero-3-phosphocholine (DMPC)) possess a bilayer that is more fluid and release drug payload faster than liposomes made with longer acyl chains (C18:0, 1,2-namely distearoyl-sn-glycero-3-phosphocholine (DSPC)). Cholesterol is a common component of liposomes that is able to modulate membrane permeability and stability: at molar ratio above 30%, it decreases the energy to melt the lipidic bilayer of liposomes and eliminates the gel-to-liquid-crystalline phase transition.[97] Furthermore, it is reported that about 30% mol of cholesterol in liposomes increase the flexibility of the bilayer that is required to decrease the opsonisation of these carriers.[95]

By comparing the lipidic composition of clinically approved Doxil® and Myocet®, it can be noticed that Doxil® contains three components: 1. the high phase-transition temperature phospholipid hydrogenated soy phosphatidylcholine (HSPC; Tm 52.5°C), 2. cholesterol and 3. $mPEG_{2kDa}$-DSPE, at a 56:39:5 molar ratio; on the other hand, Myocet® is composed of egg phosphatidylcholine (EPC), which is liquid at room temperature, and cholesterol at a 55:45 molar ratio. The EPC/Chol formulation was demonstrated to release doxorubicin fairly rapidly and showed a relatively short circulation lifetime compared to that of Doxil®, due to the steric barrier provided by the surface-grafted PEG.[86] Indeed, PEGylated stealth liposomes are slowly cleared from the bloodstream; this provides a prolonged circulation of the drug-loaded liposomes and consequently higher chances of extravasation through tumour vasculature during the first 3-4 hours after administration, because of the repeated passage through the tumour microvascular bed. Furthermore, stealth liposomes are taken up by tumours in a far greater ratio with respect to the rapidly cleared liposome formulations.[76, 68] Actually, a correlation between liposome circulation time and tumour uptake is reported.[100] Once in the tumor interstitium, intracellular delivery of drug depends on drug release from liposomes in the interstitial fluid and diffusion to the cytosol.[68] Furthermore, PEGylation can not only confer “stealth” properties to liposomes, but it is also reported to reduce nanocarrier removal by controlling the opsonisation and involvement of the complement. Indeed, it is crucial to guarantee nanocarrier coating strategies that do not activate the innate immunity response[101], which can promote the selection of resistant tumor cell lines, hence, indirectly, the tumor growth.[102-105]

Moreover, liposomes with neutral surface charge obtained with saturated phospholipids and high cholesterol content, which modulate membrane rigidity and provides uniform bilayer without surface defects, are poorly prone to opsonisation and structural destabilisation by C3 adsorption.[95, 106, 107, 108, 109] In particular, liposomes prepared from HSPC and cholesterol (15:10.5 molar ratio) were shown not to activate the human system complement.[96]

The modulation of peculiar parameters such as lipidic composition and surface with functional modifiers can dictate the tissue selectivity of liposomes. To

this aim, different molecules can be anchored to the surface of liposomes, for example functional synthetic polymers, proteins, polysaccharides, monoclonal antibodies and fluorophores (Figure 7). Those modifications allow to obtain a more specific biodistribution of the loaded drug and to reduce its systemic toxic effects.

Liposomes with positive or negative surface can be set up by including molecules with the requested charge on the lipid bilayer (Figure 7 d). The presence of electrostatic charges on the liposomal surface represents an beneficial feature to ensure colloidal stability since the electrostatic repulsion limits the natural tendency of the liposomes to aggregate. However, excessive charge has also be associated with activation of the complement and toxicity of charged liposomes.[95]

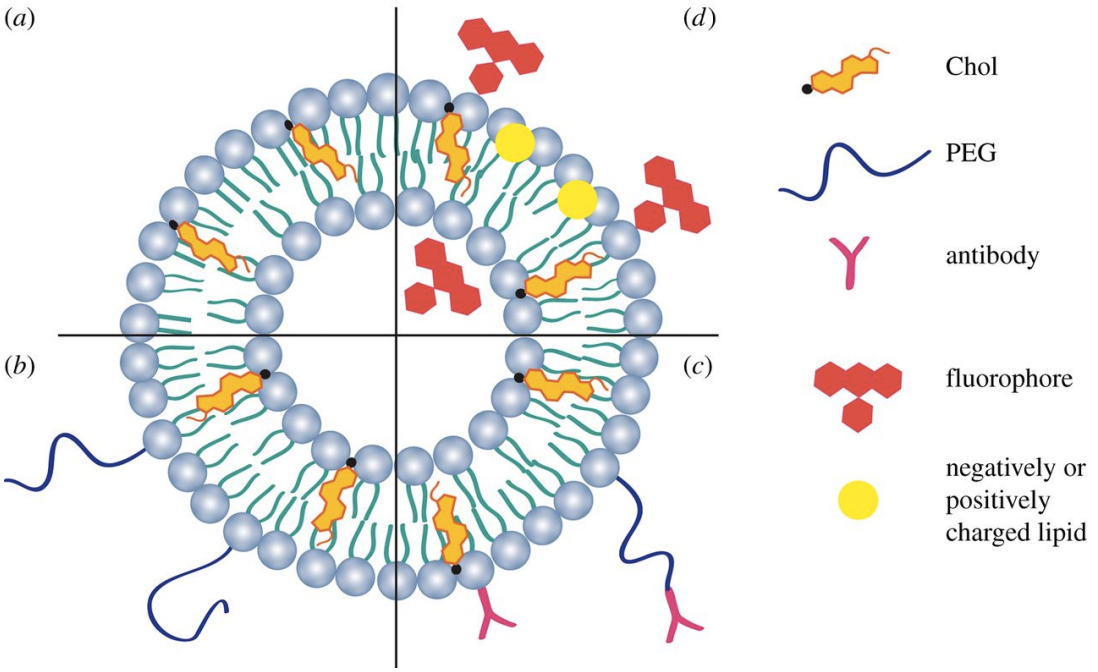

Figure 7. Liposome cross section and composition. a) Conventional vesicle; b) stealth liposome; c) ligand-targeted liposome; d) fluorescent and charged liposomes.[92]

1.4.3 Liposome classification

Liposomes classification can be based on size and structure, both deriving from the formulation process.[93]

As regards the size, the diameter of the liposomes is variable and it is generally between 20 nm and 1 micrometer. The sizes of liposomes can be ultra-small, small, medium and large. As for the structure, we can distinguish unilamellar liposomes, multilamellar and multivescicle, depending on the phospholipid bilayer spatial organization. The unilamellar liposomes are formed by a single lipid bilayer and an aqueous core. The multilamellar liposomes are formed by several concentric lipid bilayers while the multivesicular liposomes are constituted by an external vesicle, which contains other non-concentric ones.

The structural features of liposomes are important because the size and the number of bilayers of the vesicles contribute to determine the half-life of the liposomes in the blood circulation and the drug loading degree.

Figure 8 represents the major families of liposomes according to a size classification. The small and medium sized unilamellar vesicles (SUV/MUV) have sizes below 0.5 microns; they are constituted by a single bilayer and have a uniform size. The small vesicles (SUV) have a mean diameter of less than 100 nm, while medium vesicles (MUV) are between 100 and 500 nm. Large uni-lamellar vesicles (LUV) have dimensions of about 0.5 microns and consist of a single bilayer. LUV liposomes are particularly suitable to incorporate hydrophilic macromolecules (biotech drugs). These liposomes are rapidly removed by the reticuloendothelial system (RES) because of their considerable size. Finally, the large multi-lamellar vesicles (MLV) have dimensions greater than 0.5 microns and they are formed by multiple bilayers. They can efficiently incorporate hydrophobic molecules being endowed with multiple lipid bilayers in which poorly soluble drugs can dispose; MLVs possess high stability over time, they are easily uptaken by cells of the RES and can thus be exploited to deliver specific drugs to macrophages, the MPS cells (Mononuclear phagocyte system), and the Kupffer cells of the liver.

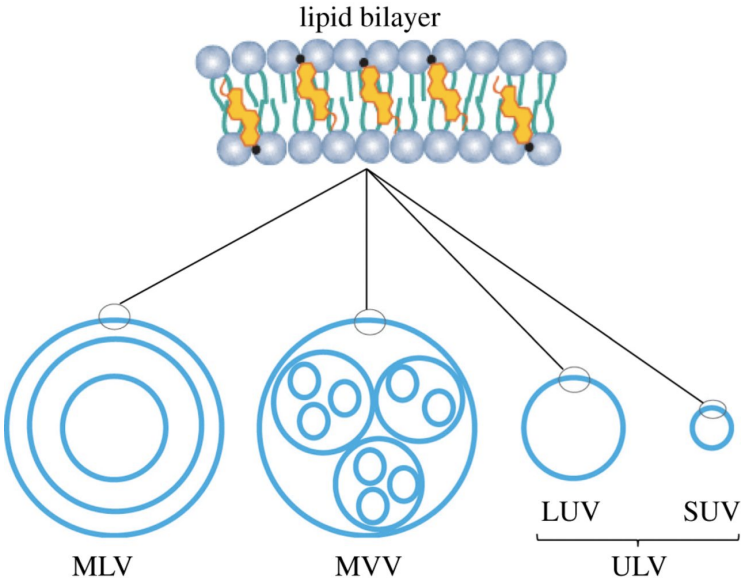

Figure 8. Liposome classification based on size and bilayer rearrangement.[92]

The experimental data reported in the literature have shown that liposomes with a diameter of less than 100 nm have significantly longer blood half-life comparing to liposomes with the same lipid composition and size.[110-112] Consequently, the production of liposomes with a defined size and structure is essential to control their biodistribution.

1.4.4 Methods for liposome preparation

Several methods are used for the preparation of liposomes that can be identified according to the technique used to disperse the lipid bilayer. The methods traditionally used in laboratory are the “Reverse Phase Evaporation”, the “Solvent Injection Method” and the “Thin-Layer rehydration”.[85, 92, 93, 113]

The reverse phase evaporation method is based on the formation of reverse micelles by sonication of the organic solution containing the hydrophobic molecules (lipids and possible drugs) with the aqueous buffer containing any hydrophilic molecule; the removal of the organic solvent results in the formation of a gel that at some point collapses, leading to the destabilisation of some of the micelles. The excess of free phospholipids self-organizes in a complete bilayer surrounding the micelles remained inverted, thus generating the liposomes. This method allows the encapsulation of high amounts of water-soluble drugs, since the

volume ratio of aqueous phase/lipids is high. These liposomes, however, are fairly large liposomes (MLVs and LUVs).

The solvent injection method involves the injection of the organic lipid solution in the aqueous buffer containing the molecule to be encapsulated; the organic solvent is then removed which yield sponataneous formation of MLVs liposomes. The type of solvent, the temperature of the buffer and the injection rate are key parameters in the modulation of the final characteristics of the formulation. In general, however, this method generates a population of liposomes that is quite polydisperse, and in some cases it is difficult to completely eliminate the organic solvent.

Finally, the thin layer-rehydration technique requires the dissolution of the lipids in the organic solvent, the evaporation of the solvent to generate a thin lipid layer and subsequent rehydration of the lipid film with a suitable buffer.[85, 114] This method allows to easily and completely remove organic solvents, but MLVs are mainly generated with a low volume of the internal aqueous core. In order to increase the internal volume of the vesicles, "freeze-thaw" treatment of initial liposomes can be applied: the lipid dispersion is subjected to a series of cyclic treatments including freezing (usually in liquid nitrogen at -96 °C) and warming to about 65 °C. This treatment breaks the lipid bilayer due to the rapid freezing and subsequent rearrangement during defrosting. Some authors[115] report that also the extent in time of the two processes of freezing and thawing, as well as the number of freeze-thaw cycles to which the formulation is subjected, can affect the size distribution of the liposomes and the loading efficiency of hydrophilic drugs. The liposomal formulation prepared by thin layer rehydration may eventually be lyophilized after adding a suitable cryoprotectant.

In order to improve the formulation quality and make the liposomes less polydisperse, smaller and homogeneous, other preparation techniques are available. However, it should be noted that reducing the size of the liposomes also leads to a decrease of their internal aqueous volume and, consequently, to a lower degree of loading of hydrophilic molecules. The most used procedure to reduce the size of liposomes and obtain SUVs from multilamellar liposomes is sonication, which can be performed either in the bath sonicator or with a sonicator tip: the

ultrasonic waves break the MLVs to form smaller liposomes with smaller polydispersity. Alternatively, the process of extrusion through membranes of polycarbonate with a specific cut-off allows to obtain vesicles of the size of the pores of the membrane choice.

1.4.5 Interactions of liposomes with the cellular membrane

In order to deliver the drug loaded in liposomes, the vesicles must be able to associate/interact with a target cell where the drug is then released. Four types of liposomes/cells interaction may occur[94, 116, 117]

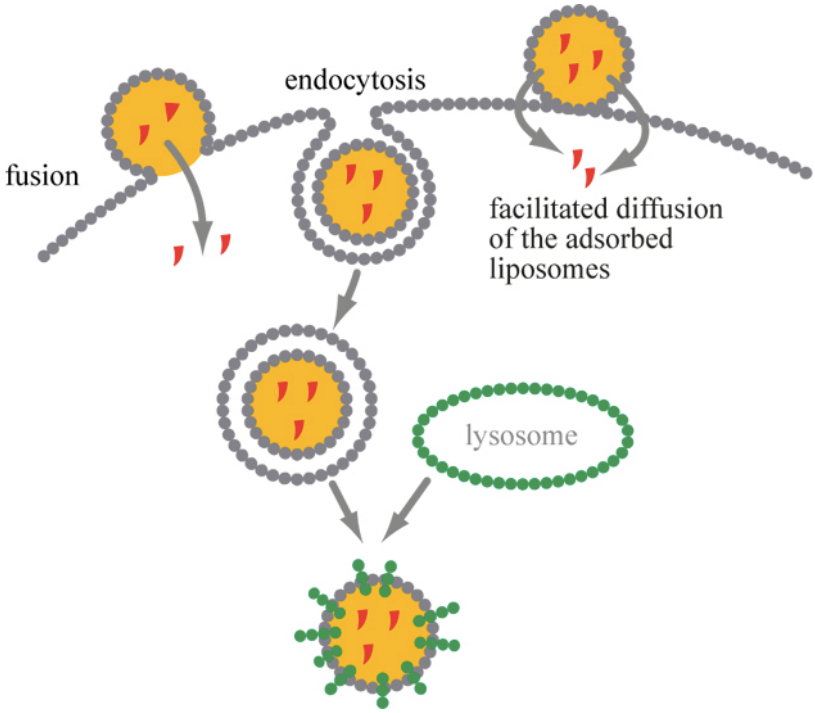

Figure 9. Mechanisms of interaction of liposomes with cells. From *Glossary of Nanothecnology and related terms* (eng.thesaurus.rusnano.com)

1. Exchange and transfer of lipids between the liposomal carrier and the cytoplasmic membrane. This mechanism does not guarantee an effective transfer of the drug from the liposome to the cytosolic compartment.

2. Adsorption of the liposome on the surface of the cytoplasmic membrane without fusion of the carrier with the cell membrane. Such interaction may alter the permeability of cells and the liposome favouring a series of events,

including the drug release in the extracellular environment or transfer within the membrane.

3. Fusion with the plasma membrane by insertion of the lipid bilayer of the liposome into the plasma membrane, with simultaneous release of liposomal content into the cytoplasm

4. Phagocytosis of the liposome by the cell followed by a migration of the carrier in subcellular organelles (endosomes and lysosomes). The lysosomes environmental acidity generally promotes the dissociation of liposomal lipids resulting in release of the drug content (Figure 9).

1.5 CELL PENETRATING PEPTIDES (CPPS)

In recent years, the discovery of peptides able to cross cellular membranes has been addressed to new challenging applications for innovative formulations. These systems allow for crucial pharmaceutical improvement of drug formulation because of their biological properties that can be advantageously exploited in drug delivery. These biologically derived molecules, most commonly called cell-penetrating peptides (CPPs) or protein transduction domains (PTDs), have opened novel perspectives in the field of drug delivery.[118-124]

After the first CPPs were discovered and the transcription activating factor (Tat) isolated from HIV-1 virus[125-127], the attention has been focused on their potential use as carriers or vectors to transfer drugs, such as peptides, proteins, oligonucleotides, plasmids, liposomes and nanoparticles, to the cell cytosol and across biological barriers. CPPs can be classified into two categories according to their chemical nature: cationic or amphipathic peptides. They have the property of translocation, which is the typical feature of the Tat from HIV-1 virus, of Antennapedia homeodomain transcription factor from Drosophila herpes simplex virus type 1 (HSV-1), of VP22 (penetrating) transcription factor and others. In particular, the Tat peptide sequence 86–102 is derived from the transcription-activating factor, which is involved in the replication of HIV. The transcription-activating factor is organized in three different functional domains: 1) an acidic N-terminal region that is important for trans activation; 2) a cysteine-rich DNA-binding

region (22-37 amino acids long) with a zinc-finger motif; and 3) a basic region (49-58 amino acids), responsible for nuclear import. This last region might also be involved in the Ca^{2+}-independent cell association of the protein. The cell penetration capacity is provided by the presence of a short peptide sequence, known as membrane traslocational signals (MTS), which consists of a specific region that corresponds to the 49-57 aminoacid sequence of the Tat protein. This sequence is very abundant in basic residues. According to this specific sequence and its primary structure, synthetic peptides have been designed with the aim to mimic Tat features, which has been achieved by including a number of arginine or lysine residues.[119, 121]

1.5.1 CPPs features

CPPs family members possess similar features that derive from the amino acid composition. Their sequence contains a high percentage of arginine (Arg, R) and lysine (Lys, L) residues that are positively charged at physiological pH. However, they differ from each other by type, number of amino acids and amino acid sequence. A 13 aminoacid sequence from Tat has been isolated, which includes 6 arginines and 2 lysines. The translocation activity of this aminoacid sequence has been intensively studied. The number of charges has a key role in promoting the peptide transport.[128]

Structure/function correlation studies have shown that the increase in the presence of arginine residues greatly favours internalization of the sequences compared to lysines.[121]

The guanidinium head group of the arginine side chain seems to be the chemical group mainly responsible for the biological activity of the peptide sequence rather than generic positive charges such as lysines. The number of arginine plays an important role, and it has been shown that the highest translocation activity is achieved with 7-15 arginine residues, which has been attributed to efficient bidentate hydrogen bond that guanidinium groups form with negatively charged phosphate, carboxylate and sulphate groups on the surface of the cell membrane. These bonds attenuate the strong polarity of guanidinium

groups by producing a polar ion pair complex capable of diffusing across the membrane.[129, 130]

It has also been found that in oligomerized arginines of synthetic polymers the association of the guanidinium group with counter anions reduce the charge repulsion between nearby guanidinium moieties. Furthermore, peptides chain length is an important factor to translocation. The translocation efficiency decreases when the sequences exceed 15 amino acidic residues. Chain linearity is not essential for the internalization process; in fact, branched CPPs are able to cross biological barriers very efficiently.

1.5.2 Cellular internalization mechanisms of CPPs

CPPs are short cationic peptides of less than 30 amino acids that possess the property of translocation across the plasma membrane and of transferring membrane impermeable macromolecules when chemically or physically associated to those molecules. In order to efficiently enable the delivery of macromolecules across plasma membrane, a methodology has been developed involving the conjugation of a suitable CPP to cargo molecules, with the purpose of favouring their passage through biological membranes and transfer them intracellularly[118, 120, 131]

The mechanism of the CPPs cellular translocation has not been fully elucidated yet, and evidences are quite controversial. It seems very likely that peptides from different translocating peptide family use different mechanisms of cell entry. The first step of the internalization process involves the peptide nonspecific interaction with the cell surface, by means of ionic bonds between the positive charges of the CPP and those anionic of the proteoglycans. This adsorption process is not specific because it does not involve selective biorecognition with specific receptors. In fact, CCPs containing D-amino acids have shown a similar internalization efficiency compared to derivatives with L isomers.[120, 132-135]

The cellular uptake mechanisms are strongly influenced by the cell characteristics and also by the features of the drug carriers, such as size and

hydrophobicity. CPPs mediated cell uptake can promote the access of drug nanocarriers to the cytoplasm according to two mechanisms, which have been recently proposed: 1. endocytotic active process and 2. direct diffusion through the phospholipidic bilayer (Figure 10).

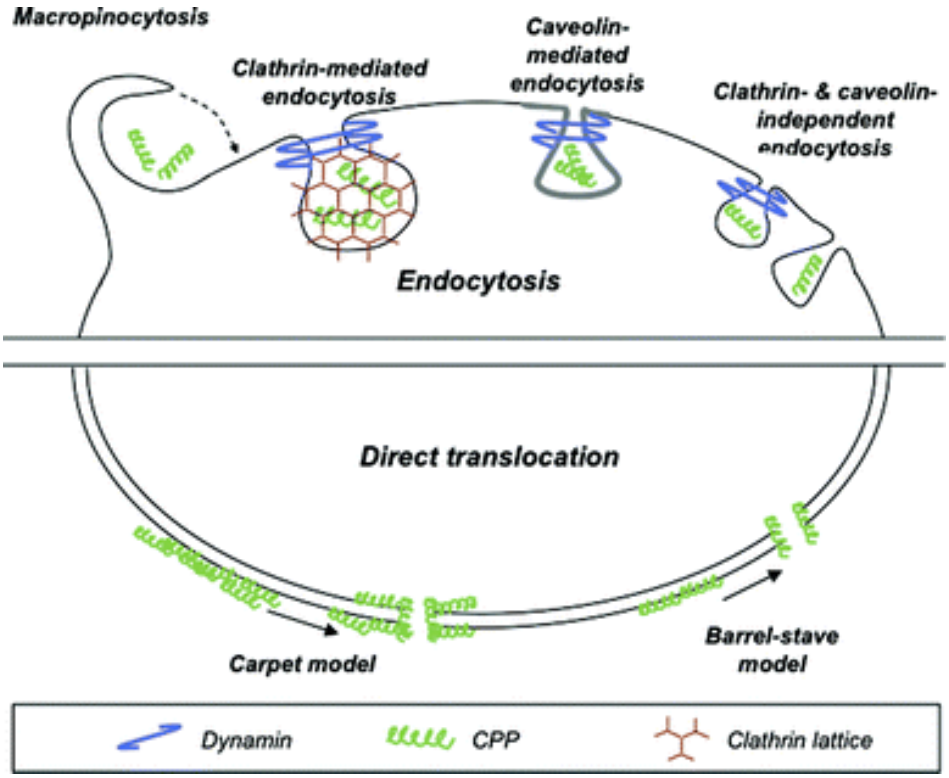

Figure 10. Mechanism of internalization of CPPs: endocytosis and direct diffusion.[138]

Endocytosis is an energy-dependent cellular process characterized by intracellular vesicle formation. Since CPPs discovery, many studies have been carried out in order to identify the real mechanism involved in internalization of these peptides. Zaro et al have shown that oligoarginine concentration in the cytosol of CHO (Chinese Hamster Ovary) cells at 4 °C is reduced by 60% compared to that of cells incubated with oligoarginines at 37 °C.[136] This result seems to support an active mechanism of cell entry of these molecules, because ATP-dependent processes are inhibited at 4 °C. The low temperature (4 °C) also greatly reduces membrane fluidity, making internalization vesicle formation difficult. Additional studies performed with endocytosis specific inhibitors have

confirmed this hypothesis. Potassium depletion and chlorpromazine, both specific inhibitors of clathrin mediated endocytosis process, inhibit 50% Tat peptide cellular uptake. Furthermore, vesicular transport mechanism depends strongly both on the drug features (namely physico-chemical and biological properties) and on the carrier to which CPPs are conjugated. For example, when Tat peptide was conjugated to proteins, endocytosis took place according to a caveolin mediated process. Similarly, a clathrin mediated process was observed when CPP was linked to a small fluorescent labelling agent.[137]

The mechanism of cell uptake of liposomes coated with polyarginine residues was intensely studied. It has been shown that the mechanism of cellular uptake varies depending on the polypeptide used to coat the liposomes and on vesicle size.[139-141]

Cell penetrating peptides were also shown to cross cellular membrane by a temperature and energy-independent process. This process involves peptides with specific properties promoting the interaction with cell membrane or capable to disrupt membrane integrity.[123] The energy independent process of cell entry of CPPs has been described by the “carpet” and the “barrel-stave” models (Figure 9). This passive access to the cytosol requires peptide accumulation on the surface of the membrane. In the first model proposed, CPPs initially adsorb with the cell membrane, remain adsorbed and generate pores through which diffusion of extracellular fluid into the cytoplasm occurs. In the second model, polyarginines and polylysines derivatives penetrate in the cell membrane and a number of them organize to form channels. This allows a direct contact of the extracellular matrix with the cytoplasmic environment and the cellular uptake of CPP.[120]

1.5.3 CPPs biodistribution, limits, degradation, toxicity

Despite the advancements of the last decade, CPPs biological behavior for therapeutic application needs to be further clarified. In particular, it is important to clearly assess their biodistribution selectivity, metabolism, immunogenicity and potential toxicity.[135, 142, 143]

To date, a selective biodistribution of CPPs has not yet been observed. Following administration, they tend to non-specifically interact with all cells with which they come in contact. This fact represents a great therapeutic limitation to the use of such peptides in drug delivery, as they promote the cellular uptake of the systems to which they are associated indiscriminately into the diseased cells and healthy ones. In order to enhance the tumour biodistribution of CPPs, Jiang et al. set up a new carrier including CPPs for selective delivery of diagnostic agents for tumor imaging. For this purpose, a fluorescently labelled oligoargininic derivative was conjugated with a polyanionic peptide able to inhibit the cellular penetration capacity, thus preventing the unspecific interaction of the ionic oligoargininic peptide with membrane proteoglycans upon parenteral administration of the carrier. In the vicinity of the tumor tissue, metalloproteinases normally overexpressed cleave the polyanionic peptide, which trigger the deshielding of the oligoarginyl derivative that can mediate the nanocarrier cell entry. Preclinical studies in rats have demonstrated the effectiveness of this strategy in vivo.[144]

The metabolic stability of the CPP is an essential requirement for the use of these peptides in the transport of drugs to target cells. The degradation of CPPs was found to be closely related to the presence of peptidases in the considered cell models. Increased proteolytic stability of cell penetrating peptides can be achieved by replacing the natural L-amino acids with the corresponding D isoforms that is not physiologically present in proteins.

A relevant body of information has been gathered concerning the toxicity of CPPs. Nath et al have reported the neurotoxicity of Tat peptide, which at certain concentration can induce cell death in primary cultures of rat neurons.[145]

The cytotoxic effect of CPPs is strongly influenced by the CPPs sequence. The 37-60 Tat sequence and the 37-53 Tat sequence, at the concentration of 100 pM and for an incubation period of 24 hours, greatly decrease the viability of HeLa cells, whereas the Tat sequences (43-60) and (47- 60) are non-toxic.[146] However, Tat-peptides at concentration 1 μM were shown to have toxic effects on all of the tested cell lines. The L-polyarginine instead, has been found to induce apoptosis in lung epithelial cells and damages the plasma membrane resulting in increased

cell permeability and loss of intercellular junctions, which regulate the permeability of the biological barrier.[147]

1.6 POLIMERIZATION

The generation of novel materials and polymers for biomedical applications requires the exploitation of very sophisticated techniques to produce them on small and subsequently on a large industrial scale. Notably, the properties of such materials must be sharply controlled to generate polymers with even physico-chemical and biological performances. In particular, the chemical identity, purity, molecular weight and polydispersity index are key features dictating the biological behaviour of such materials. Furthermore, for large production, the synthetic process has to be reproducible.

The polymerization is a process that allows the synthesis of polymers starting from the constituent monomers. There are two types of polymerization reactions that are identified according to the characteristics of the starting monomers: the polyaddition and the polycondensation. The first is a chain reaction between chemical species containing double or triple bonds which occurs at high speeds, leading to the formation of high molecular weight compounds and very polydispersed, often associated with undesirable side products such as branched polymers. The latter is a much slower reaction that can be controlled from the chemical standpoint: it takes place by condensation of reactive groups present in several species with elimination of a small molecule, usually water, and produces polymers of low molecular weight and higher homogeneity.

1.6.1 Free Radical Polymerization

The radical polymerization is the most used polyaddition process in the synthesis of polymers, in particular the vinyl-type. It takes place through three steps: an initial activation step during which reactive radical species are formed, a propagation step, that leads to the formation of the polymer and, finally, a termination reaction for the coupling of two radical species present in the reaction mixture (Figure 11).

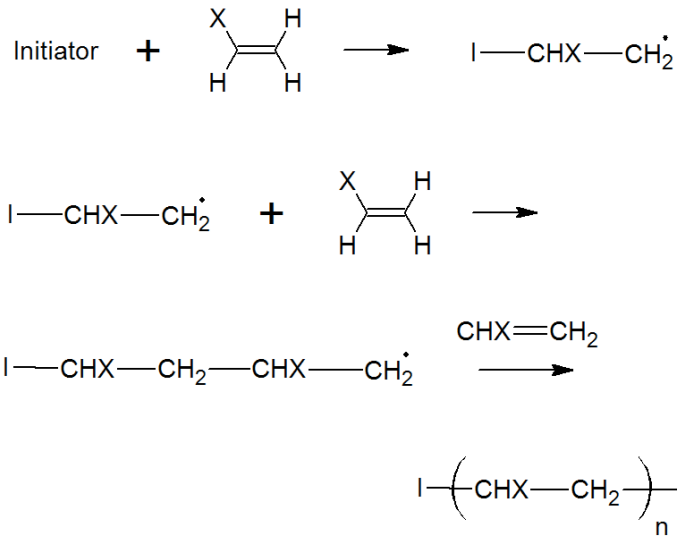

Figure 11. Free radical polymerization: reaction scheme (from polymerdatabase.com).

In the initiation phase, the primary radicals may be generated chemically or physically. The most common method used is thermal or photochemical (by UV radiation) fragmentation of relatively weak bonds. During the propagation, the radical initiator reacts with a monomer at the level of the vinyl double bond, forming a new radical with higher molecular weight, which subsequently reacts with another monomer, a process which entails the lengthening of the polymer chain. The polymerization reaction ends with the formation of stable species as consequence of the coupling of two radical species present in solution.

The length of the polymer chain which is generated with this process depends on the reaction conditions and the molar ratios of the reagents used, while physical properties of the polymer depend on monomer composition, polymerization degree, molecular weight and relative polydispersity index (PDI, Mw/Mn). Usually the polymers synthesized with this method have a wide distribution of molecular weights and show PDI values between 2 and 3.

1.6.2 Controlled/living radical polymerization (CRP)

In the literature a variety of radical polymerization techniques are described that allow to obtain polymers with well-defined physico-chemical and structural characteristics under controlled reaction conditions. In this sense, the controlled radical polymerization (Controlled Free Radical Polymerization, CFRP) of 'living' type has aroused great interest as it allows to obtain products with well-defined molecular weights and polydispersity index lower than traditional methods; it also permits to synthesize block copolymers for simple addition of different monomers in successive stages of the polymerization process.

Some examples of living polymerizations are currently exploited in the industrial field for group transfer polymerization (Group Transfer Polymerization, GTP)[148], the atom transfer radical polymerization (ATRP)[149], the controlled polymerization with the nitrosyl cation (Nitroxide-Mediated Polymerization, NMP)[150] and the chain transfer process for reversible addition-fragmentation (reversible addition-fragmentation chain transfer, RAFT).[151] These methods are all characterized by free radical polymerization because their propagation process is essentially based on a delicate balance of activation-deactivation of dormant species that when converted in the active radical state, the growth of the polymer chain proceeds to exhaustion of the monomer in solution (Figure 12).

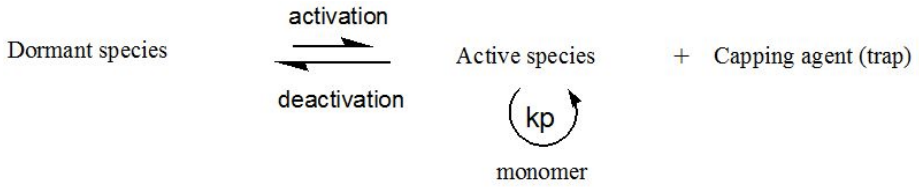

Figure 12. General equilibrium pattern of activation-deactivation (kp: polymerization costant).[152]

The activation, or reactivation, of the dormant species depends on the type of radical initiator chosen and it can occur due to thermal stimuli, UV irradiation or addition of a metallic activator.

1.6.2.1 Atom Transfer Radical Polymerization (ATRP)

Matyjaszewski and Sawamoto were among the first researchers to study the technique of Atom Transfer Radical Polymerization (ATRP), a very versatile controlled polymerization process that allows to synthesize homopolymers and copolymers of acrylic and methacrylic acid derivatives using radical initiators alkyl halides (R-Br or R-Cl). The reaction proceeds as schematically described in Figure 13.

The reaction is characterized by the existence of a dynamic equilibrium between an active radical (the radical initiator or a radical of the propagating chain), and a dormant specie which represents the predominant form. The radical species is generated by means of a reversible redox process catalyzed by a transition metal in the reduced state (activator), able to remove the halogen atom from the dormant species. The radical that is formed allows the growth of the polymer chain in the presence of the monomer and then it reacts with the oxidized metal complex (deactivator) regenerating both the dormant species and the activator.[153]

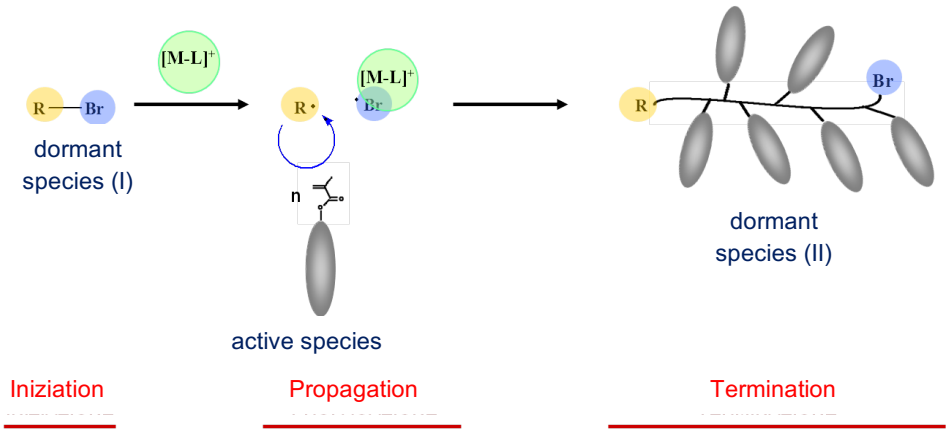

Figure 13. Representation of a controlled radical polymerization 'living' type process (R -Br: initial dormant species (I); R: radical initiator; $[ML]^+$: activator ligand-metal complex, R-polymer chain-Br: dormant final species (II)).

The catalyst plays a crucial role in ensuring a fast and reversible transfer of the halogen atom from the initial dormant species (I) to the final one (II) and is employed in a molar ratio of 0.1-1% woth respect to the monomer.[154] It is chelated by a ligand, which guarantees its solubilisation in the reaction solvent and

modulates the availability of the metal for the halogen transfer. In particular, among chelating agents, amine multidentate derivatives, that allow to obtain catalysts endowed with a higher specificity in generating active radical species, are often used.[155] The copper complexes of Cu(I) proved to be the most efficient and most used for their low toxicity, low cost and biocompatibility.[156]

The initiator/monomer molar ratio determines the molecular weight of the final polymer synthesized. Multifunctional initiators may allow the growth of branched chains. A correct initiation step of the reaction is necessary to obtain polymers with defined structure and low polydispersity.

1.6.2.2 Reversible addition fragmentation chain transfer polymerization (RAFT)

Among the most recent chemical strategies to synthesize polymers, Reversible Addition-Fragmentation Chain Transfer (RAFT) radical polymerization was set up by Commonwealth Scientific and Industrial Research Organization (CSIRO) and firstly reported in 1998 by Chiefari.[157]

In order for RAFT polymerization to take place, an equilibrium between the radical addition and fragmentation reactions must occur in the presence of a chain transfer agent, conventionally named as a RAFT agent. RAFT agents provide the "living" feature to this process by their high transfer constant, which provides the rapid exchange between the dormant and active radical species. Thus, their structure needs to be selected on the basis of the features and reactivity of the chosen monomer.[158] This is usually achieved by using thiocarbonylthio compounds that possess the structure shown in Figure 14.

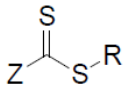

Figure 14. General structure of RAFT agents.

The key features of RAFT agents are a reactive C=S double bond and a weak S-R single bond. Transfer constants of RAFT agents are strongly dependent on "Z" and "R" substituents. The R group is the free radical leaving group and it is

selected in order for it to undergo beta scission from the RAFT-adduct radical and to be still able to re-initiate polymerization. The reactivity of the transfer agent is highly influenced by the Z group (Figure 14). It should be able to activate or deactivate the thiocarbonyl double bond in order to provide radical addition and to modify the stability of the intermediate radicals.

A variety of monomers can be used to synthesize polymers containing end or side chain functionality in a one-step process.[159]

Initiation and radical-radical termination processes take place in a conventional radical polymerization. The most common used initiators are peroxy- and azo- compounds, such as AIBN, which decomposes thermically to provide two radical species and releases N_2. In the early stage of the process, the radical reacts with a monomer unit to generate a radical species that starts an active polymerizing chain (Pn*). The propagating radical reacts with the C=S bond of the transfer agent to generate a carbon-cantered radical. This radical species undergoes beta scission and is converted to a poly-RAFT agent while liberating a new radical that consists of the 'leaving group' (R) of the RAFT agent. As mentioned before, R is a key group, since it must be able to reinitiate polymerization when in contact with a free monomer molecule and create a new propagating chain (Pm*). The central step in the RAFT polymerization process is the establishment of equilibrium between active and dormant species. To achieve control over polymerization, it is required that the dormant species concentration is favoured compared to that of the active ones, but in rapid exchange with one another. In this way the radical-radical termination is minimized and all the chains have equal probability to grow, ensuring polymers with narrow polydispersity (M_w/M_n) and low termination rate, usually <10%. Figure 15 summarizes the steps involved in the RAFT polymerization process.

Since radicals are neither formed nor destroyed during the chain-transfer reaction, RAFT is usually carried out with an external source of free radicals (initiator). The concentration of the active species is maintained low related to the dormant species. This is obtained with the control of the ratio of the initiator and terminator, which should limit termination processes and increase polymer length. Termination rate is of second order as in conventional free radical polymerizations,

while propagation steps show a dependency of first order with respect to the radical species concentration. Thus, if the concentration of radical species is reduced, propagation over termination will be promoted.

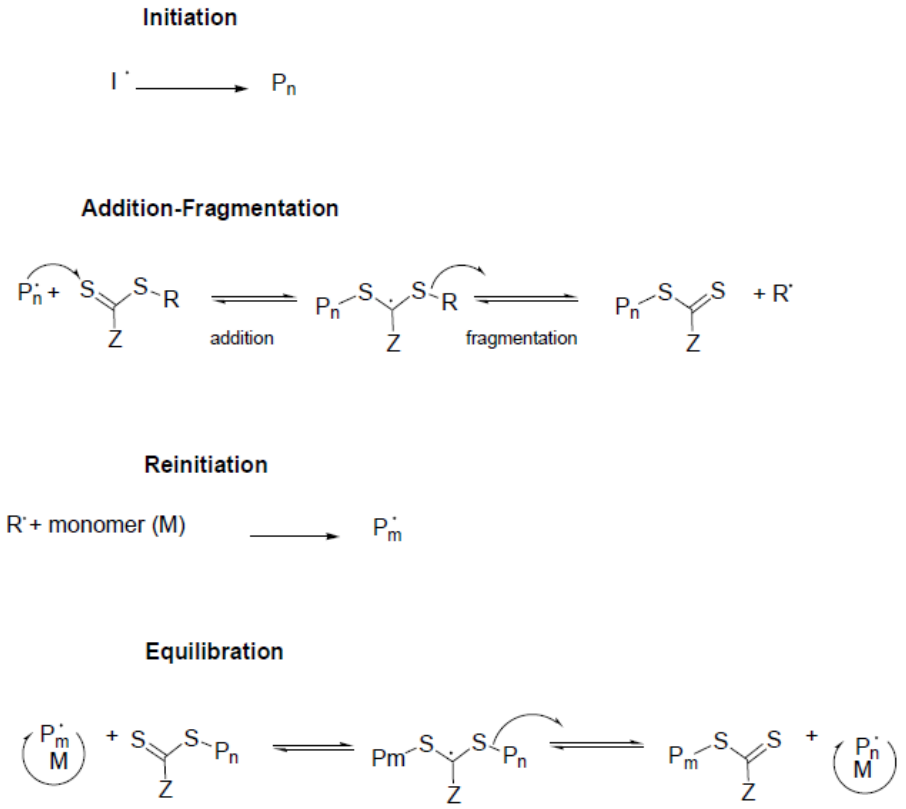

Figure 15. Schematic representation of the mechanism of the RAFT polymerization.

Transfer agent addition to the reaction mixture can affect the polymerization kinetics through an “inhibition step”, where the polymerization is slow or absent, or through a “rate retardation”, which consists of a polymerization rate slower than the one of the same reaction without the use of the RAFT agent. Inhibition can be ascribed to a pre-equilibrium phase, known as initialization, where the RAFT agent is converted to a polymeric RAFT agent. RAFT agents that mostly generate this inhibiting phenomena of polymerization are the ones that stabilize the radical adduct, e.g. Z=phenyl or other aromatic compounds. This issue can be solved using more reactive RAFT agents, e.g. trithiocarbonates. The “R” group of the RAFT agent can participate together with Z to affect the stability of the adduct during the initializing phase. A RAFT transfer agent with a weak leaving group R,

or inefficiently reactive, will not be able to control the polymerization or will induce strong inhibiting phenomena.

The advances in RAFT polymerization procedures, the knowledge of mechanism and structure-reactivity correlations have made possible the production of narrow polydisperse polymers with high conversion and commercially acceptable polymerization rates. The opportunity to carry out the reaction with a wide range of monomers, solvents and initiators makes this technique extremely fascinating for the production of polymer with complex design, like stars, blocks and hyperbranched materials, polymeric micelles and vesicles.[156]

1.7 GENERAL DESCRIPTION OF MATERIALS USED FOR THE PREPARATION OF PH SENSITIVE LIPOSOMES

1.7.1 Polyethylene Glycol (PEG)

Polyethylen glycol (PEG) is a linear synthetic polymer, which is obtained by anionic radical polymerization of ethylene oxide (Figure 16).

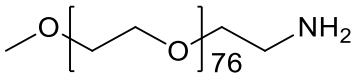

Figure 16. Chemical structure of polyethylene glycol (PEG)

PEG is commercially available in a wide range of molecular weights according to the number of monomers that constitute the polymer chain. PEG used for biomedical purposes is dimensionally homogeneous and must possess a defined chemical structure and purity as required for the development of pharmaceutical products.

The repetition of oxyethylene monomers ensures a high solubility of the polymer in both organic solvents, such as chloroform or dichloromethane, and in water. In water PEG coordinates 2-3 molecules of solvent for each oxyethylene monomer. This causes a hydrodynamic volume at least three times higher than that calculated for the not hydrated polymer. The amphiphilic nature of PEG makes

it also soluble in many polar organic solvents and, for low molecular weights, also non-polar, to the benefit of manipulation and purification processes.[160]

PEG is a neutral polymer, biocompatible, non-biodegradable, non-toxic and non-immunogenic. Only the 0.2% of the population develops anti-PEG antibodies, which however does not lead to side effects upon administration. Although it is not degradable, it can be eliminated by renal and hepatic systems without undergoing intracellular processing and chemical alterations, but the kinetics of elimination depends on its molecular weight that affects its hydrodynamic volume.[161]

This polymer is widely used in the development of drug delivery systems for controlled release of drugs.[162]

In this project PEG was used with a molecular weight of 5 kDa and terminating with a free non-reactive methoxy group. Methoxy-PEG-NH_2 was chosen for the polymerization of sulfadimethoxine methacrylate, in order to obtain a pH sensitive polymer to activate the cell penetration of the Tat-like coated liposomes in cells of the tumor that possesses an acid microenvironment.

1.7.2 Sulfadimethoxine

Sulfadimethoxine, or 4-amino-N- (2,6-dimethoxy pyrimidine-4-yl) benzensulfonamide, belongs to the pharmaceutical class of sulfonamides, which represent the first chemotherapeutic agents used systemically in the treatment of bacterial infectious diseases.

The sulfadimethoxine is a sulphonamide derivative whose basic structure is similar to that of para-aminobenzoic acid (PABA). In the clinic, sulfonamides represent a category of antimicrobial drugs that, on the basis of structural analogy with PABA, inhibits the synthesis of dihydrofolic in prokaryotes by inhibiting the activity of the enzyme dihydropteroate synthetase. The dihydrofolic acid is essential for the reactions of methylation of homocysteine to methionine (methyl cycle). The spectrum of antimicrobial activity of sulfonamides is very broad and covers both Gram positive bacterial strains of Gram-negative type.

Sulphonamide containing drugs with different physical, chemical, pharmacological and antibacterial properties are produced by chemical modification of the sulphonamide group (-SO_2-NH-R).

The sulphonamides are weakly acidic molecules with pKa values that depend on the substituent group linked to N4. There are in fact more than 15000 derivatives having a different pKa in a range from 3 to 11. Generally, the sulphonamides derivatives are soluble in a basic environment; based on the pKa value, when exposed to pH below the pKa, each derivative undergoes protonation and exist mostly in the deionized form that possesses a more hydrophobic character than the corresponding ionized anionic form (Figure 17).

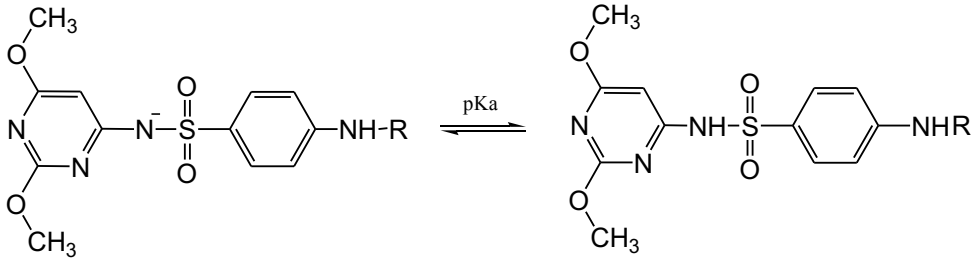

Figure 17. Sulfadimethoxine acid-base dissociation balance.

pH-sensitive polymers can be obtained by including sulphonamide containing monomers along their backbone (but also carboxylic groups, sulphate groups and sulfonate and primary and tertiary amines).

In this thesis, the sulfadimethoxine was used as the pH sensor for the polymerization of a pH responsive polymer. The sulfadimethoxine methacrylate oligomers at the tip of a PEG chains were used to superficially shield liposomes coated with the newly synthetized cell penetrating agent. To polymerize the oligomers of sulfadimethoxine, a methacrylic derivative was first synthesised and radical polymerization was then undertaken: the double bond of the methacrylic derivative quickly reacts with a radical species which in turn generate another radical allowing the propagation of the reaction and the elongation the polymeric backbone to take place (Figure 18).

Sulfadimethoxine was selected because it undergoes reversible pH-dependent protonation. According to the sulfadimethoxine pKa (6.1)[163], at pH 7.4, the sulfonamidic groups are negatively charged, while at acidic pH, they convert to

the protoned neutral form. It was shown that the higher the number of sulfadimethoxine monomers in the polymer backbone the higher is the apparent pKa of the polymer, plateauing at 7.3 with 9 SDM units. Notably, this allow to generate polymers with apparent pKa in the physiopathological range of the tumors.[164]

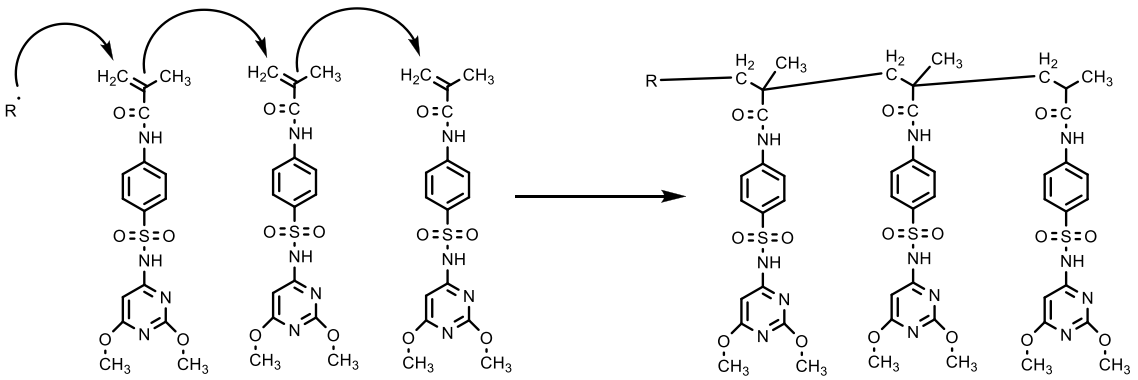

Figure 18. Scheme of radicalic polimerization reaction to obtain the pH-sensitive poly-sulfadimethoxine block of the polymer.

1.7.3 Calcein

Calcein is a fluorescent dye with excitation and emission wavelengths of 495 and 515 nm, which appears as orange crystals. Calcein chemical structure is reported in Figure 19. Calcein is commonly used as an indicator of lipid vesicle leakage and it is also traditionally employed as a complexometric indicator for titration of calcium ions with EDTA, and for fluorimetric determination of calcium.

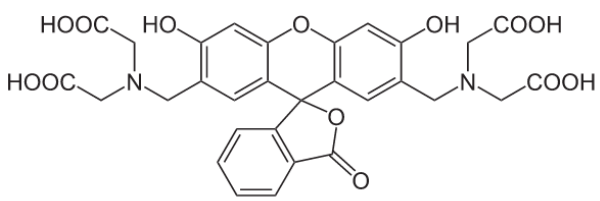

Figure 19. Chemical structure of Calcein

Calcein-release phenomena have been used as an index to characterize membrane properties of model biomembranes and to evaluate the interaction mechanisms between the closed bilayer lipid membrane of liposomes and target molecules such as proteins and peptides. In addition, the calcein-release phenomena have been used as model for the design of drug-delivery systems.[165]

In this project, calcein has been used as a proxy for hydrophilic drugs to be loaded and delivered by liposomes. Being a fluorescent molecule, it can be quantified by UV-visible spectroscopy or by spectrofluorimetry. Calcein is a very hydrophilic molecule with low permeability through lipidic bilayers, thus it can be used as model to simulate the delivery of macromolecules, such as proteins, to the cellular cytosol by using the Tat-decoared liposomes that are the platform of this thesis work.

2. MATERIALS AND METHODS

2.1 REAGENTS

- Triethylamine [TEA], potassium carbonate [K_2CO_3], 2-bromo-isobutyryl bromide [BIB], ascorbic acid [AA], copper bromide [Cu(I)Br], copper chloride [$Cu(II)Cl_2$], aqueous 5% solution of 2,4,6-trinitrobenzenesulphonic acid [TNBS], trifluoroacetic acid [TFA], iodine [I2], barium chloride [$BaCl_2$], tris-[(pyridin-2)methyl] amine [TPMA], N-hydroxy-succinimide [NHS], N,N dicyclohexylcarbodiimide [DCC], N-Ethyl-N′-(3 dimethylaminopropyl)carbodiimide hydrochloride [EDC], acetic anhydride, metacriloil chloride, sulphadimethoxin [SD], urea, bromine [Br_2], anhydrous sodium sulphate [Na_2SO_4] were bought from Sigma-Aldrich (St. Louis, MO, USA). amino-5-methoxy polyethylene glycol-kDa [mPEG-NH_2] was purchased from Laysan Bio (Arab, AL, USA).
- Boc-Arg(Pbf)-OH was purchased from Sigma-Aldrich (St. Louis, MO, USA).
- Calcein was purchased from Sigma-Aldrich (St. Louis, MO, USA).
- For the formulation of liposomes Epikuron 200 from Cargill (Minneapolis, MN, USA) has been used; Hydrogenated soy phosphatidylcholine (HSPC) was purchased from Cargill (Minneapolis, MN, USA), cholesterol was obtained from Sigma-Aldrich (St. Louis, MO, USA).
- Rhodamine-DHPE was bought from VWR International PBI s.r.l. (Milan, Italy).
- Dialysis membranes (MWCO 300 kDa) and 0.22 um PVDF filters were purchased from Sigma-Aldrich (St. Louis, MO, USA).
- All products for cell biology including Dulbecco's modified Eagle medium (DMEM), L-glutamine, trypsin, antibiotic and antimicotic solution, fetal bovine serum (FBS), phosphate saline buffer with and without Ca/Mg and plastics Greiner were obtained from Sigma-Aldrich (St. Louis, MO, USA). Chamber slides BD FalconTM for confocal microscopy were bought from SACCO S.r.l. (Cadorago, Italy).

- Vectashield® mounting medium with 4‘6-diamidine-2-phenylindole (DAPI) was provided by Vector Laboratories Inc (Burlingame, CA).
- Hela cell lines from human cervical cancer were kindly doned by Dr. Mario Zoratti (Department of Biomedical Sciences, University of Padova).
- All aqueous solutions were prepared using deionized water (milliQ-grade, 0.06 μSiemens cm^{-1}) obtained through Millipore MilliQ (MA, USA).
- Salts for buffer preparation and paraformaldehyde were provided by Riedel-de-Haen (Seelze, Germany), Fluka Analytical (Buchs SG, Switzerland) and Sigma-Aldrich (St. Louis, MO, USA). All the solvents and the remaining reagents were chosen from those specific for HPLC LC-MS or those with greater purity available in the catalogues of Sigma-Aldrich (St. Louis, MO, USA), Carlo Erba (Milan, Italy), Fluka (Milan, Italy), Merck-Novabiochem (Milan, Italy), Riedel de Haen (Milan, Italy), J.T. Baker (Milan, Italy), Cambridge Isotope Laboratories Inc. (Rome, Italy), Acros Organics (Milan, Italy), and Prolabo (Milan, Italy) and were used as received.

2.2 INSTRUMENTATION

- Spectrophotometric analysis were carried out with spectrophotometer UV-Vis λ25 Perkin Elmer (Norworlk, CT, USA).
- HPLC system Jasco, equipped with two pumps PU-2080 Plus, a detector UV-2075 Plus and Hercule 200 JMBS, and analytic column Luna (C18, 5 μm, 300 Å, 250 x 4.6 mm) from Phenomenex (Torrance, U.S.A.) was used for reverse phase chromatographic analysis (RP-HPLC).
- Samples were maintained under stirring with Rotating stirrer, MOD 708, of ASAL S.r.l..
- Lyophilization was carried out with freeze-drier Hetossic HETO Lab Equipment.
- Solvents were evaporated with Rotavapor R114 of BÜCHI Labortechnik AG (Postfach, Switzerland).

- pH measurements were carried out with pHmeter Seven Easy S20-K Mettler Toledo with electrode Mettler Toledo Inlab 413 (Schwerzenbach, Switzerland) and pHmeter Fischerbrand Hydrus600.
- Centrifuges were carried out with CENTRIKON T-42K Kontron Instruments, Z300 Hemle and with ALC microcentrifughette 4214 ALC international (Cologno Monzese, Italy).
- TLCs were run on silica gel supported on plastic (Macherey-Nagel Polygram®SIL G/UV254, silica thickness 0.2 mm), and visualized by UV detection or $KMnO_4$ oxidation. Flash chromatography was performed on silica gel (Macherey-Nagel 60, 230-400 mesh granulometry (0.063-0.040 mm)) under air pressure. Mass spectrometry analyses were performed using Agilent Technologies MSD SL Trap with an electrospray source and ionic analyser.
- NMR spectra were recorded with a Bruker AV-DPX 200 spectrometer (Fallanden, Switzerland) operating at 200 MHz for ^{1}H and 50 MHz for ^{13}C, a Bruker AV300 Ultrashield^{TM} spectrometer (Fallanden, Switzerland) operating at 300 MHz for ^{1}H and 75 MHz for ^{13}C and a Bruker AVII500 spectrometer (Fallanden, Switzerland) operating at 500 MHz for ^{1}H and 126 MHz for ^{13}C. Chemical shifts (δ) are given in ppm relative to the signal of the solvent.
- HPLC/ESI-MS analyses and mass spectra were performed with a 1100 Series Agilent Technologies system, equipped with binary pump (G1312A) and MSD SL Trap mass spectrometer (G2445D SL) with ESI source. ESI-MS positive spectra of reaction intermediates and final purified products were obtained from solutions in acetonitrile or methanol, eluting with a water:acetonitrile (or methanol) = 1:1 v/v mixture containing 0.1% formic acid. HPLC/ESI-MS analysis was used to confirm the purity (>95%) for all the synthesized compounds and intermediates.
- MALDI-TOF analysis was performed by AB Sciex 4800 Plus MALDI TOF/TOF™ Analyzer (Framingham, MA, USA).

- FT-IR spectra were recorded over the range 4000–400 cm−1 using a FT-IR Nicolet Magna 750 spectrometer (0.5 cm−1 resolution) equipped with an attenuated total reflectance (ATR) Spectra Tech Performer with diamond crystal (Thermo Fisher Scientific, Waltham, MA, USA). The data were analysed with Thermo software.
- Liposomes size analysis were performed by Dynamic Light Scattering Zetasizer NanoZS (Malvern Instruments Ltd, UK).
- Biological studies were carried out in biological safety cabinet Space, cells were grown using the incubator from PBI International and imaged with optical microscope Axiovert 40CFL Zeiss.
- Buffers were filtered with Millipore systems (Bendford, MA, USA) using 0.22 μm cellulose acetate filter.
- Fluorimetry analyses were performed using a LS 50 B Perkin-Elmer fluorimeter (Norworlk, CT, USA).
- Cytometric analyses were performed using a BD FACSDiva flow cytometer (Becton, Dickinson and Company, Buccinasco, Milan) and results were processed with BD FACSDiva Software.
- Images of confocal microscopy were obtained using confocal microscope Zeiss LSM800 (Oberkochen, Germany) equipped with a Plan- apochromat goal 63x 1.4 DIC oil immersion objective. Lasers with emitting wavelength of 405, 488, 561 and 640 nm were used to detect blue, green, orange and red emission, respectively. Images were collected at 1024x1024 pixels and results were processed with Software Zen 2, Blue edition.

2.3 METHODS

2.3.1 Cell Penetrating Enhancer structural prediction

The structure of generation 1 and 2 (G1 and G2) bis-MPA Dendrons bearing 4 and 8 arginines and functionalized with distearoyl glycerol, namely Arg_4-DAG and Arg_8-DAG respectively (Figure 20), were drawn on ChemDraw and saved as mol file. The latter were subjected to energy minimization using Force MMFF94x by Molecular Operating Environment (MOE) software (Chemical Computing Group Inc.). For data elaboration, arginine monomers were assumed as dots centred on guanidinium carbon, in order to calculate the average mutual distance of arginines.

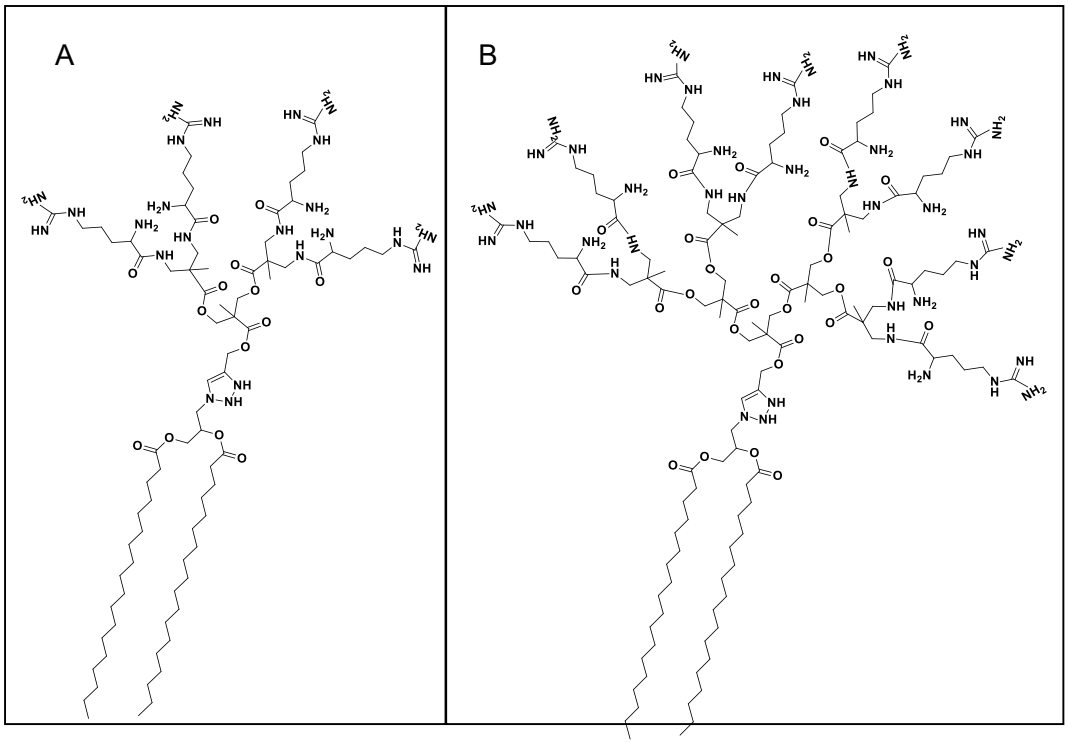

Figure 20. Structures of Arg_4-DAG (A) and Arg_8-DAG (B)

2.3.2 Synthesis of the Cell Penetrating Enhancer module (14)

2.3.2.1 Synthesis of 2,2-(bis((tert-butoxycarbonyl)amino)methyl)-propanoic acid (4)

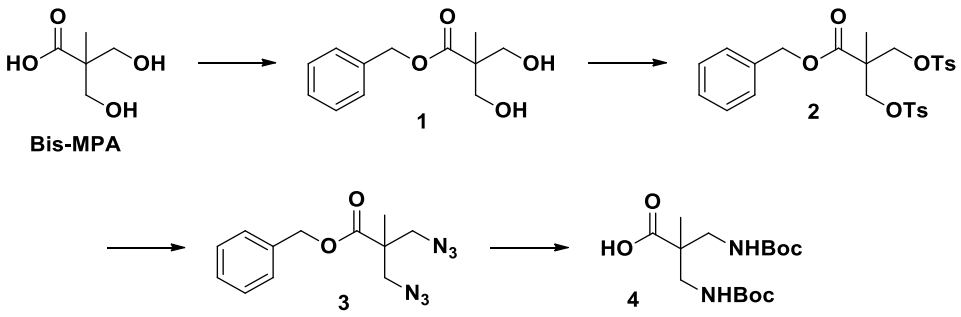

Benzyl 3-hydroxy-2-(hydroxymethyl)-2-methylpropanoate (**1**): 2,2-bis(hydroxyl-methyl)propionic acid (Bis-MPA, 10.0 g, 74.5 mmol, 1.0 eq) and KOH (4.39 g, 78.3 mmol, 1.05 eq) were dissolved in 50 mL of DMF under stirring at 100 °C. After 1 h, benzyl bromide (15.3 g, 89.5 mmol, 1.2 eq) was added dropwise and the reaction mixture was stirred at r.t. for 15 h. DMF was evaporated under reduced pressure and the residue was dissolved in 250 mL of DCM. The organic phase was washed with deionized water (3 × 50 mL) and dried over $MgSO_4$. After filtration, the solvent was removed under reduced pressure and the residue was purified by flash chromatography using 85:15 DCM/acetone (R_f = 0.27) as eluent to afford **1** (13.1 g, 80% yield) as a white powder.^{1}H-NMR (300 MHz, $CDCl_3$) δ (ppm) = 7.41 – 7.31 (m, 5H), 5.21 (s, 2H), 3.93 (d, *J* = 11.3 Hz, 2H), 3.73 (d, *J* = 11.3 Hz, 2H), 1.09 (s, 3H). ^{13}C NMR (75 MHz, $CDCl_3$) δ (ppm) =175.82, 135.81, 128.74, 128.41, 127.96, 68.13, 66.77, 49.41, 17.23. ESI-MS (ion trap) = 225 m/z $[M+H]^+$.

Benzyl 2-methyl-3-(tosyloxy)-2-((tosyloxy)methyl)propanoate (**2**): a solution of **1** (6.6 g, 29.3 mmol, 1.0 eq), pyridine (7.1 mL, 87.8 mmol, 3.0 eq) and DMAP (9.0 g, 73.1 mmol, 2.5 eq) in dry DCM (60 mL) was stirred at 0 °C for 15 minutes. Then, a solution of p-toluenesulfonyl chloride (TsCl, 14.0 g, 73.1 mmol, 2.5 eq) in DCM (60 mL) was added dropwise and the resulting mixture was stirred at 60 °C for 4 h. The organic phase was washed with 0.5 M HCl (2 × 150 mL) and dried over $MgSO_4$. After filtration, the solvent was removed under reduced pressure and the residue was purified by flash chromatography using 80:20 v/v petroleum ether/ethyl acetate (R_f = 0.20) as eluent to afford **2** (12.4 g, 80% yield) as a white powder. ^{1}H-

NMR (500 MHz, $CDCl_3$) δ (ppm) = 7.71 (m, 4H), 7.37 – 7.30 (m, 5H), 7.25 – 7.22 (m, 4H), 5.04 (s, 2H), 4.14 (d, *J* = 9.6 Hz, 2H), 4.06 (d, *J* = 9.6 Hz, 2H), 2.44 (s, 6H), 1.17 (s, 3H). ^{13}C-NMR (126 MHz, $CDCl_3$) δ (ppm) = 171.05, 145.32, 135.10, 132.28, 130.13, 128.78, 128.62, 128.16, 128.13, 69.54, 67.46, 46.77, 21.84, 17.63. ESI-MS (ion trap) = 533 m/z $[M+H]^+$.

Benzyl 3-azido-2-(azidomethyl)-2-methylpropanoate (**3**): sodium azide (3.3 g, 58.3 mmol, 6.0 eq) was added to a solution of **2** (5.1 g, 9.7 mmol, 1.0 eq) in dry DMF (45 mL). The resulting suspension was stirred at 90 °C for 16 h. DMF was evaporated under reduced pressure and the residue was purified by flash chromatography using 60:40 v/v DCM/petroleum ether (R_f = 0.30) as eluent to afford **3** (2.3 g, 85% yield) as a light yellow viscous oil. ^{1}H-NMR (500 MHz, $CDCl_3$) δ (ppm) = 7.44 – 7.30 (m, 5H), 5.19 (s, 2H), 3.63 (d, *J* = 12.2 Hz, 2H), 3.52 (d, *J* = 12.2 Hz, 2H), 1.24 (s, 3H). ^{13}C-NMR (126 MHz, $CDCl_3$) δ (ppm) = 173.06, 135.40, 128.78, 128.61, 128.31, 67.30, 54.92, 47.82, 19.42. ESI-MS (ion trap) = 275 m/z $[M+H]^+$.

3-((tert-butoxycarbonyl)amino)-2-methyl-2-(pivalamidomethyl)propanoic acid **(4)**: PtO_2 (150 mg) was added to a stirred solution of **3** (1.5 g, 5.5 mmol, 1.0 eq) and $(Boc)_2O$ (2.5 g, 11.5 mmol, 2.1 eq) in MeOH (25 mL). After three nitrogen/vacuum purge cycles, the flask atmosphere was saturated with hydrogen and the solution kept under stirring for 4 h. After reestablishment of a hydrogen atmosphere 10% Pd/C (180 mg) was added. After three nitrogen/vacuum purge cycles, the flask atmosphere was saturated with hydrogen and the mixture was stirred for other 3 h. The resulting suspension was filtered over celite and the solvent was removed under reduced pressure. The residue was purified by flash chromatography using 93:7 v/v DCM/acetone + 1% of acetic acid as eluent to afford **4** (1.63 g, 90% yield) as a white solid. ^{1}H NMR (300 MHz, $CDCl_3$) δ (ppm) = 5.13 (s, 2H), 3.47 (d, *J* = 14.3 Hz, 2H), 3.12 (d, *J* = 14.3 Hz, 2H), 1.43 (s, 18H), 1.13 (s, 3H). ^{13}C NMR (75 MHz, $CDCl_3$) δ (ppm) = 175.32, 156.80, 79.55, 66.79, 49.05, 43.57, 28.50, 19.13. ESI-MS (ion trap) = 333 m/z $[M+H]^+$.

2.3.2.2 Synthesis of propargyl 2,2-bis(hydroxymethyl)propanoate (8)

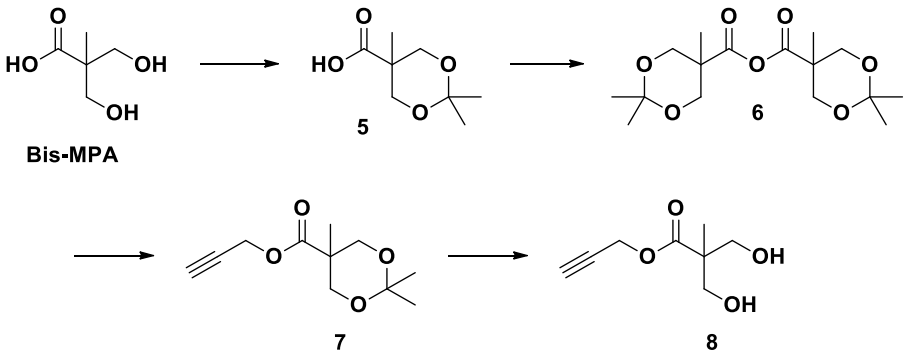

2,2,5-trimethyl-1,3-dioxane-5-carboxylic acid (**5**): a solution of Bis-MPA (10.0 g, 74.5 mmol, 1.0 eq), 2,2-dimethoxypropane (13.8 mL, 111.8 mmol, 1.6 eq) and p-toluenesulfonic acid monohydrate (0.71 g, 3.7 mmol, 0.05 eq) in dry acetone (50 mL) was stirred for 2 h at room temperature. The catalyst was neutralized by the addition of 2 M ammonia solution in EtOH (2 mL) and the resulting mixture was dried under reduced pressure. The residue was dissolved in DCM (250 mL) and extracted with water (2 × 20 mL). The organic phase was dried over $MgSO_4$. After filtration, the solvent was removed under reduced pressure and the residue was purified by flash chromatography using 85:15 v/v DCM/acetone (R_f = 0.27) as eluent to afford **5** (10.2 g, 78% yield) as a white powder. ^{1}H-NMR (500 MHz, $CDCl_3$) δ (ppm) = 4.18 (d, *J* = 12.0 Hz, 2H), 3.68 (d, *J* = 12.0 Hz, 2H), 1.45 (s, 3H), 1.42 (s, 3H), 1.21 (s, 3H). ^{13}C-NMR (126 MHz, $CDCl_3$) δ (ppm) = 179.76, 98.53, 66.08, 41.83, 25.60, 21.86, 18.49. ESI-MS (ion trap) = 175 m/z $[M+H]^+$.

2,2,5-trimethyl-1,3-dioxane-5-carboxylic anhydride (**6**): a suspension of DCC (3.0 g, 14.4 mmol, 1.0 eq) in dry DCM (5 mL) was added dropwise to a stirred suspension of **5** (5.1 g, 28.8 mmol, 2.0 eq) in dry DCM (15 mL) under nitrogen atmosphere. The reaction mixture was stirred for 4 hours at room temperature. The suspended solid DCU side product was filtered off by using a glass filter. The residue was dried under reduced pressure to afford **6** (4.7g, 100% yield) as a viscous oil. The obtained anhydride was used without further purification. ^{1}H NMR (300 MHz, $CDCl_3$) δ (ppm) = 4.22 (d, *J* = 11.9 Hz, 4H), 3.70 (d, *J* = 11.9 Hz, 4H), 1.45 (s, 6H), 1.41 (s, 6H), 1.25 (s, 6H). ^{13}C NMR (75 MHz, $CDCl_3$) δ (ppm) = 169.64, 98.55, 65.82, 43.81, 25.53, 21.90, 17.86. ESI-MS (ion trap) = 331 m/z $[M+H]^+$.

Prop-2-yn-1-yl 2,2,5-trimethyl-1,3-dioxane-5-carboxylate (**7**): a solution of propargyl alcohol (0.6 g, 10.6 mmol, 0.75 eq) and DMAP (0.2 g, 1.65 mmol, 0.1 eq) dissolved in dry pyridine (15 mL) was added dropwise to a solution of **6** (4.7 g, 14.2 mmol, 1.0 eq) in dry DCM (50 mL). The solution was stirred for 15 h at room temperature. The solvent was evaporated under reduced pressure and the residue was dissolved in 150 mL of DCM. The resulting mixture was then washed with 0.5 M HCl (100 mL) and deionized water (2 × 100 mL). The organic phase was dried over $MgSO_4$. After filtration, the solvent was removed under reduced pressure and the residue was purified by flash chromatography using 85:15 v/v petroleum ether/ethyl acetate as eluent to afford **7** (2.15 g, 71% yield) as a colourless oil. ^{1}H NMR (300 MHz, $CDCl_3$) δ (ppm) = 4.69 (d, *J* = 2.5 Hz, 2H), 4.15 (d, *J* = 11.9 Hz, 2H), 3.60 (d, *J* = 11.9 Hz, 2H), 2.45 (t, *J* = 2.5 Hz, 1H), 1.38 (s, 3H), 1.34 (s, 3H), 1.17 (s, 3H). ^{13}C NMR (75 MHz, $CDCl_3$) δ (ppm) = 173.43, 98.15, 75.08, 65.88, 52.36, 41.92, 24.53, 22.76, 18.48. ESI-MS (ion trap) = 213 m/z $[M+H]^+$.

Prop-2-yn-1-yl 3-hydroxy-2-(hydroxymethyl)-2-methylpropanoate (**8**): a solution of **7** (1.0 g, 4.8 mmol) in MeOH (20 mL) was stirred in presence of DOWEX 50W-X8 resin (H^+ form, 1.5 g) for 6 h. The resin was filtered off and the filtrate was dried under reduced pressure to afford **8** (0.76 g, 92% yield) as a colorless oil. ^{1}H NMR (300 MHz, $CDCl_3$) δ (ppm) = 4.76 (d, *J* = 2.5 Hz, 2H), 3.92 (dd, *J* = 11.3, 6.2 Hz, 2H), 3.73 (dd, *J* = 11.3, 6.2 Hz, 2H), 2.49 (t, *J* = 2.5 Hz, 1H), 1.10 (s, 3H). ^{13}C-NMR (75 MHz, $CDCl_3$): δ (ppm) = 175.20, 75.38, 68.24, 68.22, 52.62, 49.47, 17.12. ESI-MS (ion trap) = 173 m/z $[M+H]^+$.

2.3.2.3 Synthesis of alkynic tetra-Boc-Arginyl(Pbf) scaffold (10)

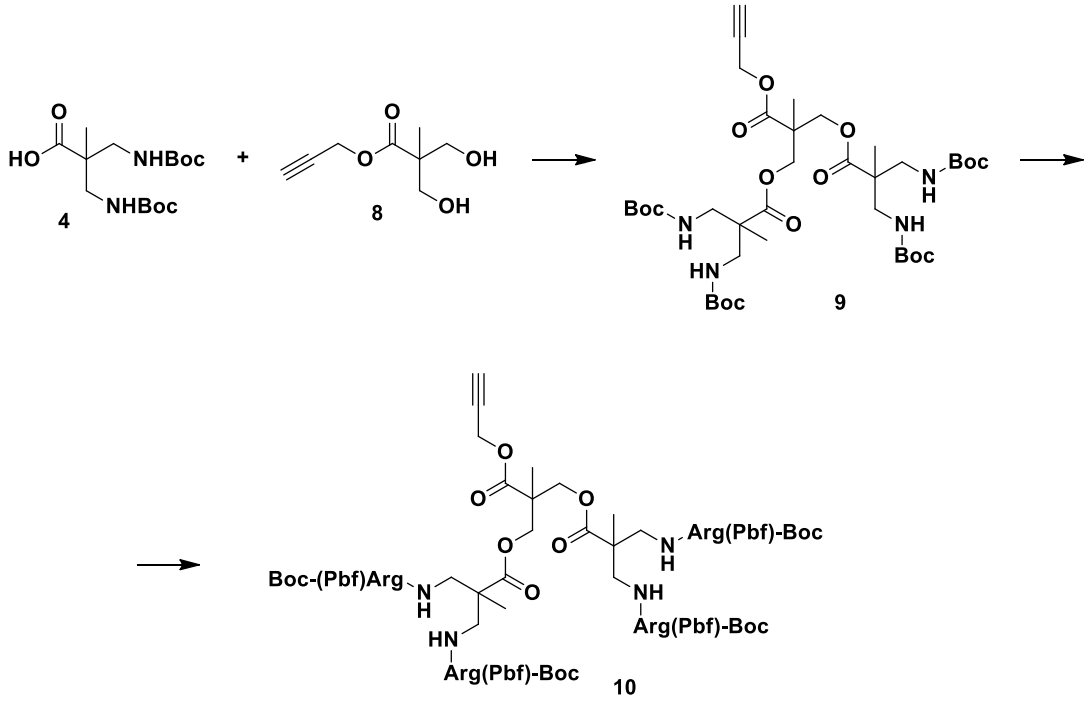

2-methyl-2-((prop-2-yn-1-yloxy)carbonyl)propane-1,3-diyl bis(3-((tert-butoxycarbonyl)amino)-2-(((tert-butoxycarbonyl)amino)methyl)-2-methylpropanoate) (**9**): a suspension of DCC (1.2 g, 5.81 mmol, 0.55 eq) in DCM (20 mL) was added to a stirred solution of **4** (3.5 g, 10.56 mmol, 1.0 eq) in dry DCM (10 mL) and stirred at room temperature for 16 h. The suspended solid DCU side product was filtered off by using a glass filter and the solvent was removed under reduced pressure. The obtained anhydride was used without further purification.

The anhydride (3.4 g, 5.3 mmol, 3.0 eq) dissolved in DCM (5 mL) was added to a stirred solution of **8** (303 mg, 1.76 mmol, 1.0 eq), dry pyridine (1.8 mL, 17.6 mmol, 10.0 eq) and DMAP (215 mg, 1.76 mmol, 1.0 eq) in dry DCM (20 mL). The reaction was stirred at room temperature for 16 h. The solution was diluted with 50 mL of DCM and washed with 0.5 M HCl (2 × 100 mL); the organic phase was dried with $MgSO_4$ and filtered. The solvent was removed under reduced pressure and the residue was purified by flash chromatography using a gradient 80:20 to 70:30 v/v of petroleum ether/ethyl acetate to afford **9** (1.00 g, 71% overall yield) as a white solid. ^{1}H NMR (200 MHz, $CDCl_3$) δ (ppm) = 5.52 (s, 3H), 4.78 – 4.70 (m, 2H), 4.40 – 4.11 (m, 4H), 3.55 – 3.33 (m, 4H), 3.22 – 2.96 (m, 4H), 2.56 (s, 1H), 1.44 (s, 36H), 1.31 (s, 3H), 1.10 (s, 6H). ^{13}C NMR (50 MHz, $CDCl_3$) δ (ppm) = 174.85,

172.08, 156.86, 79.58, 75.94, 65.01, 52.99, 49.26, 46.77, 43.50, 28.49, 19.16. ESI-MS (ion trap) = 801 m/z $[M+H]^+$.

2-methyl-2-((prop-2-yn-1-yloxy)carbonyl)propane-1,3-diyl bis(3-(2-((tert-butoxycarbonyl)amino)-5-(3-((2,2,4,6,7-pentamethyl-2,3-dihydrobenzofuran-5-yl)sulfonyl)guanidino)pentanamido)-2-((2-((tert-butoxycarbonyl)amino)-5-(3-((2,2,4,6,7-pentamethyl-2,3-dihydrobenzofuran-5-yl)sulfonyl)guanidino)pentanamido)methyl)-2-methylpropanoate) (**10**): a solution of **9** (240 mg, 0.3 mmol) in a 50:50 v/v DCM/TFA (4 mL) was stirred for 2.5 h at room temperature. Then, the solvent was removed under high reduced pressure for 30 min and the obtained amine was used without further purifications.

DIPEA (0.93 g, 7.2 mmol, 24.0 eq) was added dropwise to a solution of Boc-Arg(Pbf)-OH (1.26 g, 2.4 mmol, 8.0 eq), HOBt (324 mg, 2.4 mmol, 8.0 eq) and EDC (0.46 g, 2.4 mmol, 8.0 eq) in dry DMF (4 mL) at 0 °C and the resulting mixture was stirred for 20 min. Then, the amine obtained above was dissolved in DMF (3 mL) and added dropwise at 0 °C. After this time, the ice bath was removed and the solution was stirred at room temperature for 16 h. The resulting mixture was diluted with 70 mL of ethyl acetate and washed first with a 50:50 v/v 0.5 M HCl/brine mixture then with brine (2 × 70 mL). The organic phase was dried with $MgSO_4$ and filtered. The solvent was removed under reduced pressure and the residue was purified by flash chromatography using 80:20 v/v EtOAc/DCM until the elution of all the by-products and then 50:50 v/v petroleum ether/acetone to afford **10** (768 mg, 0.25 mmol, 83% yield) as a white solid. ^{1}H NMR (500 MHz, $CDCl_3$) δ (ppm) = 7.61 (m, 4H), 6.32 (m, 10H), 5.72 (s, 3H), 4.73 (s, 2H), 4.48 – 3.98 (m, 8H), 3.75 – 3.02 (m, 16H), 2.93 (s, 8H), 2.54 (s, 12H), 2.47 (s, 12H), 2.07 (s, 12H), 1.69 (m, 17H), 1.44 (s, 32H), 1.36 (s, 32H), 1.30 (s, 3H), 1.13 (s, 6H). ^{13}C NMR (126 MHz, $CDCl_3$) δ (ppm) = 173.92, 172.37, 158.83, 156.57, 155.96, 138.35, 132.78, 132.27, 124.70, 117.59, 86.48, 86.47, 79.87, 52.97, 46.54, 43.29, 28.66, 28.39, 28.36, 25.60, 19.42, 19.41, 18.07, 12.54. ESI-MS (ion trap) = 811 m/z $[M+3H]^{3+}$.

2.3.2.4 Synthesis of 3-azidopropane-1,2-diyl distearate (12)

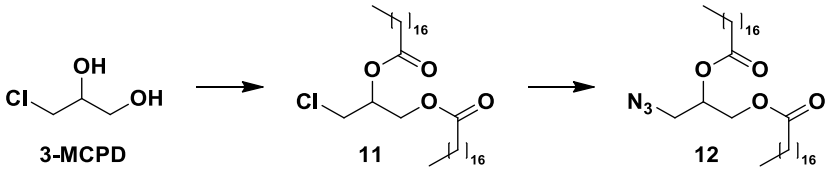

3-chloropropane-1,2-diyl distearate (**11**): a solution of stearoyl chloride (3.6 g, 11.8 mmol, 2.5 eq) in dry DCM (15 mL) was added dropwise to a solution of 1-chloro-2,3-propanediol (0.52 g, 4.7 mmol, 1.0 eq) and pyridine (0.76 mL, 9.4 mmol, 2.0 eq) in dry DCM (5 mL) and the resulting mixture was stirred at room temperature for 16 h. The reaction mixture was then extracted with 0.5 M HCl (100 mL) and the organic phase was dried with $MgSO_4$ and filtered. The solvent was removed under reduced pressure and the residue was purified by flash chromatography using 90:10 v/v petroleum ether/diethyl ether (R_f = 0.4) to afford **11** (2.9 g, 97% yield) as a white waxy solid. ^{1}H NMR (300 MHz, $CDCl_3$) δ (ppm) = 5.28 – 5.17 (m, 1H), 4.45 – 4.16 (m, 2H), 3.75 – 3.58 (m, 2H), 2.32 (q, *J* = 7.3 Hz, 4H), 1.70 – 1.54 (m, 4H), 1.25 (s, 60H), 0.87 (t, *J* = 6.6 Hz, 6H). ^{13}C NMR (126 MHz, $CDCl_3$) δ (ppm) = 173.32, 172.92, 70.38, 62.37, 42.41, 34.32, 34.20, 32.07, 31.03, 29.90, 29.85, 29.83, 29.80, 29.76, 29.62, 29.51, 29.41, 29.25, 29.21, 25.03, 22.83, 14.24. ESI-MS (ion trap) = 644 m/z $[M+H]^+$.

3-azidopropane-1,2-diyl distearate (**12**): a suspension of **11** (0.5 g, 0.8 mmol, 1.0 eq) and NaN_3 (0.5 g, 7.7 mmol, 10.0 eq) in dry DMF (20 mL) was stirred at 100 °C for 15 h. The solvent was evaporated under reduced pressure and the residue was diluted with EtOAc (100 mL) and extracted with a mixture of 1:1 v/v deionized water/brine (5 × 100 mL). The organic phase was dried with $MgSO_4$ and filtered. The solvent was removed under reduced pressure and the residue was purified by flash chromatography using 90:10 v/v petroleum spirit/diethyl ether (R_f = 0.35) to afford **12** (0.46 g, 92% yield) as a white waxy solid. ^{1}H-NMR (500 MHz, $CDCl_3$): δ (ppm) = 5.26 – 5.10 (m, 1H), 4.34 – 4.06 (m, 2H), 3.48 – 3.41 (m, 2H), 2.40 – 2.25 (m, 4H), 1.69 – 1.55 (m, 4H), 1.25 (s, 60H), 0.88 (t, *J* = 6.6 Hz, 6H). ^{13}C NMR (126 MHz, $CDCl_3$) δ (ppm) = 173.33, 172.97, 70.02, 62.44, 51.05, 34.33, 34.19, 32.07, 29.84, 29.80, 29.76, 29.62, 29.50, 29.41, 29.26, 29.22, 25.01, 24.96, 22.83, 14.24. ESI-MS (ion trap) = 651 m/z $[M+H]^+$.

2.3.2.5 Synthesis of the first generation dendronic cell penetration enhancer (Arg_4-DAG) (14)

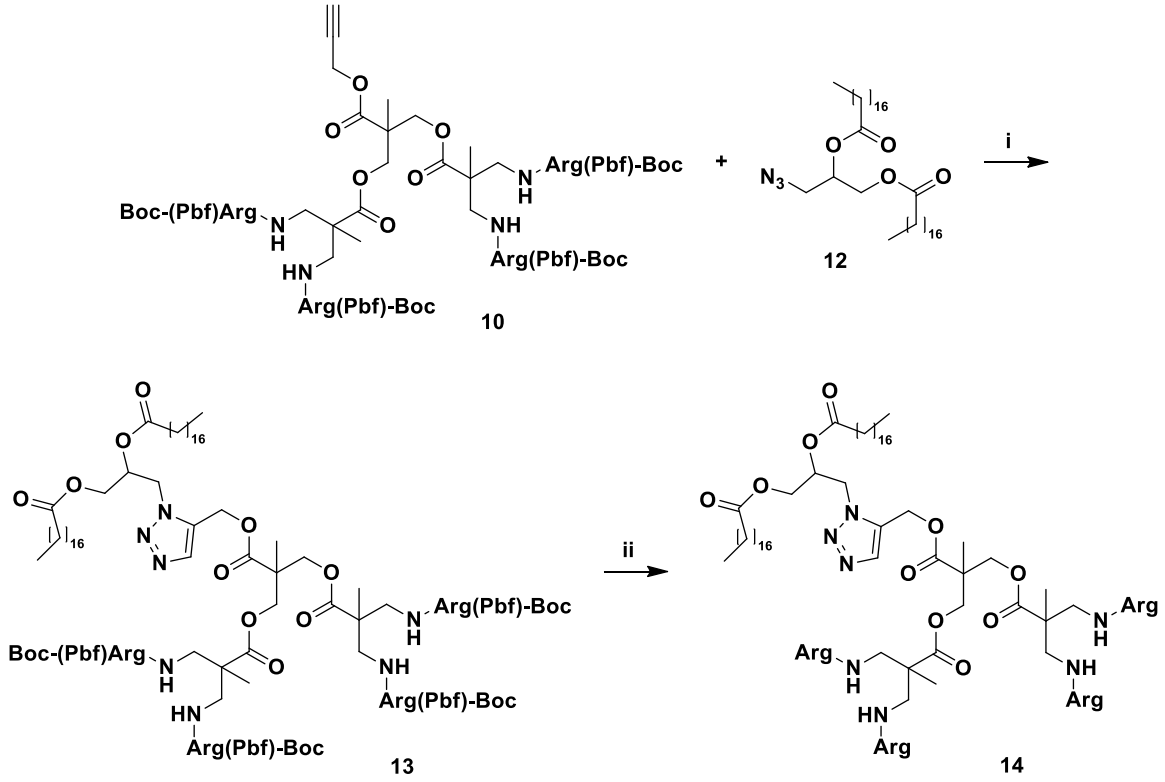

2-(((1-(2,3-distearoylpropyl)-1H-1,2,3-triazol-4-yl)methoxy)carbonyl)-2-methylpropane-1,3-diyl bis(3-(2-((tert-butoxycarbonyl)amino)-5-(3-((2,2,4,6,7-pentamethyl-2,3-dihydrobenzofuran-5-yl)sulfonyl)guanidino) pentanamido)-2-((2-((tert-butoxycarbonyl)amino)-5-(3-((2,2,4,6,7-pentamethyl-2,3-dihydrobenzofuran-5-yl) sulfonyl)guanidino)pentanamido)methyl)-2-methylpropanoate) (**13**): AcOH (20 mol-%), DIPEA (20 mol-%), CuI (10 mol-%) and sodium L-ascorbate (10 mol-%) were added to a stirred solution of **10** (550 mg, 0.28 mmol, 1.05 eq) and **12** (162 mg, 0.25 mmol, 1.0 eq.) in anhydrous DCM (5 mL). After 24 hours of reaction the solution was purified by flash chromatography using 55:45 v/v petroleum ether/acetone as eluent to afford **13** (627 mg, 0.20 mmol, 82% yield). ^{1}H NMR (500 MHz, $CDCl_3$) δ (ppm) = 8.10 – 7.84 (m, 1H), 7.79 – 7.45 (m, 3H), 6.67 – 6.10 (m, 10H), 5.76 (s, 2H), 5.45 – 5.19 (m, 2H), 4.64 (s, 2H), 4.41 – 3.95 (m, 9H), 3.68 – 3.05 (m, 12H), 2.97 – 2.91 (m, 10H), 2.87 (s, 2H), 2.55 (s, 12H), 2.48 (s, 12H), 2.30 (t, *J* = 7.5 Hz, 2H), 2.25 (t, *J* = 7.1 Hz, 2H), 2.07 (s, 12H), 1.88 – 1.49 (m, 21H), 1.44 (s, 25H), 1.36 (s, 35H), 1.24 (s, 64H), 1.14 – 1.00 (m, 5H), 0.86 (t, *J* = 6.9 Hz,

6H). ^{13}C NMR (126 MHz, $CDCl_3$) δ (ppm) = 174.19, 173.59, 173.04, 162.92, 159.13, 156.86, 156.28, 138.66, 133.13, 132.58, 124.99, 117.88, 86.75, 80.13, 69.71, 62.60, 46.80, 43.59, 36.87, 34.34, 32.28, 31.81, 31.29, 30.06, 30.01, 29.87, 29.72, 29.67, 29.50, 29.40, 28.96, 28.66, 25.88, 25.19, 25.10, 23.04, 19.70, 18.36, 18.04, 14.48, 12.83. ESI-MS (ion trap) = 1543 m/z $[M+2H]^{2+}$.

3-(4-(12,17-diamino-4-(((3-(2-amino-5-guanidinopentanamido)-2-((2-amino-5-guanidinopentanamido) methyl)-2-methylpropanoyl)oxy)methyl)-8-((2-amino-5-guanidinopentanamido)methyl)-17-imino-4,8-dimethyl-3,7,11-trioxo-2,6-dioxa-10,16-diazaheptadecyl)-1H-1,2,3-triazol-1-yl)propane-1,2-diyl distearate (Arg_4-DAG) (**14**): **13** (350 mg, 0.11 mmol) in a mixture of dry DCM (2.5 mL) and TFA (1 mL) was stirred for 1 hour at 0 °C and then for other 23 h at room temperature. The solvent was removed under reduced pressure. The residue was dissolved in a mixture (1:1) of water (with 0.05% of TFA) and ACN and filtered through anionic exchange resin (Amberlite IRA-900 Cl form) eluting with a 1:1 v/v water (with 0.05% of TFA)/ACN mixture. The resulting solution was freeze dried to afford the final product as a white powder **14** (180 mg, 0.107 mmol, 95% yield). ^{1}H NMR (500 MHz, MeOD) δ (ppm) = 8.48 – 8.36 (m, 1H), 8.26 – 8.18 (m, 1H), 5.55 – 5.49 (m, 1H), 5.32 (s, 2H), 4.84 – 4.68 (m, 2H), 4.55 – 4.44 (m, 1H), 4.39 – 4.22 (m, 4H), 4.19 – 4.03 (m, 5H), 3.66 – 3.35 (m, 8H), 2.36 (t, *J* = 7.4 Hz, 2H), 2.32 – 2.25 (m, 2H), 2.08 – 1.89 (m, 8H), 1.82 – 1.70 (m, 8H), 1.66 – 1.50 (m, 4H), 1.29 (s, 66H), 1.17 (s, 6H), 0.90 (t, *J* = 6.9 Hz, 6H). ^{13}C NMR (126 MHz, MeOD) δ (ppm) = 175.05, 174.85, 174.32, 174.30, 170.83, 170.66, 158.66, 71.05, 67.42, 63.63, 58.90, 54.19, 51.48, 44.71, 41.84, 34.96, 34.88, 33.09, 30.82, 30.70, 30.49, 30.29, 30.25, 30.16, 29.84, 26.05, 25.95, 25.62, 25.56, 23.74, 19.49, 18.13, 14.46. ESI-MS (ion trap) = 418 m/z $[M+4H]^{4+}$.

2.3.3 Synthesis of pH-sensitive copolymer m-PEG-(polymethacyiloil)sulfadimethoxine) ($mPEG_{5kDa}$-SDM_8) (17)

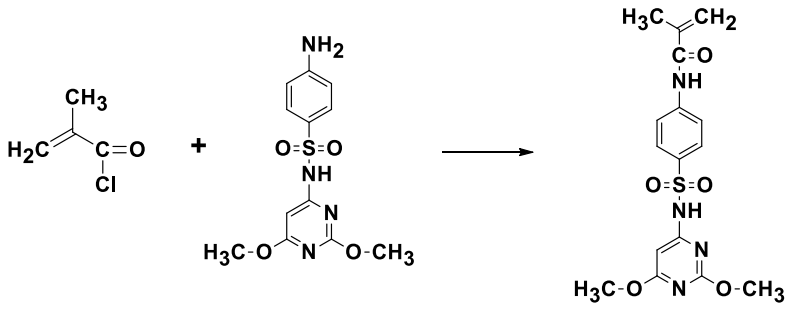

Methacryloyl sulfadimethoxine (SDM) (**15**): Sulfadimethoxine (1.5 g, 5 mmol) was dissolved in 10 mL of 1:1 v/v 0.25 M NaOH/acetone mixture. The aqueous/organic mixture was cooled in an ice bath at 0 °C, and methacryloyl chloride (0.253 g, 5 mmol) was dropwise added under vigorous stirring. The white precipitate formed was recovered by filtration, washed three times with deionised water and dried under vacuum, to give **15** as white powder (yield 92%). ^{1}H NMR (300 MHz, DMSO-d6) δ (ppm) = 11.51 (s, 1H), 10.17 (s, 1H), 7.89 (broad s, 4H), 5.92 (s, 1H), 5.84 (broad s, 1H), 5.58 (bs, 1H), 3.79 (s, 3H), 3.76 (s, 3H), 1.94 (s, 3H), δ). ESI-MS: 379.10 m/z $(M+H)^{1+}$ [calc. for SDM $(M+H)^{1+}$: 379.107].

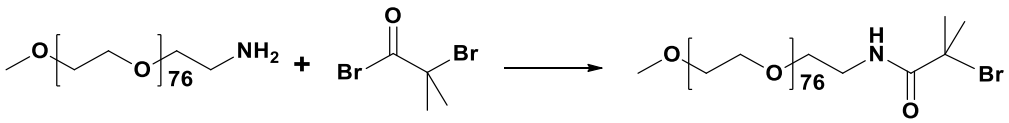

*m-PEG-NH-CO-C-$(CH_3)_2$-Br (*mPEG-Br) (**16**): $mPEG_{5kDa}$-NH_2 (300 mg, 60 μmol) was dissolved in 50 mL of toluene and azeotropically treated for 30 min to remove traces of moisture. The residual toluene was removed under vacuum, and the solid residue was redissolved with 4 mL of anhydrous dichloromethane. Triethylamine (8 μL, 60 μmol) and α-bromoisobutyryl bromide (37 μL, 0.3 mmol) were sequentially dropwise added to the polymer solution. The reaction mixture was kept at room temperature under stirring overnight and then isolated by precipitation in cold diethyl ether and washed three times with the same solvent to

give **16** as white solid (90% yield). ^{1}H NMR (300 MHz, $CDCl_3$) δ (ppm) = 3.64 (s, 448H), 3.38 (s, 3H), 1.96 (s, 6H), 1.24 (s, 28H).

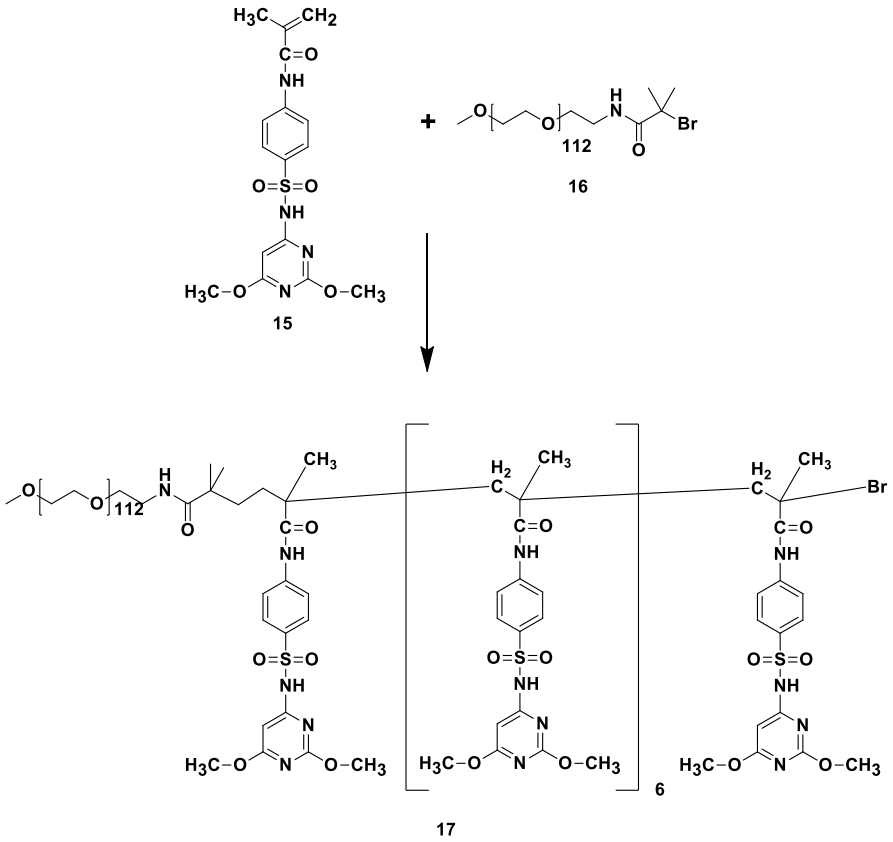

mPEG-(polymethacyiloil)sulfadimethoxine) (mPEG$_{5kDa}$-SDM$_8$) (**17**): m-PEG-NH-CO-C-$(CH_3)_2$-Br (200 mg, 36 μmol) and SDM (175.6 mg, 432 μmol) were dissolved in 1 mL of 150 mM NaOH. A volume of 200 μL of a tris(pyrydilmethyl)amine (TMPA)/$CuCl_2$ (1:1 molar ratio) in 150 mM NaOH was dropwise added to m-PEG-NH-CO-C-$(CH3)_2$-Br and SDM. The reaction was carried out under nitrogen atmosphere, and 100 μL of a 14 mM ascorbic acid solution in 150 mM NaOH was dropwise added to the reaction mixture, which was then maintained at 35 °C overnight. The reaction mixture was diluted with 20 mL of 4:1 v/v water/acetic acid and extracted 4 times with 15 mL of CH_2Cl_2. The organic phase was dried over anhydrous $MgSO_4$ and the solvent was removed under reduced pressure. The residue was poured into 200 mL of cold diethyl ether under vigorous stirring and the powder was exsiccated under vacuum. The product [mPEG$_{5kDa}$-SDM$_8$] was characterized by RP-HPLC, ^{1}H NMR, iodine test and UV-Vis spectroscopy at 265 nm to determine PEG/SDM molar ratio. ^{1}H NMR (300

MHz, DMSO-d6) δ (ppm) = 7.80 (broad s, 32H), 5.91 (s, 8H), 3.74 (broad s, 48H), 3.50 (s, 448H), 3.23 (s, 3H).

2.3.4 pH-sensitive polymer characterization

2.3.4.1 Snyder's test

In order to test the conversion of primary ammino group of mPEG-NH_2 to mPEG-Br, a Snyder's test was carried out. The mPEG-NH_2 and mPEG-Br solutions to be tested were prepared in 5 mL of borate buffer. Three dilutions of mPEG-NH_2 and mPEG-Br were prepared, 30 μL of 5% w/v TNBS (in milliQ water) were added to each dilutions that were then tested after 30 minutes incubation by spectroscopic analysis at 420 nm. The three samples were analysed in triplicate and borate buffer was used as blank.

The absorption of the chromophore generated when TNBS react with primary ammines is directly proportional to the concentration of the primary amino groups in solution. The test allows to determine the degree of modification of the compounds whose amino groups have been conjugated. The degree of conversion of the amino group of mPEGNH_2 to mPEGBr was calculated on the basis of the difference between the absorbance values of solutions of the starting material (mPEG-NH_2) used as reference and that of equimolar samples of the conjugated derivative as:

Abs of mPEG-NH_2: 100 = Abs of mPEG-Br: x

% of modification = 100 – x

where x = % of non reacted amino groups in mPEG-Br

2.3.4.2 Iodine test

PEG concentration in aqueous solutions was assessed with the iodine assay according to the method described by Sims and Snape.[166] The iodine assay, in combination with the Snyder's test, allows to quantify the derivatization of mPEG-NH_2 with 2-bromo-isobutyryl bromide, as well as PEG/SDM molar ratio in the pH-sensitive polymer $mPEG_{5kDa}$-SDM_8.

A calibration curve was generated from a 100 μg/mL solution of mPEG-NH_2 in milliQ water that was diluted at several concentrations in milliQ water providing samples of 1 mL. A blank sample was generated with 1 mL of milliQ water. Then 250 μL of barium chloride (5% m/v in 1M HCl) and 250 μL of iodine solution (1.27g of I_2 in a 2% KI solution in milliQ water) were added to the mPEG-NH_2 dilutions. After 15 minutes, absorbance values were measured in triplicate at spectrophotometrically at 535 nm to generate the calibration curve (Figure 21).

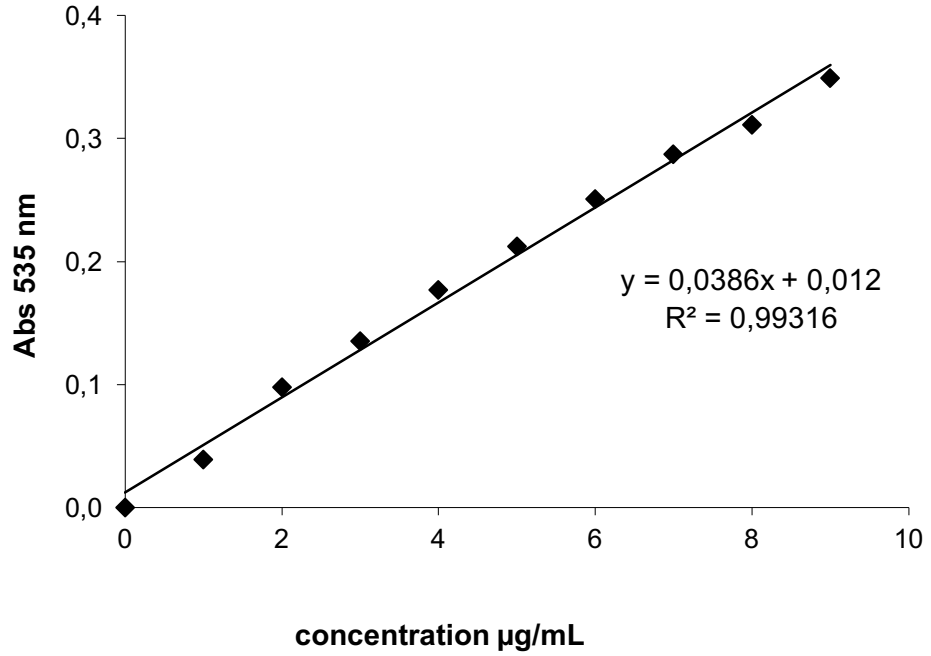

Figure 21. Calibration curve for the iodine test

The iodine test was performed on solutions of mPEG-Br and $mPEG_{5kDa}$-SDM_8 to assess the concentrations of the polymer. Eighty μL of a 100 μg/mL polymer solution in milliQ water were suitably diluted in 920 μL of milliQ water. Blank was generated with 1 mL of milliQ water. Then 250 μL of barium chloride (5% m/v in 1 M HCl) and 250 μL of iodine solution (1.27 g of I_2 added to a 2% KI solution in milliQ water) were added to the sample solution. After 15 minutes, absorbance values were measured in triplicate at 535 nm. The concentration was derived from the calibration curve (Figure 21).

2.3.4.3 Assessment of sulfadimethoxine

The concentrations of sulfadimethoxine (SD) and methacryloylsulfadimethoxine (SDM) in solution were determined spectrophotometrically by UV-Vis analysis.

First, the molar extinction coefficient of SD and SDM was assessed in NaOH. Ten mg of SD, or 10.0 mg of SDM, were exactly weighted and dissolved in 10 mL of 0.1 N NaOH and 1 mL of this solution was diluted with 0.1 N NaOH to a subsequently volume of 10 mL. The samples obtained were then analysed by UV-Vis spectroscopy and the absorbance at 265 nm was recorded. From the absorbance values measured and the known concentration of the SD or SDM, the ε the sample was derived using the Lambert-Beer equation:

$$A = \varepsilon \, l \, [conc]$$

where l is the optical path length (1 cm) and [conc] is the known concentration in the analysed solution. The molar extinction coefficients in 0.1 N NaOH was found to be 21300 $M^{-1\ cm-1}$ for the SD and 28710 $M^{-1\ cm-1}$ for the SDM.

2.3.4.4 Chromatographic analysis

SD, SDM and $mPEG_{5kDa}$-SDM_8 aqueous dilutions were analysed by RP-HPLC system to assess sample purity. The chromatographic system was equipped with a Luna C18 column and the UV-Vis detector was set at 265 nm. The column was eluted with acetonitrile (eluent A) and MilliQ water (eluent B) both supplemented with 0.05% TFA in a gradient mode (eluent B from 40 to 90% in 14 minutes).

2.3.5 pH titration analysis

One mg/mL of $mPEG_{5kDa}$-SDM_8 dispersion in water was added of 5 µL of 2 N NaOH and maintained under gentle stirring for 15 min to allow complete dissolution. The solution was titrated under stirring with 0.1 N HCl and pH was detected with pH meter. The solution pH values were plotted versus the HCl

volume added to the $mPEG_{5kDa}$-SDM_8 solution. The apparent pK_a of the polymer was calculated by the second derivative analysis of the titration curve.

2.3.6 Tagging reaction of Bovine Serum Albumin (BSA) with a fluorescent probe

2.38 mL of Rhodamine-NHS dissolved in DMSO at 10 mg/mL (23.8 mg, 46.16 mmol), were slowly added to 83.3 mL of a 12 mg/mL BSA solution in 0.1 M bicarbonate buffer at pH 8 (15.05 mmol). The volume of Rhodamine-NHS solution was added as 40 µL aliquots every ten minutes. The reaction was performed under mild stirring and protected from light for 24 hours. The reaction mixture was then dialyzed against water by a Float-A-Lyzer system with a 50 kDa cut-off membrane for 72 hours. Afterwards, the solution was lyophilized. The Rhodamine-labeled BSA (Rho-BSA) conjugate was dissolved in 10.0 mL of 0.1 M 2-(N-morpholino) ethane sulfonic acid (MES buffer), pH 4.6 and purified by dialysis with a 50 kDa cut-off membrane for 72 hours. Finally, the solution was freeze-dried to recover the biocongiuted protein.

2.3.7 Rho-BSA characterization

2.3.7.1 Spectrophotometric analysis

The ratio of BSA and Rho in the Rho-BSA conjugate was assessed by quantifying their concentration on a Rho-BSA solution using UV-Vis analysis at 280 nm and 550 nm, respectively. The molar extinction coefficients of BSA and Rhodamine in PBS at pH 7.4 are 43824 $M^{-1\ cm-1}$ and 80000 $M^{-1\ cm-1,}$ respectively. When quantifying the concentration of BSA, the contribution of Rhodamine at 280 nm was subtracted.

2.3.7.2 ESI-TOF

Electrospray ionization mass spectrometry (ESI-TOF) was performed to detect traces of free rhodamine after the Rho-BSA purification. This technique is

conventionally exploited to determine low molecular weight compounds in the range of 2 kDa. The ESI-TOF analysis was key since the contamination of the bioconjugate with free Rhodamine may hamper the reliability of the quantification of Rhodamine labelled BSA.

2.3.7.3 MALDI-TOF

Matrix-assisted laser desorption/ionization time-of-flight mass spectrometry (MALDI-TOF-MS) allows the detection of the molecular weight of macromolecules and thus their identification. It consists on a rapid photo-volatilization of samples embedded in a UV-absorbing matrix followed by time-of-flight mass spectrum analysis.[167] Ten µL solution of Rho-BSA at a concentration of 0.2-2 mg/mL in a 1:3 v/v water/acetonitrile mixture containing 0.05 v/v% TFA was prepared and 3 µL of this solution was added to 3 µL of a 4'-hydroxyazobenzene-2-carboxylic acid (HABA) solution in a 1:1 MilliQ water/acetonitrile mixture added of 0.05% TFA.

2.3.7.4 Chromatographic analysis

Twenty µL of protein solutions containing BSA and Rho-BSA dissolved in bicarbonate buffer at pH 8 were analyzed by RP-HPLC using Luna C18 column eluted at 1.0 mL/min with a linear gradient of 20 minutes ranging from 35 to 95% of acetonitrile (+0.05% TFA) in milliQ water (+0.05% TFA). The chromatograms were recorded at 280 nm for BSA and 580 nm for rhodamine.

2.3.8 Liposome preparation

Liposome formulations were prepared according to the “thin film rehydration” method, using 2:1 mol/mol hydrogenated soy phosphatidylcholine/cholesterol mixtures. Briefly, 10 mg of lipids was dissolved in 1.5 mL of CH_2Cl_2, the organic solvent was removed under reduced pressure and then stored overnight under vacuum to remove any trace of CH_2Cl_2. The lipid film was rehydrated with 200 µL of buffer (0.01 M phosphate, 0.15 M NaCl at pH 7.4 or 0.01 M HEPES, 0.15 M NaCl at pH 7.4 or 0.01 mM MES, 0.15 M NaCl at pH 6.5)

and processed with ten freeze-thawing cycles. Liposome suspension was then added of 1-8% mol with respect to lipids of Arg_4-DAG from a 5 mg/mL solution in the same buffer (CPE-coated liposomes), or 4% mol of 5 kDa PEG-DSPE from a 5 mg/mL solution in the same buffer (pegylated liposomes). Liposomes were then sonicated for 60 sec at 20% power. The samples were diluted with the same buffer to a lipid concentration of 10 mg/mL and extruded at 60°C eleven times through a polycarbonate membrane with a 200-nm cut-off. The formulations were incubated at 37 °C for 1 hour.

Fluorescently labelled liposomes were prepared by including the lipid film with 0.2 mol% of Rhodamine-DHPE, respect to lipids.

2.3.9 Particle size and zeta potential measurements

The size, polydispersity and zeta potential of decorated liposomes were assessed by Dynamic Light Scattering analysis after dilution of liposomes in different buffers: 0.01 M phosphate and 0.15 M NaCl at pH 7.4 and 6.5; 0.01 M phosphate and 300 mM mannitol at pH 7.4 and 6.5; 0.01 M HEPES and 0.15 M NaCl at pH 7.4; 0.01 M MES and 0.15 M NaCl at pH 6.5, 0.01 M HEPES and 300 mM mannitol at pH 7.4; 0.01 M MES and 300 mM mannitol at pH 6.5. Liposome size was expressed as average diameter (z-average).

Liposomes decorated with 4 mol% of Arg_4-DAG in 0.01 M HEPES (or MES), 0.15 M NaCl at pH 7.4 and 6.5 were incubated with increasing molar ratio of $mPEG_{5kDa}$-SDM_8 from 0 to 1 mol % with respect to Arg_4-DAG and underwent zeta potential analysis.

2.3.10 Liposomes colloidal stability in serum

10 mg/mL liposomes prepared according to the procedure reported above and decorated with 4 mol% of Arg_4-DAG and coated with 0, 0.25, 0.5 and 1 mol % of $mPEG_{5kDa}$-SDM_8 with respect to the Arg_4-DAG module were diluted to 1 mg/mL with 10 mM HEPES, 0.15 M NaCl at pH 7.4 in the presence of 2.5% of mice serum that was freshly isolated from blood by centrifugation at 1000 rpm for 10 minutes

at 4°C. After 1 hour of incubation at 37 °C, the samples underwent zeta potential analysis.

2.3.11 MP-SPR measurements

Surface plasmon resonance measurements were performed with a SPR Navi™ 200 (BioNavis Ltd., Ylöjärvi, Finland) instrument. The setup was equipped with two incident laser wavelengths, 670 nm and 785 nm, two independent flow channels, inlet tubing and outlet (waste) tubing. Both of the flow channels were measured in parallel with 670 nm and 785 nm incident light. The measurement temperature was kept constant at 20 °C, and the flow rates used for CPE coated liposome immobilization and for $mPEG_{5kDa}$-SDM_8 interactions were 50 and 100 µL/min, respectively. The pH responsive polymer solutions were flow at pH 7.4 and at pH 6.5 to assess liposome/polymer association. Liposomes were captured and immobilized on SPR sensors consisting of a thin 6-kD carboxymethyl dextran hydrogel layer functionalized with dodecyl lipid anchors.[168, 169]

The SPR sensors were used repeatedly after rejuvenation with an injection series of Hellmanex II 2% or CHAPS 20 mM, ethanol 80% and Milli-Q water. In between measurements, the sensors were stored immersed in CHAPS at 4 °C. During the SPR measurements, the functionalized gold sensor slides were first subjected to the running buffer for respective liposome for approximately 5–10 min until a stable baseline was achieved. In the second phase, the liposomes were injected into both flow channels for 10 min, and lastly, sensor surfaces containing the immobilized liposome species were subjected to pH sensitive polymer at pH 7.4 and 6.5.

2.3.12 Liposome loading with Rho-BSA

Liposomes loaded with Rhodamine labelled BSA (Rho-BSA) were prepared by rehydrating the lipidic film with 200 µL of a 10 mg/mL Rho-BSA solution in PBS pH 7.4. After freezing and thawing treatment and extrusion, the non-loaded Rho-BSA was removed by dialysis according to a validated protocol: 1 mL of 10 mg/mL liposomes was dialyzed for 72 hours using a 300-kDa cut-off Float-A-Lyser® G2

system using 1 L of PBS at pH 7.4 as receiving medium. Rho-BSA concentration in the liposomes suspension was assessed with a RP-HPLC system equipped with a Luna C18 column. The UV detector was set at 220 nm. The column was eluted with acetonitrile (eluent A) and MilliQ water (eluent B) both supplemented with 0.05% TFA in a gradient mode (eluent B from 30 to 90% in 13 minutes). The Rho-BSA concentration (y) was derived from the eluted peak area (x) using a standard curve obtained with Rho-BSA dilutions [y (µg Rho-BSA/mL) = 1661,1 x (peak area); R^2 = 0.9982]. The encapsulation efficiency was calculated as the percentage of loaded Rho-BSA after dialysis with respect to the Rho-BSA fed to hydrate the liposomes. The liposome loading capacity was expressed as the amount of encapsulated Rho-BSA (after dialysis) per mg of lipid (w/w).

2.3.13 Rho-BSA release study

Rho-BSA release profile from Arg_4-DAG decorated liposomes was investigated at 25 °C in PBS at pH 7.4 and acetate buffer at pH 5.0. Two mL of 1 mg/mL Rho-BSA loaded liposomes were transferred in a 300 kDa MW Cut-Off Float-A-lyzer® and dialyzed against PBS at pH 7.4 or acetate buffer at pH 5.0. At scheduled times, 50 µL of each liposome sample were withdrawn and analysed by RP-HPLC to assess the Rho-BSA concentration. The variation of concentration was plotted versus time.

2.3.14 Liposome loading with Calcein

A 15 mM (9.34 mg/mL) solution of calcein in PBS (0.01 M phosphate and 0.15 M NaCl) at pH 7.4 was prepared and the pH was set at 7.4 by adding 1M NaOH. The calcein concentration was assessed by UV-VIS spectroscopy.

A dried 10 mg lipid film was rehydrated with 200 µL of the calcein solution in PBS pH 7.4, then subjected to freezing and thawing cycles and extruded. The non-loaded calcein was removed by dialysis: 1 mL of 10 mg/mL liposomes was dialyzed overnight using a 300-kDa Float-A-Lyser® G2 system against 1 L of PBS at pH 7.4. Calcein concentration assessment was carried out by

spectrofluorometric analysis with an excitation wavelength of 493 nm and emission of 515 nm.

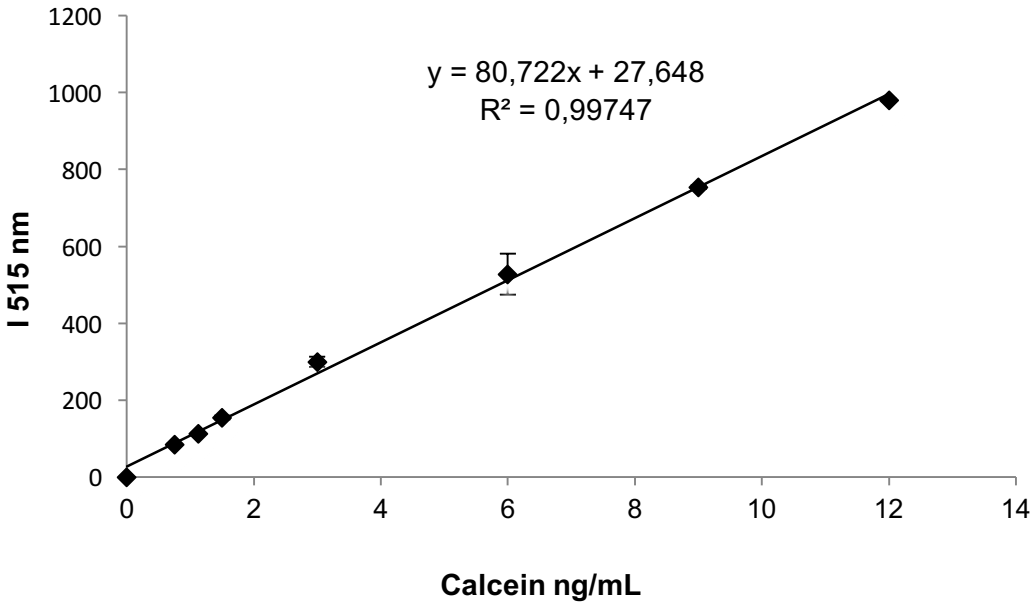

Figure 22. Titration curve of calcein by fluorescence analysis.

The concentration of calcein in the sample solutions was derived from a titration curve (Figure 22) obtained by dilutions of a 1 mg/mL calcein solution in PBS pH 7.4 (triplicate samples).

The encapsulation efficiency was expressed as the percentage of loaded calcein after dialysis with respect to the calcein fed to hydrate the liposomes. The liposome loading capacity was expressed as the amount of encapsulated calcein (after dialysis) per mg of lipid (w/w).

2.3.15 Calcein release study

Calcein release studies from Arg_4-DAG decorated liposomes were performed at 25 °C in PBS at pH 7.4 and acetate buffer at pH 5.0. Two mL of 1 mg/mL calcein loaded liposomes were transferred in a Float-A-lyzer® with a 300 kDa MW Cut-Off and dialyzed against PBS at pH 7.4 or acetate buffer at pH 5.0. At scheduled times, 20 microliters of each liposome suspension was withdrawn, diluted 10000 times with PBS pH 7.4 and spectrophotometrically monitored for

calcein concentration. The decrease of calcein concentration in the liposome suspension was plotted versus time.

2.3.16 Cellular uptake study

2.3.16.1 Cell cultures

Hela cells (human cervical cancer) were grown at 37 °C, in 5% CO_2 atmosphere, in DMEM medium supplemented with 10% (v/v) heat-inactivated fetal bovine serum (FBS), 2 mM L-glutamine, 100 IU/mL penicillin, 100 µg/mL streptomycin and 0.25 µg/mL of amphotericin B. In all studies cells were subcultured every 2-3 days.

2.3.16.2 Cytofluorimetric analysis

Hela cells were used to evaluate the internalization of surface engineered liposomes (naked, PEGylated, coated with 2% or 4% of Arg_4-DAG, coated with 4% Arg_4-DAG and 4% $mPEG_{5kDa}$-SDM_8; empty liposomes labelled with Rhodamine-DHPE and liposomes loaded with Rho-BSA or calcein) according to the pH of incubation. Cells were seeded in a 6 well plate at a density of 28×10^4 cells/well. After 24 hours the cells were washed two times with PBS and incubated 1 hour at 37 °C with 1 mL of 0.1 mg/mL liposomal dilutions in DMEM supplemented with 10% of FBS at pH 7.4 or 6.5 (buffering with 0.1 M MOPS).[170] The medium was removed and cells were rinsed three times with fresh PBS and treated for 2 min with 300 µL of 0.5 mg/mL trypsin in PBS without calcium and magnesium. One mL of DMEM supplemented of 10% FBS was added to each well and cells were recovered and centrifuged at 1000 rpm for 5 minutes. The cellular pellet was resuspended in PBS, washed twice with PBS and recovered by centrifugation at 1000 rpm for 5 minutes. Cell samples were resuspeded in 300 µL of PBS.

Cell samples underwent flow cytometric analysis using a BD FACScanto II flow cytometer (Biosciences, San Jose, Canada). Analysis were acquired by FACSDIVA software package and cell population were gated using forward versus side scatter to exclude debris and dead cells.

2.3.16.3 Confocal microscopy

The cellular uptake and interaction of liposomes (Rhodamine-DHPE labelled naked, pegylated, coated with 4% Arg_4-DAG, coated with 4% Arg_4-DAG and 4% $mPEG_{5kDa}$-SDM_8; and the Rho-BSA or calcein loaded version of the same liposomes) were studied by confocal microscopic analysis.

Hela cells were seeded onto 4-chamber tissue culture microscope slides at a 1×10^5 cells/chamber density. After 24 hours (90% confluence), cells were washed 2 times with PBS at pH 7.4 and replaced with 0.5 mL of 0.1 mg/mL liposome suspensions in DMEM supplemented with 10% of FBS at pH 7.4 or 6.5. After incubation of 1 hour at 37 °C, the medium was removed and cells were gently washed three times with fresh PBS, and finally fixed by treatment with 4% paraformaldehyde in PBS for 10 min in ice bath. Cell membranes were stained by incubating the cells with 5 µg/mL Alexa Fluor 633 conjugated wheat-germ agglutinin in PBS for 10 minutes at room temperature. The cells were then washed with PBS and the samples were covered with a glass slide using Vectashield as mounting medium containing 1.5 µg/mL DAPI for nucleus staining and kept at 4°C in the dark until microscopic examination.

Samples were analysed by confocal microscopy using a 63X oil immersion objective lens. Lasers with an emission wavelength at 405, 488, 561 and 640 nm were used to detect DAPI, calcein, rhodamine-DHPE and Alexa Fluor germ agglutinin, respectively.

2.3.17 Statistical analysis

Statistical analyses were performed with XLSTAT software (New York, USA). Two-way analysis of variance was used to calculate the threshold of significance. Statistical significance was set at $p < 0.05$.

3. RESULTS

3.1 CELL PENETRATING ENHANCER DESIGN AND STRUCTURAL PREDICTION

In order to predict the charge density for the G1 and G2 arginine-decorated Dendrons (Figure 20), the average mutual distance of arginines was calculated applying Molecular Operating Environment (MOE) software. The simulation showed that arginine guanidinum carbons possess distance values of 10.3 Å and 13.8 Å, respectively for the G1 and G2 structures (bearing 4 and 8 arginines). This prediction showed that arginines are closer in the G1 derivative and thus the have a higher charge density. Moreover, the [hydrophobic alkyl chains]/[polycationic dendritic block] weight ratios of the 4-arginine and 8-arginine derivatives are 1:2.8 and 1:4.6 respectively which corresponds to a higher molecular weight ratio of the hydrophobic moiety of the G1 dendron with respect to G2. This anticipates that the G1 Dendron may undergo a stronger association to the liposome membrane (Table 2).

Table 2. Structural prediction of Arg_4-DAG and Arg_8-DAG

Compound	**Arg_4-DAG**	**Arg_8-DAG**
Dendron generation	G1	G2
number of arginines	4	8
MW	1677 Da	2762 Da
Arginine average mutual distance	10.3 Å	13.8 Å
[hydrophobic alkyl chains]/[polycationic dendritic block] weight ratio	1:2.8	1:4.6

3.2 CELL PENETRATING ENHANCER SYNTHESIS AND CHARACTERIZATION

The first-generation cell penetration enhancer Dendron, Arg_4-DAG, (**14**, Figure 23), based on 2,2-bis(hydroxymethyl)propionic acid (**bis-MPA**) and 2,2-

bis(amminomethyl)propionic acid (**bis-AMPA**) scaffolds with four arginines on one side and a 3-(1,2,3-triazol)propane-1,2-distearate anchoring unit for liposome association on the other side was synthesized by the Cu(I)-catalyzed Huisgen 1,3-dipolar cycloaddition ("click" reaction) between the azide terminated distearoyl propane anchoring unit (**12**) and the alkynic tetra-Boc-arginyl(Pbf) dendron (**10**) followed by TFA mediated deprotection of the arginine protecting groups (**xiii** and **xiv**, Figure 23).

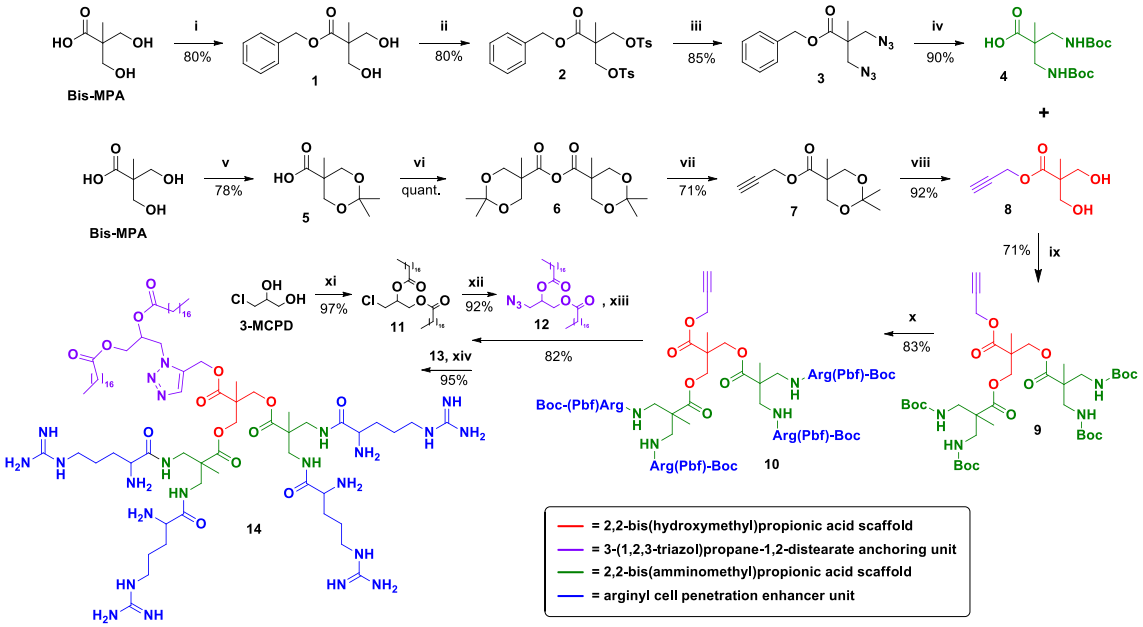

Figure 23. Scheme of the synthesis of the first-generation tetra-arginyl dendritic 3-(1,2,3-triazol)propane-1,2-distearate cell penetration enhancer for the decoration of liposomes (14)[a].

[a]Reagents and conditions: (i) BnBr, KOH, DMF, 100 °C, 15 h; (ii) TsCl, Py, DMAP, CH_2Cl_2, 60 °C, 4 h; (iii) NaN_3, DMF, 90 °C, 16 h; (iv) 1) PtO_2, H_2, $(Boc)_2O$, MeOH, rt, 4 h; 2) 10% Pd/C, H_2, MeOH, rt, 3 h (v) DMP, PTSA, Acetone, rt, 2 h; (vi) DCC, CH_2Cl_2, rt, 4 h; (vii) 2-propyn-1-ol, Py, DMAP, CH_2Cl_2, rt, 15 h; (viii) Dowex 50W-X8 (H^+-form), MeOH, rt, 6 h; (ix) 1) **4**, DCC, CH_2Cl_2, rt, 16 h; 2) **8**, Py, DMAP, CH_2Cl_2, rt, 16 h; (x) 1) CH_2Cl_2/TFA (1:1), rt, 2.5 h; 2) Boc-Arg(Pbf)-OH, HOBt, EDC, DIPEA, DMF, rt, 16 h; (xi) stearoyl chloride, Py, CH_2Cl_2, rt, 16 h; (xii) NaN_3, DMF, 100 °C, 15 h; (xiii) CuI (10 mol %), AcOH (20 mol %), DIPEA (20 mol %), sodium ascorbate (10 mol %), CH_2Cl_2, rt, 24 h; (xiv) 1) CH_2Cl_2/TFA (2.5:1), rt, 24 h; 2) CH_3CN/H_2O + 0.05% TFA (1:1), Amberlite IRA-900 (Cl^--form).

3-azidopropane-1,2-distearate (**12**) was prepared according to a two-step procedure from commercially available (±)-3-chloro-1,2-propanediol (**3-MCPD**): 1.

acylation reaction of stearic acid to generate stearoyl chloride, 2. nucleophilic substitution of chloride with azide (**xi** and **xii**, Figure 23). The product was obtained with high yield as expected.

The synthesis of the four branched alkynic tetra-Boc-arginyl(Pbf) scaffold (**10**) was achieved via anhydride coupling between 2,2-(bis((*tert*-butoxycarbonyl)amino)methyl)-propanoic acid (**4**) and propargyl 2,2-bis(hydroxymethyl)propanoate (**8**) to obtain **9** (**ix**, Figure…), followed by TFA mediated Boc deprotection and coupling with Boc-Arg(Pbf)-OH (**x**, Figure 23).

The compound **8** was synthesized according the procedure reported by Barnard et al.[171] with slight modifications (**v** - **viii**, Figure 23). The derivative **4** was synthesized by benzylation of the carboxylic function of Bis-MPA followed by tosylation of the two free hydroxyl groups and nucleophilic substitution of the tosylate with azide yielding **3** which was then reduced with hydrogen in presence of PtO_2 and reacted with Boc-anhydride to obtain the corresponding Boc-protected diamine. Aftrewords, the intermediate was further reduced in presence of Pd/C to cleave the benzyl protecting group and obtain **4** (**i** - **iv**, Figure 23).

The final alkylated oligo arginine Dendron Arg_4-DAG **14** was obtained with high purity, as proved by the ^{1}H and ^{13}C NMR spectra (Figure 24 and 25) The m/z signal at 418 of the $[M+4H]^{4+}$ ion confirmed its identity. The spectra of all intermediates are reported in the Appendix Chapter.

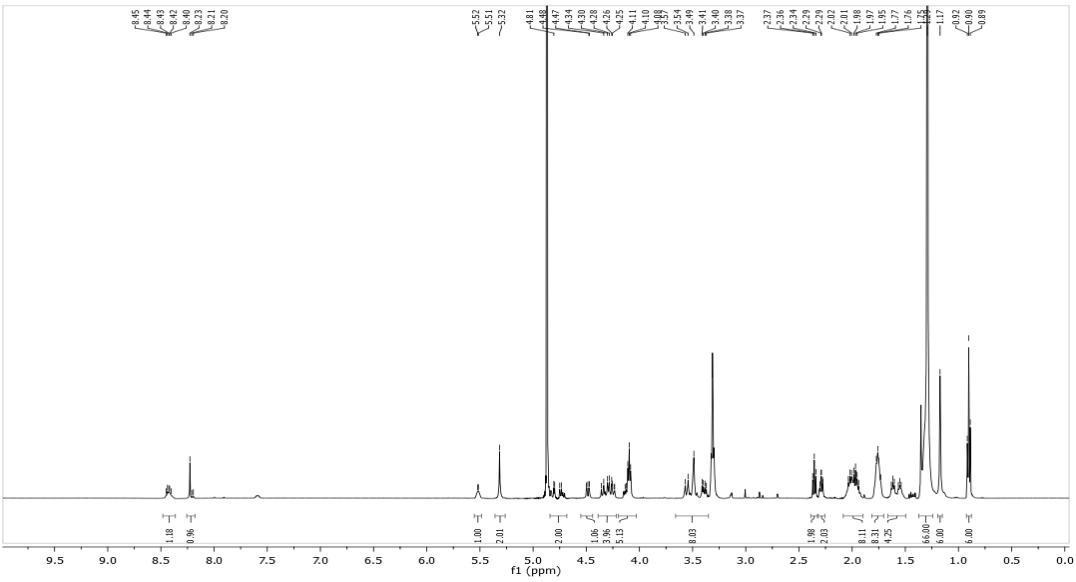

Figure 24. ^{1}H-NMR (500 MHz) in MeOD of Arg_4-DAG.

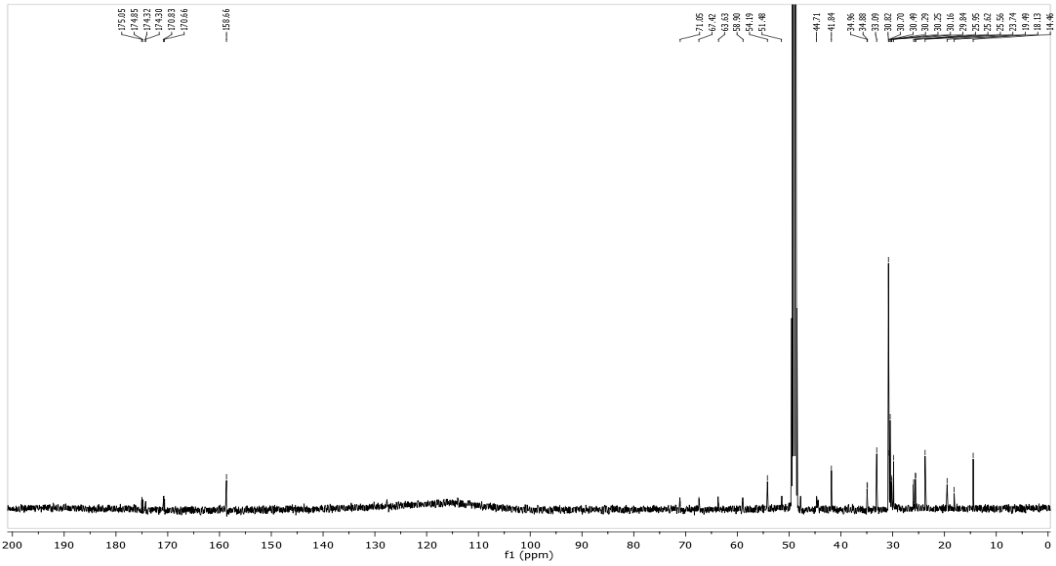

Figure 25. ^{13}C-NMR (126 MHz) in MeOD of Arg_4-DAG.

3.3 pH-SENSITIVE POLYMER SYNTHESIS AND CHARACTERIZATION

The acid-sensitive m-PEG-poly-methacryloyl-sulfadimethoxine ($mPEG_{5kDa}$-SDM_8) co-polymer **17** was synthetized according to a three-step procedure adapting a strategy reported in the literature[90], showed in Figure 26.

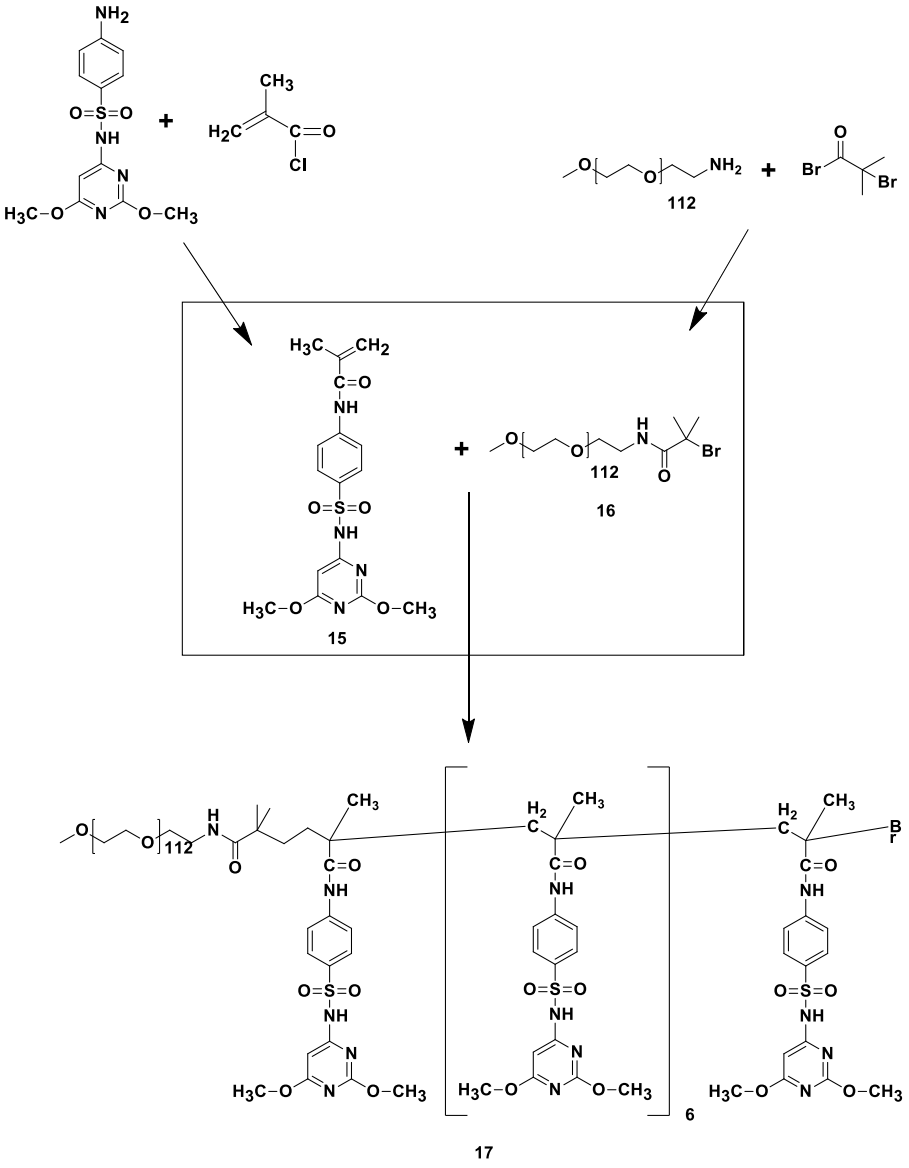

Figure 26. Scheme of the synthesis of the pH-sensitive polymer ($mPEG_{5kDa}$-SDM_8).

After nucleofilic substitution of sulfadimethoxine primary amines with the methacriloyl chloride, the SDM pH sensor **15** was recovered by spontaneous precipitation from the reaction mixture.[163]

The identity of the SDM was confirmed by ESI-TOF mass spectrometry in positive mode. The spectrum showed the presence of a single signal at 379.10 m/z $(M+H)^{1+}$ corresponding to the molecular weight of SDM ($C_{16}H_{18}N_4O_5S$, theoric molecular weight: 378.10 Da). The signal at 311.09 m/z $(M+H)^{1+}$ corresponding to the starting reagent sulfadimethoxine ($C_{12}H_{14}N_4O_4S$, theoric molecular weight: 310.07 Da) has a negligible intensity.

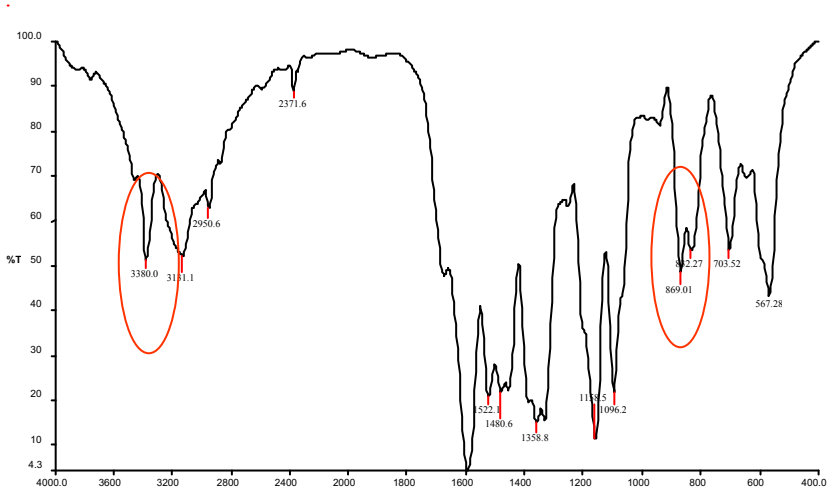

Figure 27. FT-IR spectrum of SD.

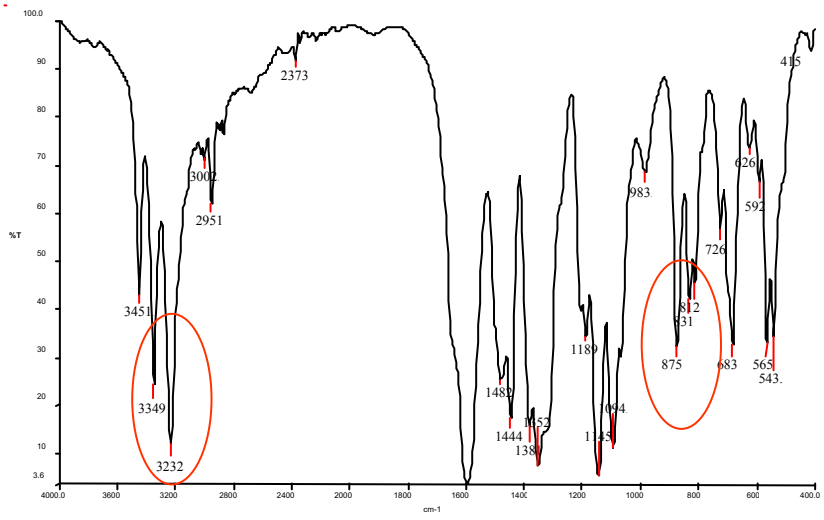

Figure 28. FT-IR spectrum of SDM.

The FT-IR spectra of starting sulfadimethoxine and of methacryloyl sulfadimethoxine derivative reported in Figure 27 and 28 show the differences of the peculiar bond stretching of the two molecules. Figure 27 shows the presence

of the characteristic band at 3232 cm^{-1} that corresponds to the signal of the secondary amide NH bond stretching originated from the amine of the aniline of methacryloyl sulfadimethoxine; this signal is absent in the FT-IR spectrum of the starting reagent (Figure 27). The bands corresponding to the bending of the methacrylic group are detectable between 880 and 860 cm^{-1}.

The chemical structure of the monomer was confirmed by ^{1}H NMR analysis (see Appendix chapter). The integrals of the signals of the pyrimidine ring of SD at 5.92 ppm and of the methacrylamide methoxy group at 1.94 ppm were consistent with a 1:1 SD/methacrylamide molar ratio.

In order to determine the purity of methacryloyl sulfadimethoxine, a RP-HPLC chromatographic analysis was performed. The chromatograms reported in Figure 29 show an eluted peak at 7.17 minutes corresponding to the sulfadimethoxine (which has been preliminary tested by injection in the same chromatographic system as a reference, dotted line) and a peak at 10.45 minutes attributed to methacryloyl sulfadimethoxine.

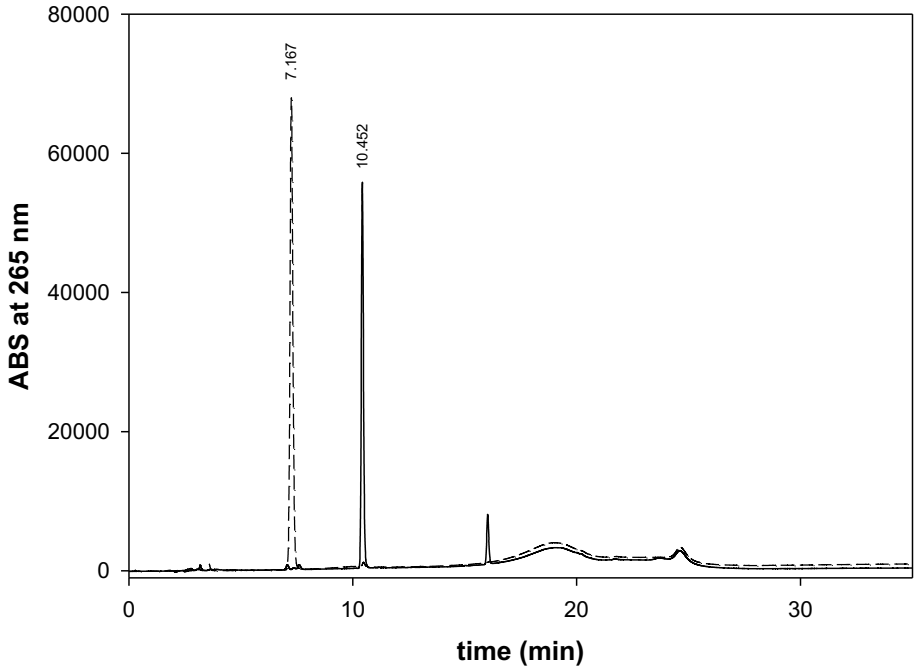

Figure 29. Overrlay of SD (---) and SDM (—) chromatographic analysis

The degree of purity of SDM was calculated from the ratio of the chromatographic peak areas and it was found to be 93%.

Activated mPEG-NH-CO-C-$(CH_3)_2$)-Br **16** was obtained by α-bromoisobutyryl bromide reaction with $mPEG_{5kDa}$-NH_2 under anhydrous conditions followed by precipitation in cold diethyl ether for 3 times. The TNBS colorimetric analysis confirmed the complete functionalization of the amino groups of mPEG–NH_2 with α-bromoisobutyryl bromide. The integrals of the ^{1}H NMR signals of the mPEG-NH-CO-C-$(CH_3)_2$)-Br **16** (3.64 ppm for the oxyethylene monomers of PEG and 1.96 ppm for the two methyl groups of the α-bromoisobutyryl amide) were in agreement with a 1:1 PEG/α-bromoisobutyryl amide molar ratio (see Appendix chapter).

The synthesis of $mPEG_{5kDa}$-SDM_8 **17** was performed by AGET-ATRP polymerization of methacryloyl sulfadimethoxine **15** using mPEG-NH-CO-C-$(CH_3)_2$)-Br as polymerization initiator, using a 1:12 α-bromoisobutyryl bromide/SDM molar ratio, Cu(II)/TPMA as catalyst and ascorbic acid as reducing agent to regenerate the Cu(I) as catalyst.

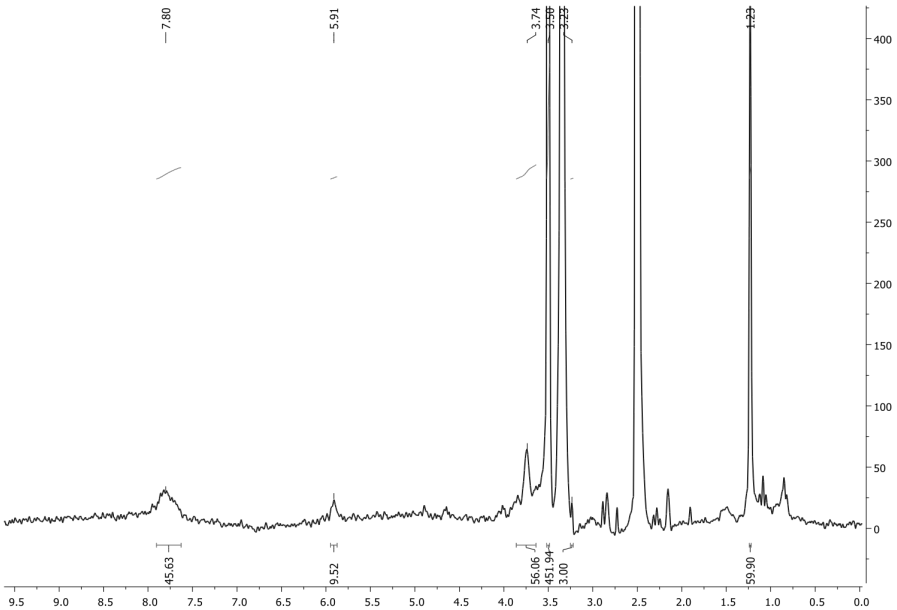

Figure 30. ^{1}H-NMR spectrum of $mPEG_{5kDa}$-SDM_8.

The ^{1}H NMR spectrum of the $mPEG_{5kDa}$-SDM_8 shows the signals at 5.91 ppm and 3.5 ppm (Figure 30), corresponding to the pyrimidyl hydrogen of SDM and the PEG oxyethylene monomers, respectively. The integrals of these signal confirmed that the co-polymer includes, on average, 8 methacryloyl sulfadimethoxine monomers. The UV–Vis analysis and iodine assay confirmed that a co-polymer with a 1:8 PEG/SDM molar ratio was obtained.

The polymer was purified by sequential extraction and precipitation procedures. The purity of pH sensitive $mPEG_{5kDa}$-SDM_8 **17** was determined by RP-HPLC analysis.

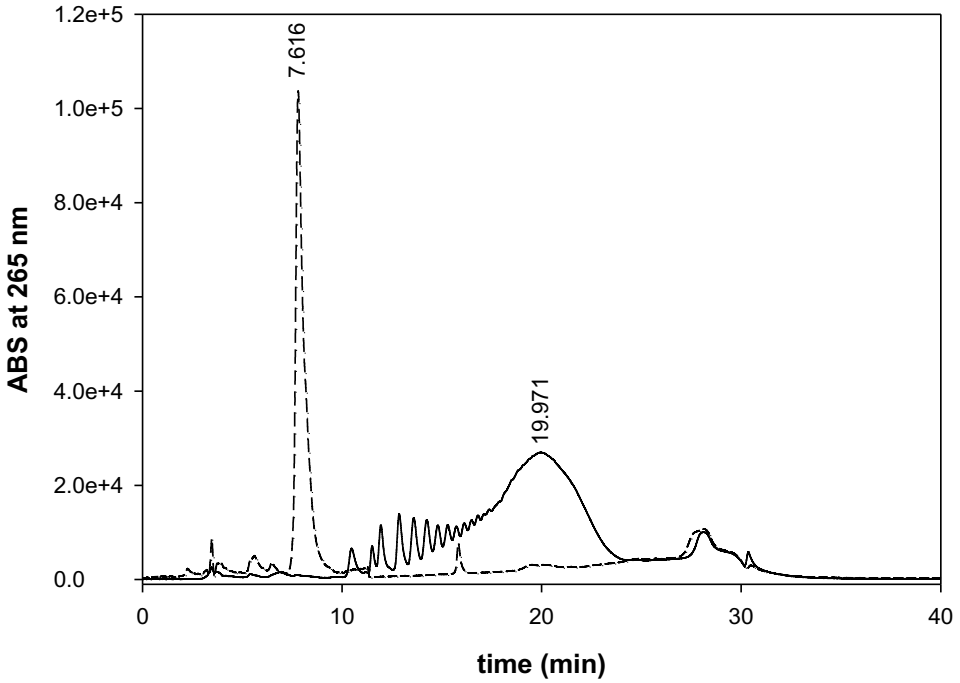

Figure 31. RP-HPLC chromatographic profile of SDM (---) and $mPEG_{5kDa}$-SDM_8 (—) .

Figure 31 shows that $mPEG_{5kDa}$-SDM_8 elutes with a quite broad peak which is expected for polymeric water soluble products (19.77 minutes). SDM was injected (dashed line chromatogram) as control. Notably, the profile of $mPEG_{5kDa}$-SDM_8 did not show traces of unreacted SDM proving that the synthetic and purifications procedures allow to remove very efficiently the non-polymerized free SDM monomers.

3.4 ASSESSMENT OF $mPEG_{5KDA}$-SDM_8 pKa

The pKa of $mPEG_{5kDa}$-SDM_8 was assessed by potentiometric titration using HCl as titrant.[172] The potentiometric profile displayed in Figure 32 shows that the $mPEG_{5kDa}$-SDM_8 co-polymer possesses an apparent pKa of 7.1. The result is in agreement with similar polymers obtained from PEG derivatives and SDM reported in the literature.[163, 164, 173]

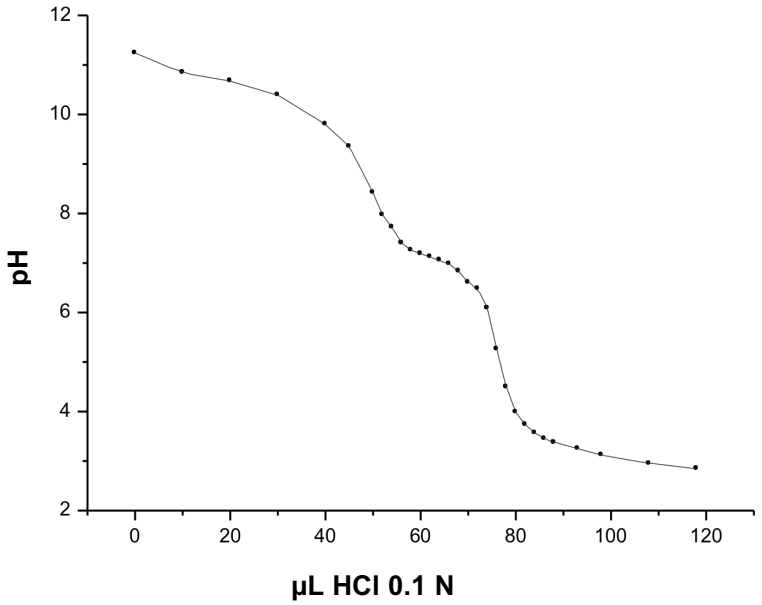

Figure 32. Potentiometric titration profile of $mPEG_{5kDa}$-SDM_8.

3.5 FLUORESCENT LABELLING OF BSA

The conjugation of NHS-Rhodamine to BSA was carried out by previously dissolving NHS-Rhodamine in DMSO and BSA in bicarbonate buffer pH 8. Then, small aliquots of the NHS-Rhodamine solution were added to BSA solution. The activated rhodamine used in this reaction is very reactive with primary amines in proteins and particularly under alkaline conditions yielding stable, highly fluorescent, derivatives. In order to facilitate the labelling yield, a NHS-Rhodamine/BSA molar ratio of 3:1 was used.

The ESI-TOF spectrum (Figure 33) showed that the fluorescently labelled BSA (Rho-BSA) is devoid of free rhodamine or NHS-Rhodamine since few peaks were

detected in proximity of the expected NHS-Rhodamine (527.52 MW) and Rhodamine (479.02 MW) m/z and none of them corresponded to neither of the two fluorescent molecules.

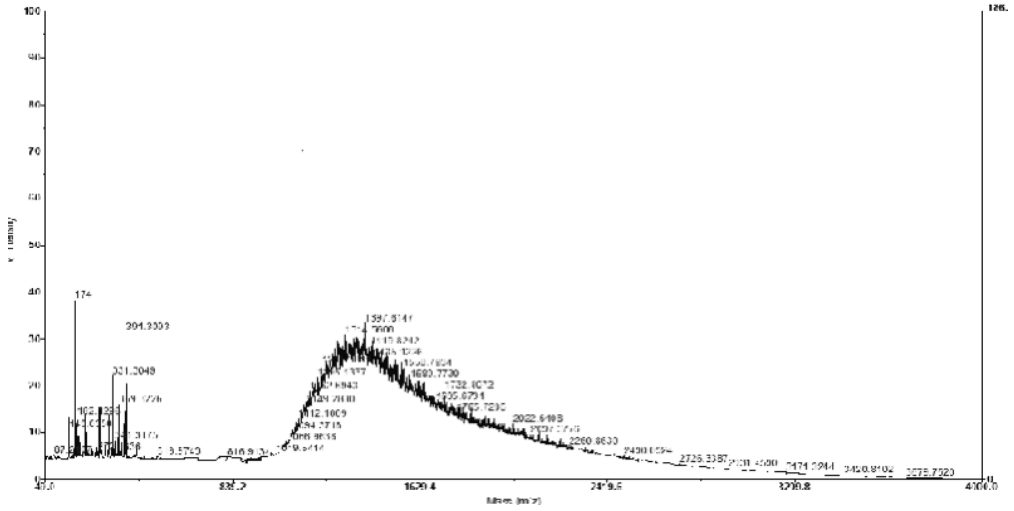

Figure 33. Rho-BSA ESI-TOF spectrum.

The signal on the MALDI-TOF spectrum of Figure 34A confirmed that an average of 2.5 molecules of Rhodamine has been conjugated to BSA, as also proved by spectrophotometric determination. The m/z was found to be 68308.49. BSA MALDI-TOF analysis was also performed as control which showed a 67063.3 m/z of the native protein (Figure 34B).

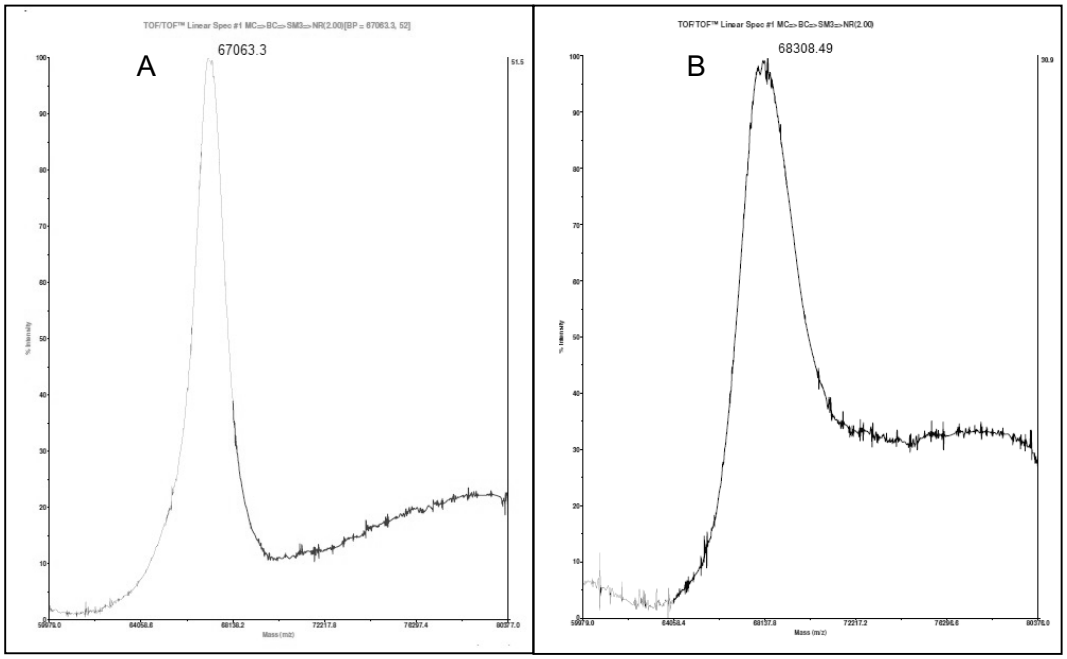

Figure 34. Native BSA (A) and Rho-BSA (B) MALDI-TOF spectra

Non labelled BSA and Rhodamine labelled BSA (Rho-BSA) solutions were analysed by RP-HPLC chromatography using the conditions described in the Methods chapter. Figure 35A reports the chromatographic profile of native BSA that elutes with a sharp peak with a retention time (Rt) of 9.813 minutes.

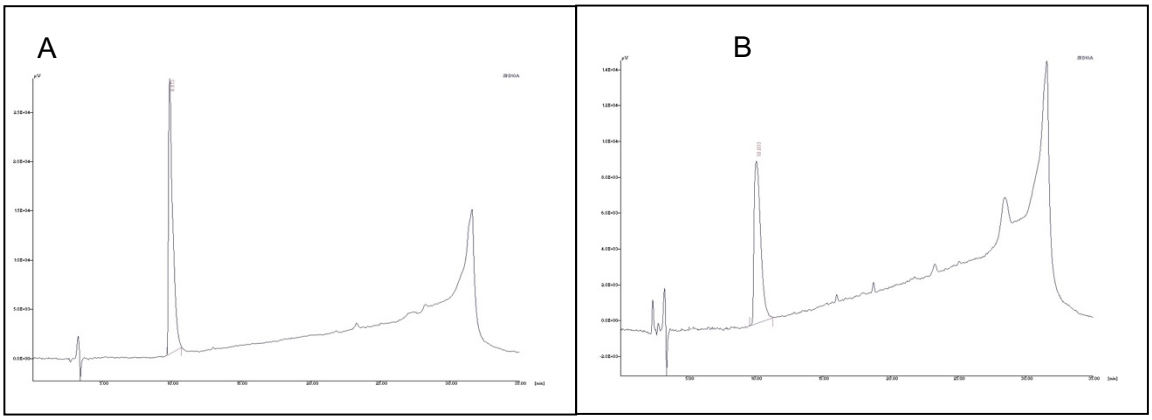

Figure 35. HPLC-RP chromatographic profile of BSA (A) and Rho-BSA (B) recorded at 280 nm.

Figure 35B shows the chromatographic profile at 280 nm of Rho-BSA that elutes with a peak having retention time (Rt) of 10.033 minutes. The peak shifting of the Rho-BSA with respect to BSA proves that BSA has been chemically modified upon reaction with the NHS-Rho. The analysis of the conjugate was also carried out at 550 nm, the wavelength at which rhodamine absorbs: in this case the rhodamine peak overlaps with that obtained at 280 nm, confirming the conjugation. Furthermore, the profile in Figure 11B also shows the high purity degree of the conjugate Rho-BSA since no traces of native BSA nor free NHS-Rhodamine or Rhodamine were detected.

3.6 LIPOSOMES FORMULATION AND CHARACTERIZATION

3.6.1 Arg_4-DAG Coated Liposomes

Arg_4-DAG decorated liposomes were assembled by thin layer rehydration technique.[85] Lipids were dissolved in DCM and the dried film was rehydrated with 10 mM PBS, 0.15 M NaCl. Arg_4-DAG was incorporated in the preformed liposomes by dilution from a 5 mg/mL solution in the same buffer, using the post-insertion technique via spontaneous micelle transfer.[87, 174, 175] The cartoon of the Arg_4-DAG decorated liposome conformation is reported in Figure 36.

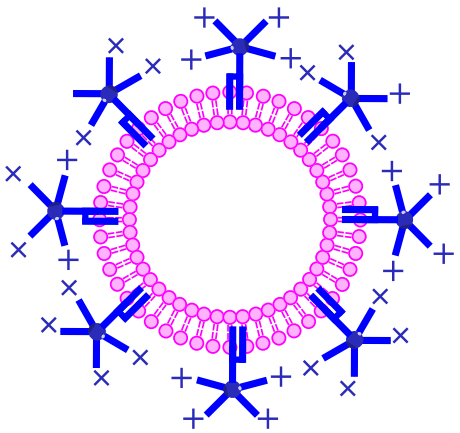

Figure 36. Cartoon of Arg_4-DAG decorated liposome

The incorporation process was promoted by ultrasound treatment. Liposomes were finally extruded. The extrusion process was found to remove the Arg_4-DAG non-associated to the liposomes, which was preliminarily shown by

filtering a Arg_4-DAG solution with the same filter used to extrude liposomes. Liposomes were decorated with increasing Arg_4-DAG component from 1 to 8 mol% with respect to lipids. This percentage was selected based on information reported in the literature for liposomes decorated with TAT-like derivatives.[122, 176, 177] The Arg_4-DAG is a cationic charged molecule, thus its association to the liposomes was confirmed by zeta potential analysis. Upon post insertion treatment with the Arg_4-DAG, the zeta potential on liposomes was found to increase up to 26 mV when the Arg_4-DAG/lipid ratio was 8 mol% with respect to total lipids (Figure 37). The zeta potential tended to a plateaux when a 4 mol% of Arg4-DAG was included in the lipid bilayer. Notably, the non-coated liposomes (Arg4-DAG free liposomes) possess a zeta potential of -1 mV.

All formulations showed a size of 200 ± 10 nm with a polydispersity index of 0.06, and do not change size when adding the CPE. Dimensional analysis also demonstrated that there are no free micelles.

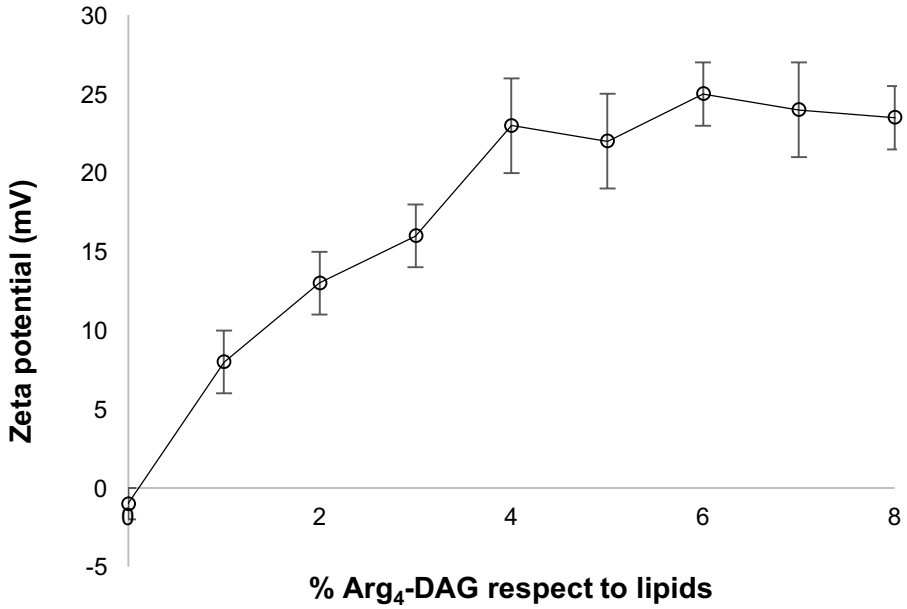

Figure 37. Zeta potential profile (mV) of liposomes coated with increasing Arg_4-DAG/lipid ratio at pH 7.4 in PBS.

After inclusion of the synthetic CPE, the zeta potential was also measured in different buffers at pH 6.5 and 7.4, which were selected as conditions that mimic the tumor environment and the blood, respectively. The study was aimed at evaluating the influence of the buffer components (negative charged phosphate vs zwitterionic HEPES/MES) and osmotic agents (NaCl vs mannitol) on Arg_4-DAG coated liposomes charge shielding. The zeta potential values ranged from +22 mV to +33 mV depending on the buffers and the osmotic agent used, which further proved the Arg_4-DAG association with liposome surface (Figure 38). Notably, the two buffers used, namely phosphate and HEPES/MES, affected the liposome zeta potential showing that the buffer ionic species associate to the arginines of the Arg_4-DAG which may shield the poly-cationic surface charges of the liposomes, thus altering the zeta potential of the vesicles. The phosphate buffer was found to slightly decrease the zeta potential of liposomes with respect to the buffer generated with HEPES, while no significant difference was shown when mannitol and NaCl were compared as osmotic agents. The zeta potential of Arg_4-DAG decorated liposomes was only slightly affected by the pH.

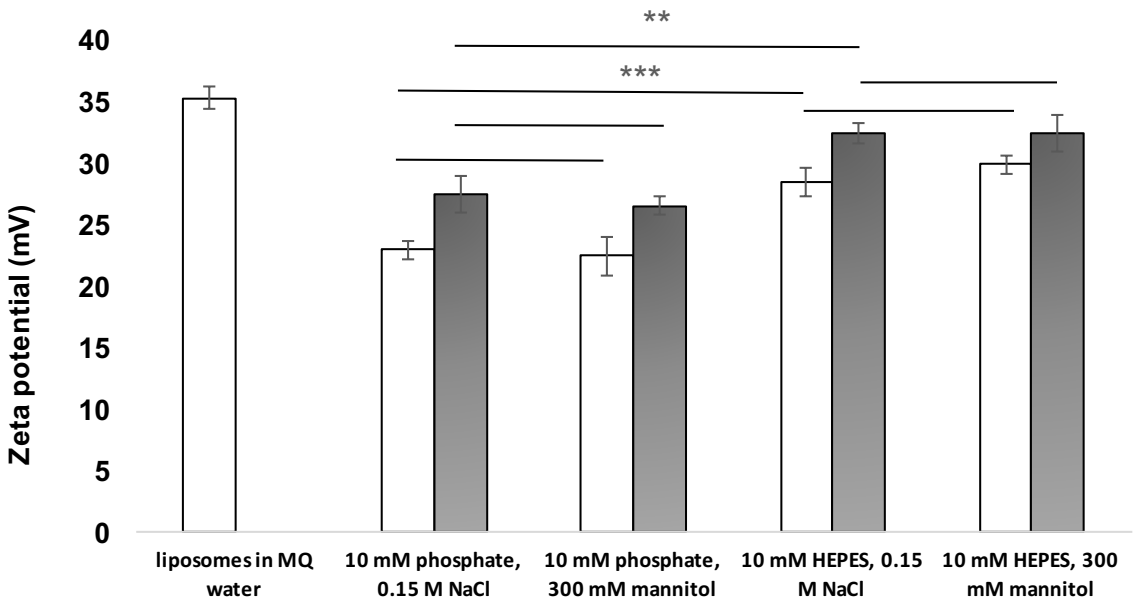

Figure 38. Zeta potential (mV) of liposomes coated with 4 mol% CPE at pH 7.4 (□), 6.5 (■) in different buffers.

Based on the zeta potential analysis, 0.01 M HEPES (at pH 7.4 or MES at pH 6.5), 0.15 M NaCl was selected as buffer for further investigations since it showed a low ability to mask the cationic charges on liposomes surface derived from the oligo-arginines of the bilayer associated CPE.

3.6.2 Liposome pH-controlled shielding

The oligo-arginines shielding capacity of $mPEG_{5kDa}$-SDM_8 copolymer was found to depend on the pH-sensitive polymer/Arg_4-DAG molar ratio in the liposome formulation. The zeta potential analysis of the liposomes was performed by stepwise increase of the pH-sensitive polymer/Arg_4-DAG molar ratio from 0 to 1. The presence of $mPEG_{5kDa}$-SDM_8 in the CPE decorated liposome suspension at a final 1:1 $mPEG_{5kDa}$-SDM_8/Arg_4-DAG molar ratio was showed to reduce the zeta potential from +28 of the liposomes in the absence of the pH responsive polymer to -1 mV at pH 7.4 as consequence of the ionic association of the oligo-arginines of Arg_4-DAG and oligo-SDM of $mPEG_{5kDa}$-SDM_8. This charge-to-charge interaction provides for the arginine charge screening. On the contrary, when the polymer was incubated with liposomes at pH 6.5, the zeta potential remained positive (+10 mV). Five kDa mPEG-OH (at same concentration of the pH sensitive polymer) and sulfadimethoxine (SD, at the same concentration of the methacroloyl monomers of the pH sensitive polymer) used as controls were not able to shield the Arg_4-DAG coated liposomes at pH 7.4 and zeta potential remained unchanged. Thus $mPEG_{5kDa}$-SDM_8 efficiently associates with Arg_4-DAG through a charge-to-charge cooperative complexation that is favoured by the multiple charges of the two components, providing for liposome physical PEGylation at pH 7.4 (Figure 39) while dissociating at pH 6.5 as consequence of the sulfadimethoxine charge loss, which reveals the Arg_4-DAG moieties.

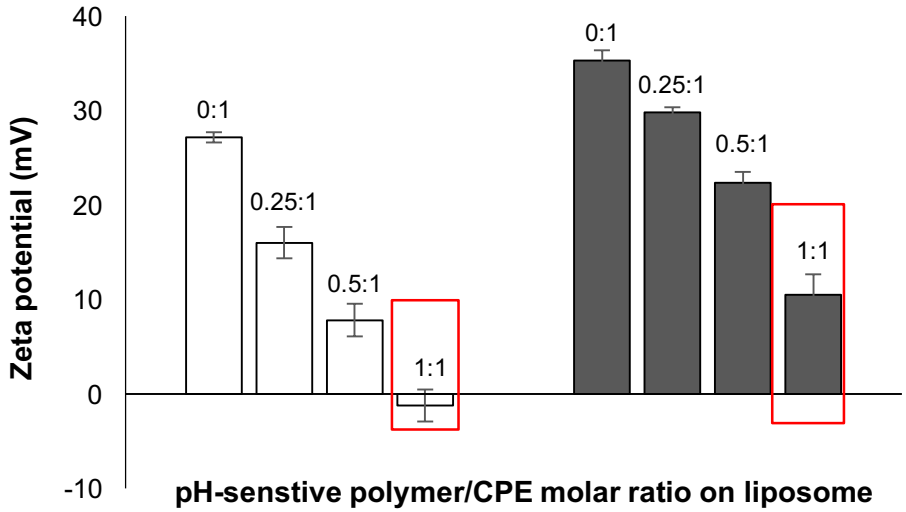

Figure 39. Zeta potential of Arg_4-DAG decorated liposomes in the presence of $mPEG_{5kDa}$-SDM_8 at 0.25:1, 0.5:1 and 1:1 $mPEG_{5kDa}$-SDM_8/Arg_4-DAG molar ratio, at pH 7.4 (□), 6.5 (■).

Notably, the decrease of the liposome zeta potential was proportional to the $mPEG_{5kDa}$-SDM_8ratio with respect to the Arg_4-DAG.

We investigated the liposome pH response in the presence of serum. Four mol% CPE decorated vesicles coated with increasing ratio of the pH-sensitive polymer with respect to the Arg_4-DAG underwent zeta potential analysis. The data in Figure 40 report the zeta-potential of CPE coated and CPE coated PEGylated formulations in diluted serum. It is evident that, whereas serum proteins do not affect the charge of naked liposomes, CPE-decorated vesicles, proteins tend to bind and strip $mPEG_{5kDa}$-SDM_8 from liposome surface at lower molar ratio with respect to the CPE but not from the liposomes coated with a 1:1 $mPEG_{5kDa}$-SDM_8/Arg_4-DAG molar ratio (corresponding to 4 mol% with respect to lipids of each module). The zeta potential of liposomes decorated with 1 and 2 mol % of $mPEG_{5kDa}$-SDM_8 tends to become positive over time when incubated with serum since the CPE is exposed. This result confirms that 4% mol of $mPEG_{5kDa}$-SDM_8 is necessary to ensure a sufficiently strong CPE/$mPEG_{5kDa}$-SDM_8 association on the liposome surface that endow “stealth” properties to the liposomes while circulating in the blood stream.

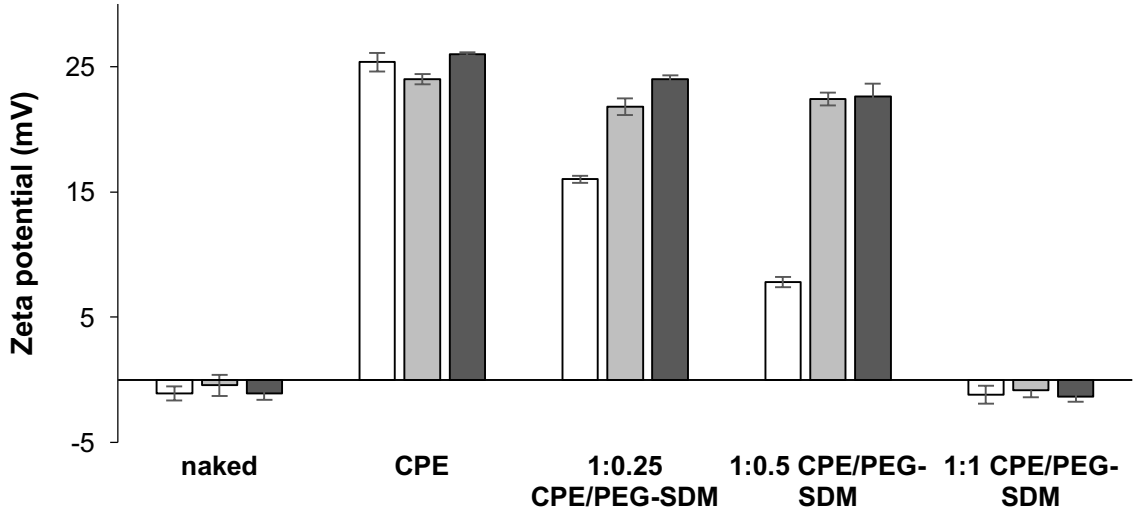

Figure 40. Zeta potential of naked and Arg_4-DAG decorated liposomes in the presence of $mPEG_{5kDa}$-SDM_8 at 1:0.25, 1:0.5 and 1:1 Arg4-DAG/$mPEG_{5kDa}$-SDM_8 molar ratio. The measurements were performed in HEPES buffer at pH 7.4 after liposome preparation (□), in HEPES at pH 7.4 supplemented of 2.5 vol. % of serum immediately after addition (■) and after 1 h incubation at 37°C (■).

3.6.3 MP-SPR measurement

The SPR studies were conducted at the University of Helsinki in the laboratory of prof. Tapani, in order to test the association of the pH sensitive polymer at different pHs and serum proteins with naked and CPE decorated liposomes.

Figure 41 shows typical SPR responses when different liposomes at different pH were adsorbed onto a SPR sensor functionalized with 6kD dextran/decylamine according to Granqvist et al.[168] The signal level indicates that the liposomes adsorbs as intact vesicles because a lipid bilayer would induce a signal response in the range of 0.7-0.8. The star marks the time point when rinsing with the running buffer starts.

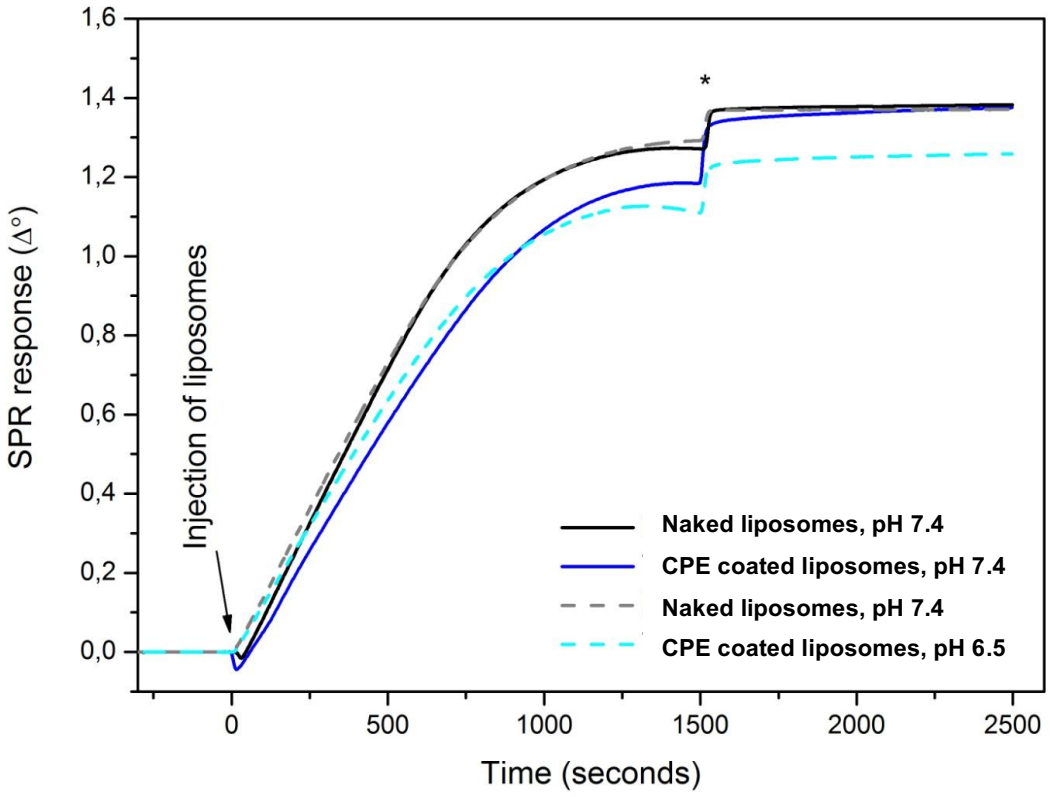

Figure 41. MP-SPR sensogram for imobilization of naked and CPE coated liposomes at pH 7.4 and 6.5.

As observed in the SPR profile, CPE coated liposomes immobilized on the sensor chip with the same efficiency regardless the conditions pH. Notably, the presence of the Arg4-DAG does not affect the efficiency of liposome immobilization with respect to the naked controls.

Figure 42 shows SPR responses when an increasing concentration of the $mPEG_{5kDa}$-SDM_8 is allowed to interact with the sensor chip adsorbed liposomes. Stars mark the time points where rinsing with the running buffer is taking place. The data obtained confirmed a significant interaction of the CPE decorated liposomes with the pH sensitive polymer at pH 7.4, compared to the contact with $mPEG_{5kDa}$-SDM_8 at pH 6.5. Naked liposomes interaction with the pH sensitive polymer was negligible at both pHs.

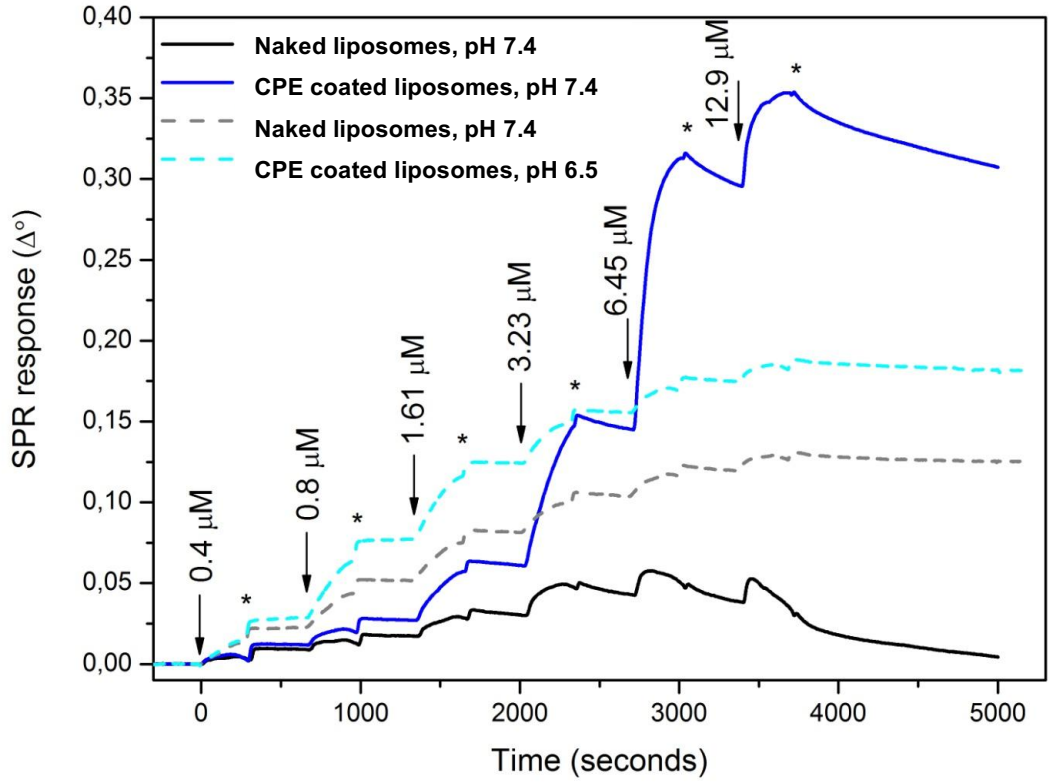

Figure 42. MP-SPR sensogram for imobilization of naked and CPE coated liposomes at pH 7.4 and 6.5, with PEGylation in situ at timepoints.

Figure 42 proves that association of the pH responsive polymer can be measured efficiently using a plasmon resonance approach and that the pH controlled adhesion of the polymer rises a detectable weight change of the liposomes.

3.6.4 Rho-BSA Loading and Release

Rho-BSA loaded liposomes were obtained by rehydrating the lipid film to a final 10 mg/mL lipid concentration using a 2 mg/mL Rho-BSA solution. The procedure was performed according to previously results published by the research group where this thesis was carried out.[178]

The vesicles showed a diameter of 201 ± 6 nm with a polydispersity index of 0.197. After removal of the non-loaded Rho-BSA, RP-HPLC analysis indicated

a Loading Capacity of 25.2 µg Rho-BSA/mg lipids and an Encapsulation efficiency of 2.52%.

Rho-BSA release profile reported in Figure 43 indicates that approximately 30% of the loaded protein was released in 24 h.

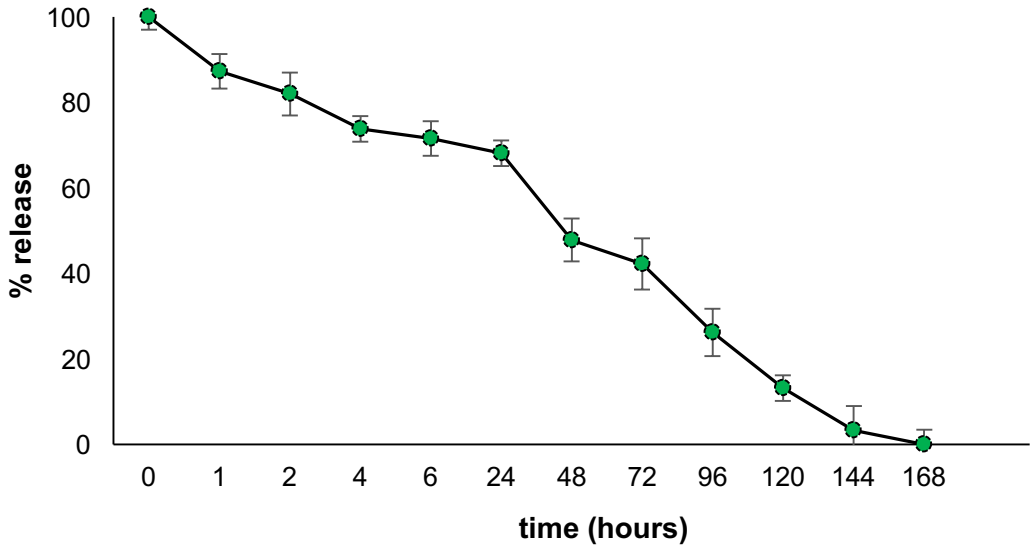

Figure 43. Rho-BSA release from liposomes at pH 7.4.

Notably, Rho-BSA release was complete in about 7 days. The coating of liposomes with CPE, as well as the pH conditions, neither altered the loading capacity nor the release profile.

3.6.5 Calcein Loading and release

Calcein loaded liposomes were obtained by rehydrating a lipid film to a final 10 mg/mL lipid concentration using a rehydration buffer containing 1.87 mg/mL calcein concentration. Calcein was selected as model hydrophilic molecule that do not cross lipid bilayers.[165]

The calcein loaded vesicles showed a main diameter of 197 ± 8 nm with a polydispersity index of 0.117, a Loading Capacity of 52 µg calcein/mg lipids and an Encapsulation efficiency of 5.6%.

The release study was performed on CPE coated liposomes in buffer at pH 7.4 and pH 5.0 mimicking the blood and intracellular liposomal conditions, respectively.

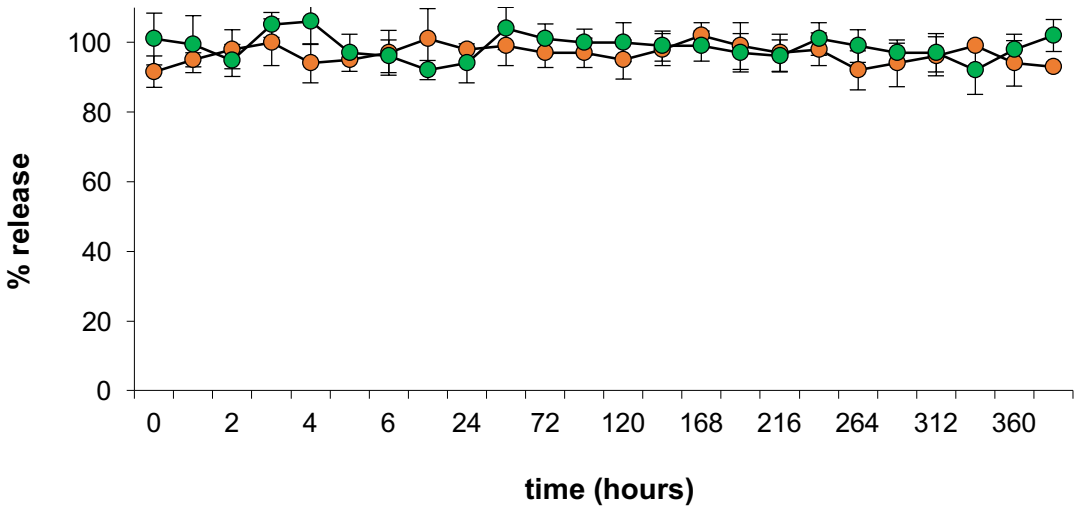

Figure 44. Calcein release profile from liposomes at pH 7.4 (green) and 5.0 (orange).

The profiles in Figure 44 highlight that the encapsulated calcein is not released by liposomes either at pH 7.4 or at pH 5.0 for at least 16 days in virtue of the low permeability of calcein across the lipid bilayer. This behaviour is relevant for the studies performed with cells that were incubated with liposomes for only 1 hour during which no release takes place. Preliminary studies have shown that calcein fluorescence is not affected by the pH.

The coating of liposomes with CPE neither altered the loading capacity nor the release profile.

3.7 Biological Studies

3.7.1 CPE-coated Liposome association with cells

CPE-coated liposomes interaction with cells was assessed by FACS analysis and confocal microscopy. Liposomes were labelled with trace amounts of

rhodamine-DHPE. Rhodamine-DHPE is a convenient fluorescent label that is conventionally used to tag vesicles and nanoparticles when studying their intracellular trafficking. Liposomes coated with 2 and 4 mol % of the CPE with respect to the lipids showed a 65% and 99% of fluorescence positive cells, respectively, demonstrating a significant Arg_4-DAG surface density-dependent association of coated liposomes with respect to naked vesicles (Figure 45). The increase of the uptake profile was in agreement with the increase of the zeta-potential values of the tested formulations, which were of -1 mV, 13 mV and 26 mV for naked liposomes, and liposomes decorated with 2 and 4 mol% of the CPE with respect to the lipids, respectively.

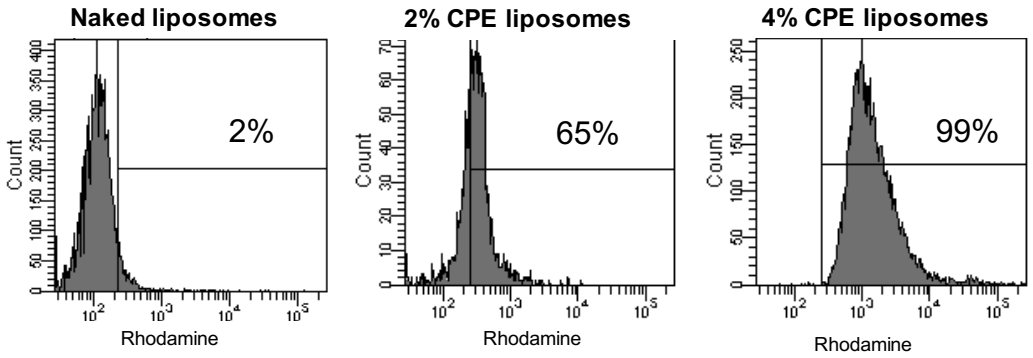

Figure 45. Cytofluorimetric profile of cells incubated with liposomes; from left to right: naked liposomes and liposomes coated with 2 and 4 mol% of Arg_4-DAG.

The cellular disposition of liposomes was then imaged by confocal microscopic analysis. Figure 46 confirms that the liposome association to cells is enhanced by the CPE component and show the vesicle disposition in the cytoplasmic compartment. This information was derived by a dedicated line-scanning analysis (Figure 3D) of the cell image in Figure 3C, which highlight the localization of liposomes (red profile), within the cell membrane (green profile) and the cytosol but not within the nucleus (blue profile). The fluorescence intensities displayed in Figure 3D were calculated along the white arrow of the cell in Figure 3C.

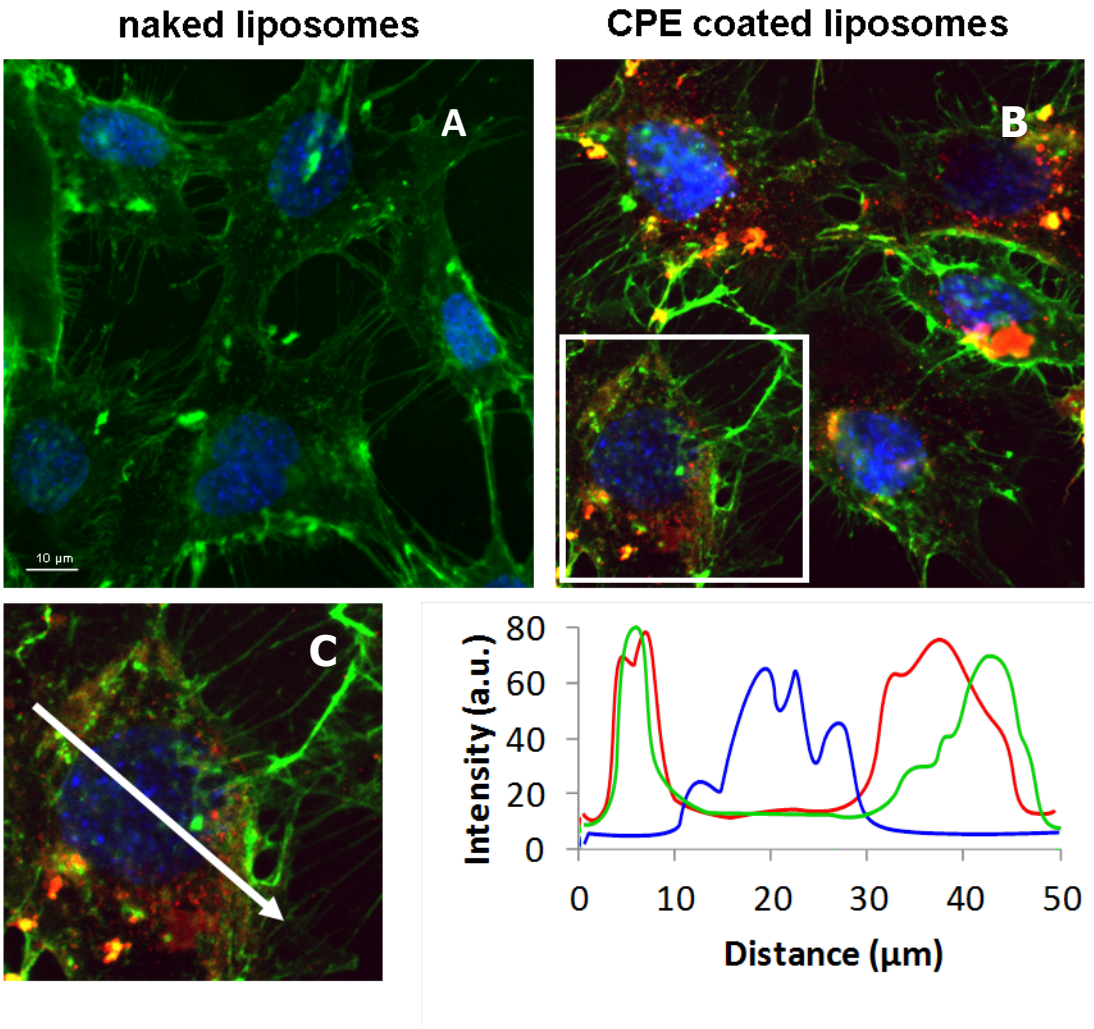

Figure 46. Confocal microscopic image showing the Hela cell association of fluorescently labelled liposomes: A. naked liposomes; B. liposomes coated with 4 mol% of DAG-Arg_4; C. magnification of the white square in B.; D. line-scanning analysis of the cell cross section indicated by the white arrow in C.: (—) DAPI, (—) rhodamine, (—) Alexa Fluor 633.

3.7.2 pH-controlled liposomes association to cells

Liposomes engineered with 4 mol% Arg_4-DAG with respect to lipids and a 1:1 Arg_4-DAG/pH-sensitive polymer molar ratio were investigated for the pH-controlled cell uptake resulting from the shielding/unshielding of $mPEG_{5kDa}$-SDM_8.

The cytofluorimetric profiles reported in Figure 47A and B show that, after 1 h of incubation at pH 6.5, 98% of Hela cells was positive for CPE-coated liposomes either formulated or non-formulated with the pH-sensitive polymer. The

MFI for these cell samples was found to be over 4000 indicating that liposomes underwent massive cell association.

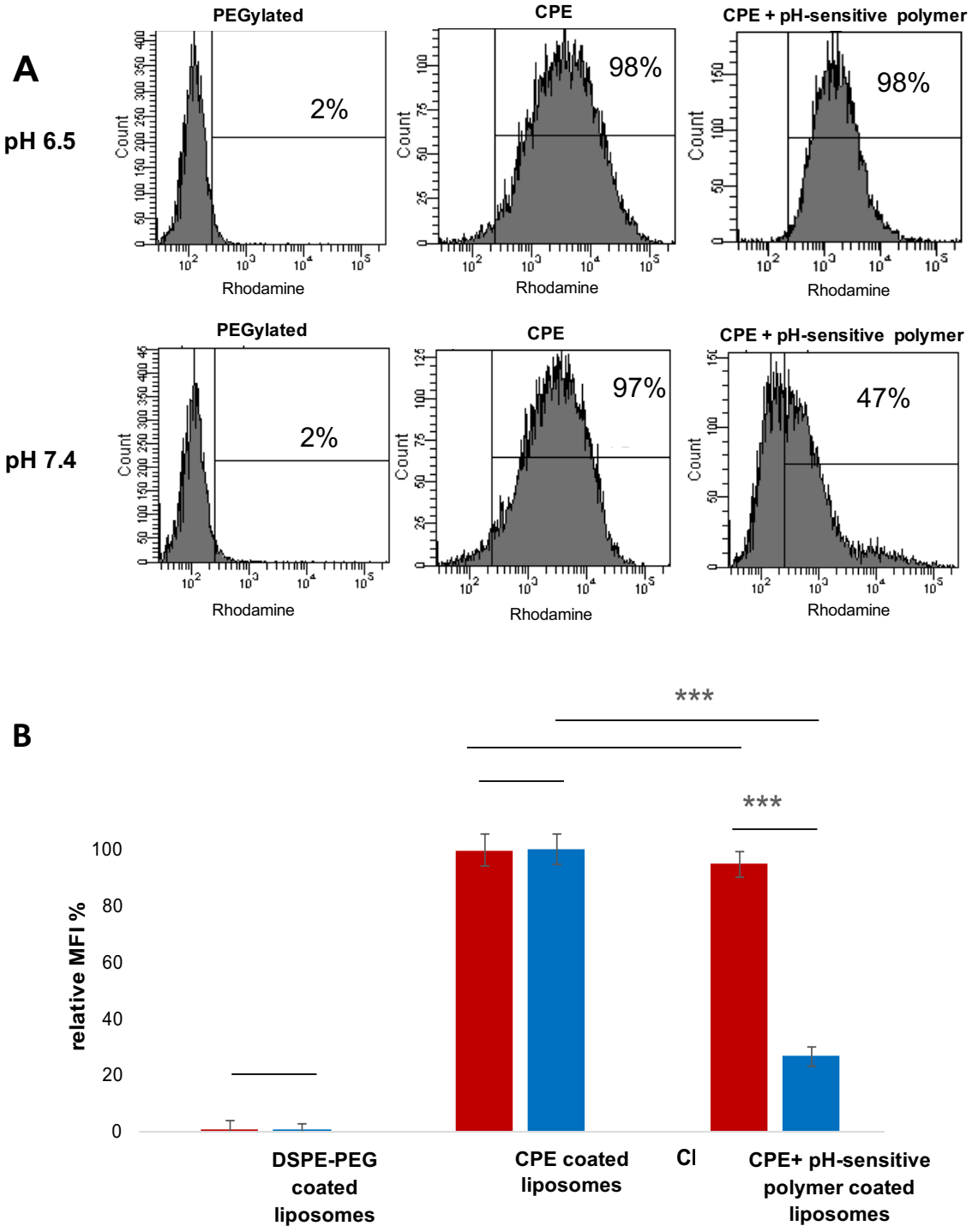

Figure 47. Cell association of rhodamine-DHPE liposomes with Hela cells. (A) percentage of cells with associated liposomes and (B) relative MFI% at pH 7.4 (■) and 6.5 (■). *** $p < 0.001$

At pH 7.4, 97% of cells were fluorescently positive when incubated with CPE-coated liposomes (no $mPEG_{5kDa}$-SDM_8 in the formulation), whereas when liposomes were generated with the $mPEG_{5kDa}$-SDM_8 53% of cells resulted fluorescently negative. The cells incubated with CPE/$mPEG_{5kDa}$-SDM_8 coated liposomes at pH 7.4 displayed an 80% lower relative MFI with respect to CPE-coated liposomes, indicating a very low association with cells compared to formulations without $mPEG_{5kDa}$-SDM_8 at both pHs and liposomes generated with CPE/$mPEG_{5kDa}$-SDM_8 and incubated at pH 6.5. Liposomes PEGylated with commercial DSPE-PEG used as control yielded a quite low cell association at both pHs (2% fluorescently positive cells).

Confocal microscopy (Figure 48) confirmed the cell association of the CPE-coated liposomes when incubated with cells at both pHs. Notably, an intense cytosolic fluorescence was detectable when CPE/pH-responsive polymer coated liposomes were incubated with cells at pH 6.5. This condition promoted the anionic charge loss of the pH responsive block copolymer and its prompt dissociation from the Arg_4-DAG unimers on liposome surface which guided the association with cells and internalization. In physiological conditions (pH 7.4), the CPE/pH-responsive polymer coated liposomes were only detected on the plasma membrane of the cells. Only few fluorescent spots were detectable. This finding is in agreement with FACS analysis that showed a limited association to cells of these liposomes when incubated at pH 7.4. This behaviour could be probably due to the interaction of the polymeric corona of the liposomes with the dendrites of the cells.

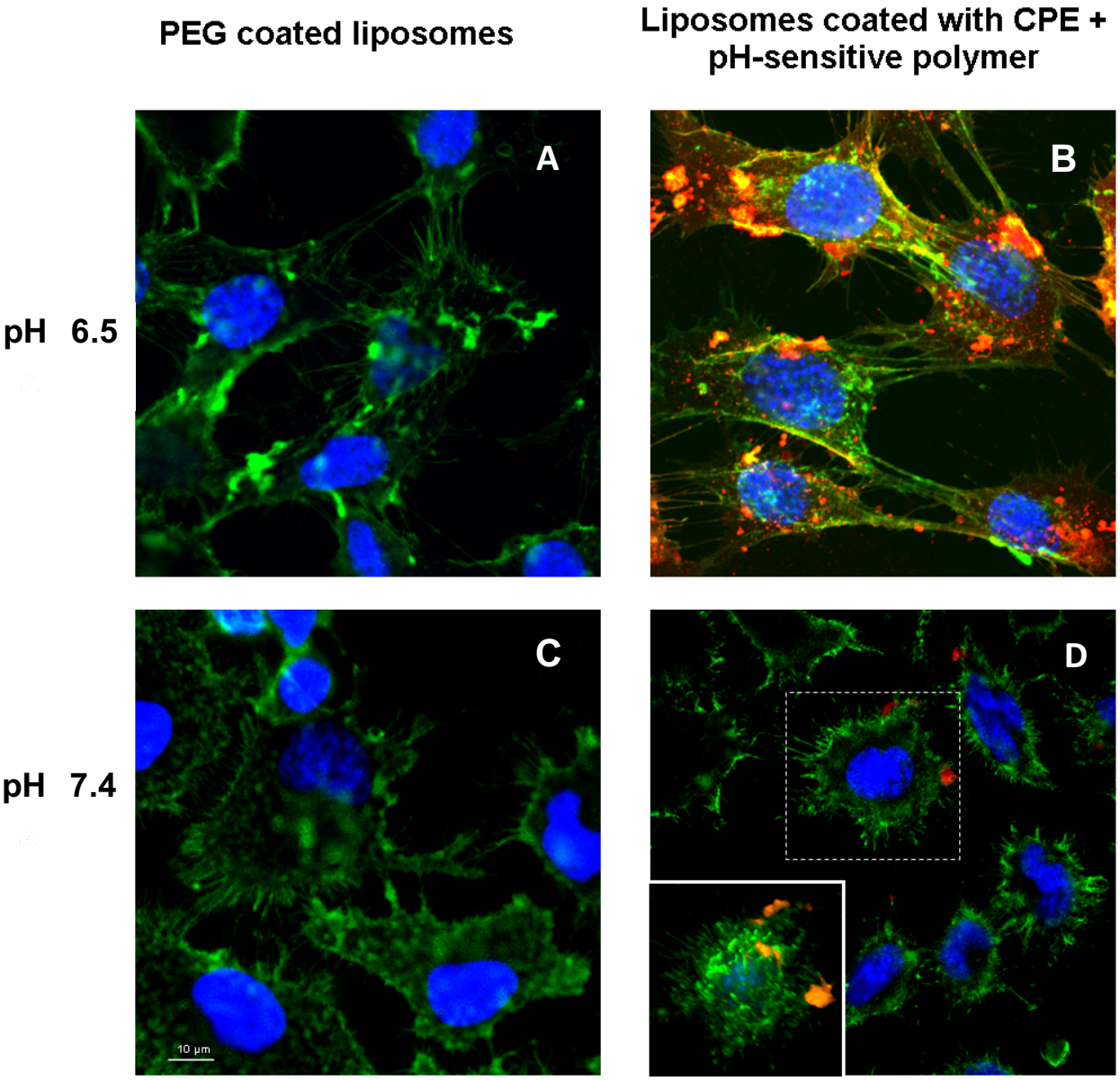

Figure 48. Confocal microscopic images of HeLa cells incubated with: 4 mol% $mPEG_{5kDa}$-DSPE coated liposomes at pH 6.5 (A) and (C) 7.4; liposomes decorated with 1:1 $mPEG_{5kDa}$-SDM_8/DAG-Arg_4 molar ratio at pH 6.5 (B) and (D) 7.4. The white squared area at the bottom left of panel D reports a 3D reconstruction of the cell in the white dotted square.

3.7.3 Rho-BSA intracellular delivery with CPE coated liposomes

In order to investigate the capacity of the CPE coated liposomes to deliver biological macromolecules intracellularly, we have loaded the liposomes with Rhodamine labelled BSA used as model. The cytofluorimetric data reported in Figure 49A and B show that after 1 h of incubation with Rho-BSA loaded CPE-coated liposomes, 33% cells were fluorescently positive while free Rho-BSA and naked liposomes loaded with Rho-BSA yielded negligible cell association. The relative mean fluorescence intensity of cells incubated with Rho-BSA loaded CPE-coated liposomes was about 100% higher with respect to that of cells treated with free Rho-BSA and loaded in naked liposomes.

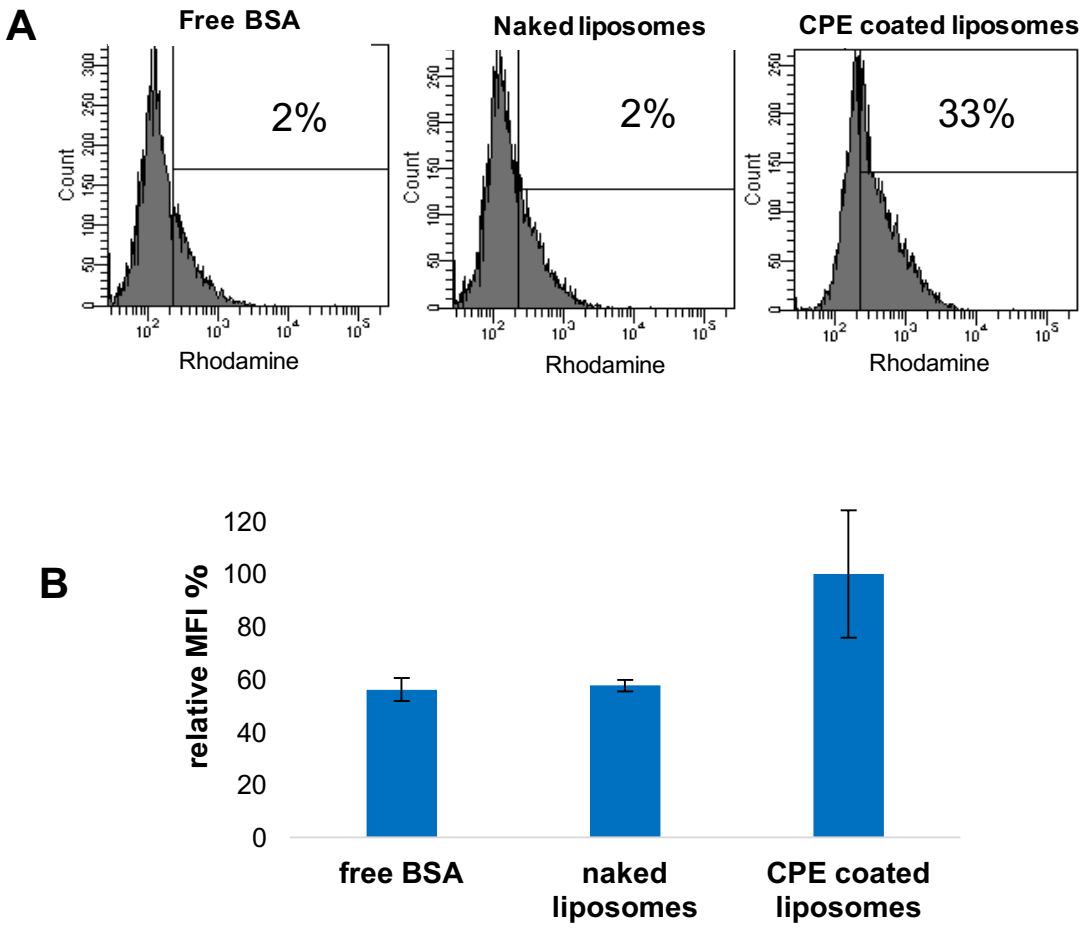

Figure 49. Cell association of Rho-BSA loaded liposomes with Hela cells. (A) Percentage of cells with associated liposomes and (B) relative MFI% at pH 7.4.

Confocal microscopy (Figure 50) demonstrated that the Rho-BSA loaded liposomes decorated with the CPE moiety localize intracellularly, which was not observed for control liposomes and free Rho-BSA. Despite the low intensity of the fluorescent signal that can be ascribed to the low loading of the protein in the liposomes, the microscopic images confirmed the cytofluorimetric data. This result is very relevant for the intracellular delivery of biotherapeutics that is a key challenge for drug delivery science.

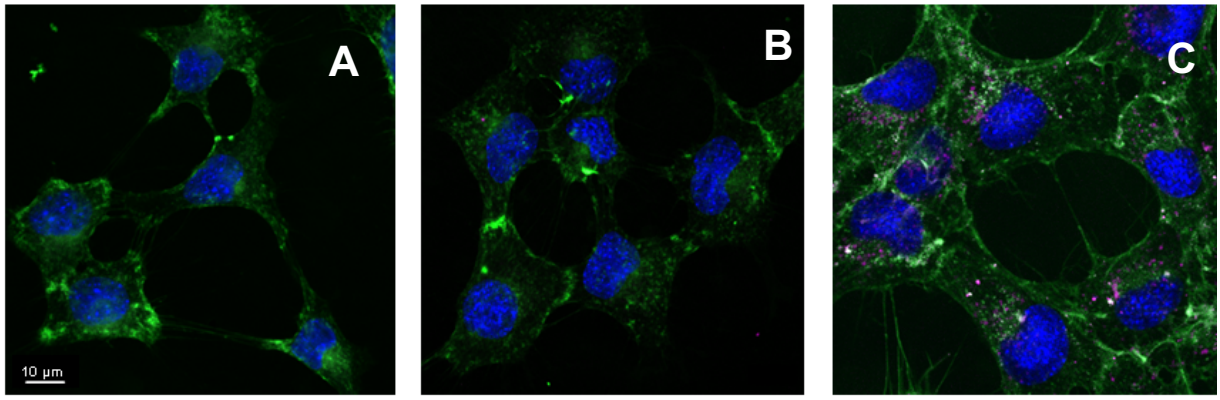

Figure 50. Confocal microscopic images of Hela cells treated with free Rho-BSA (A), naked liposomes (B) or CPE coated liposomes (C) loaded with Rho-BSA.

3.7.4 Liposomes loaded with Calcein

Liposomes were also tested for the delivery of calcein that is conventionally used as model molecule with low permeability through biological membranes. The results of the flow cytometric investigation and confocal microscopy, reported respectively in Figure 51A and B, confirm the ability of the CPE-coated liposomal formulation to deliver calcein to the cytosol of Hela cells while the free calcein did not associate to the cells. The CPE coated liposomes underwent significant cell association, which was not affected by the pH of cell incubation.

The FACS analysis showed that calcein delivery to the cells is controlled by pH environment when liposomes were generated with the CPE/mPEG$_{5kDa}$-SDM$_8$ coating. In fact, while almost 100% of cells resulted calcein positive when incubated with CPE/mPEG$_{5kDa}$-SDM$_8$ coated liposomes at pH 7.4, only 55% of cells

become fluorescently positive when incubated with the same formulation at pH 7.4 and the relative MFI was only 11% with respect to the one observed at pH 6.5.

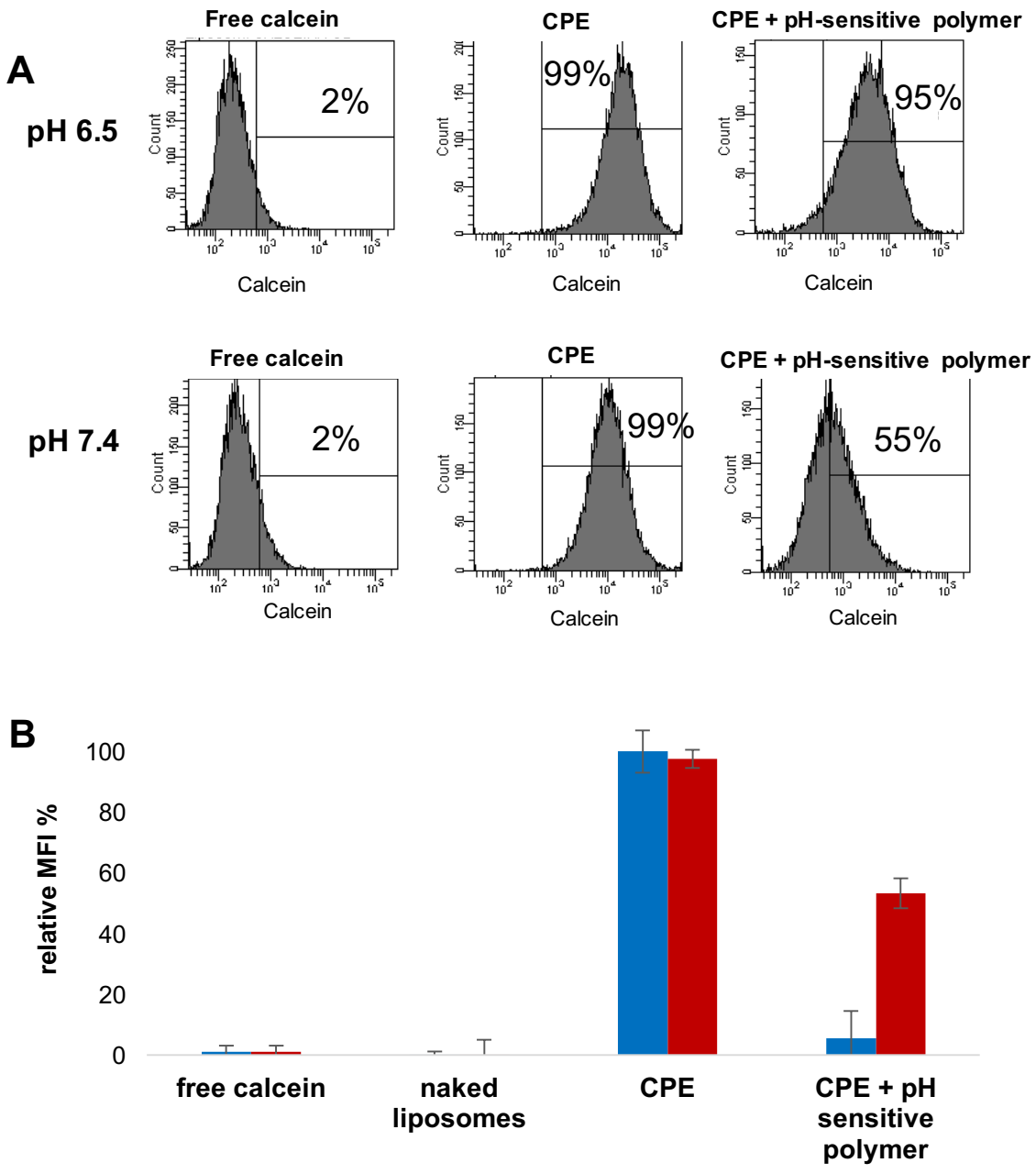

Figure 51. Cell association of rhodamine-DHPE liposomes with Hela cells. (A) % of cells with associated liposomes and (B) relative MFI% at pH 7.4 (■) and 6.5 (■)

Indeed, calcein fluorescence was not detectable under microscopic investigation, indicating a negligible association with Hela. On the contrary, very

dense fluorescence spots were observed in the cytosol of cells treated with CPE coated calcein loaded liposomes incubated with cells at both pHs.

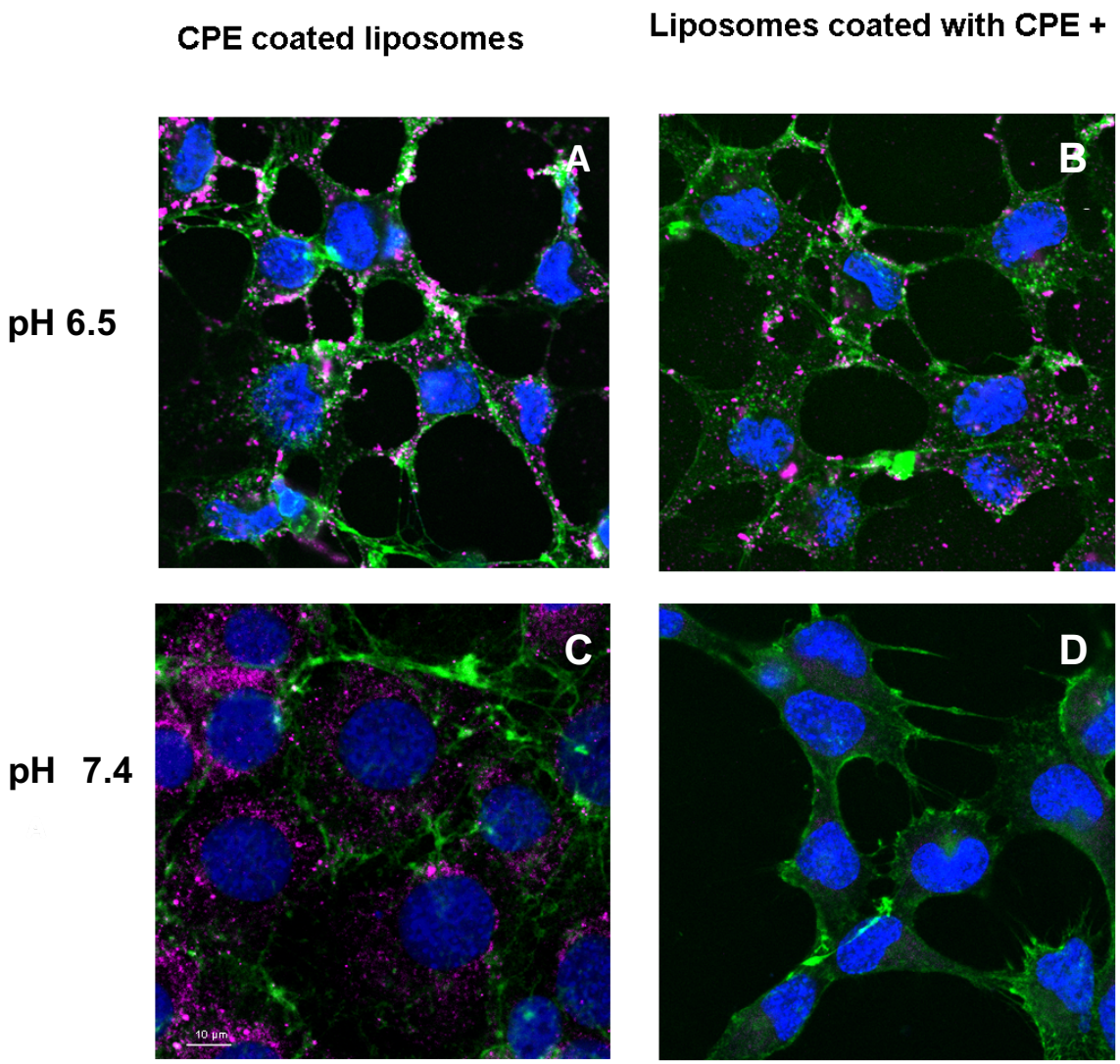

Figure 52. Confocal microscopic images of HeLa cells treated with: CPE coated calcein loaded liposomes at pH 6.5 (A) and (C) 7.4; calcein loaded liposomes decorated with 1:1 CPE/mPEG$_{5kDa}$-SDM$_8$ molar ratio at pH 6.5 (B) and (D) 7.4.

The imaging study (Figure 52) also confirmed that calcein delivery by the CPE/mPEG$_{5kDa}$-SDM$_8$ coated liposomes takes place selectively at pH 6.5, which yielded intracellular well defined fluorescent spots. The intracellular delivery of calcein was also confirmed by a zeta-stack image analysis of a cell (Figure 53). On

the other hand, negligible cell associated fluorescence was observed when cells were incubated with the same pH responsive liposomal formulation at pH 7.4.

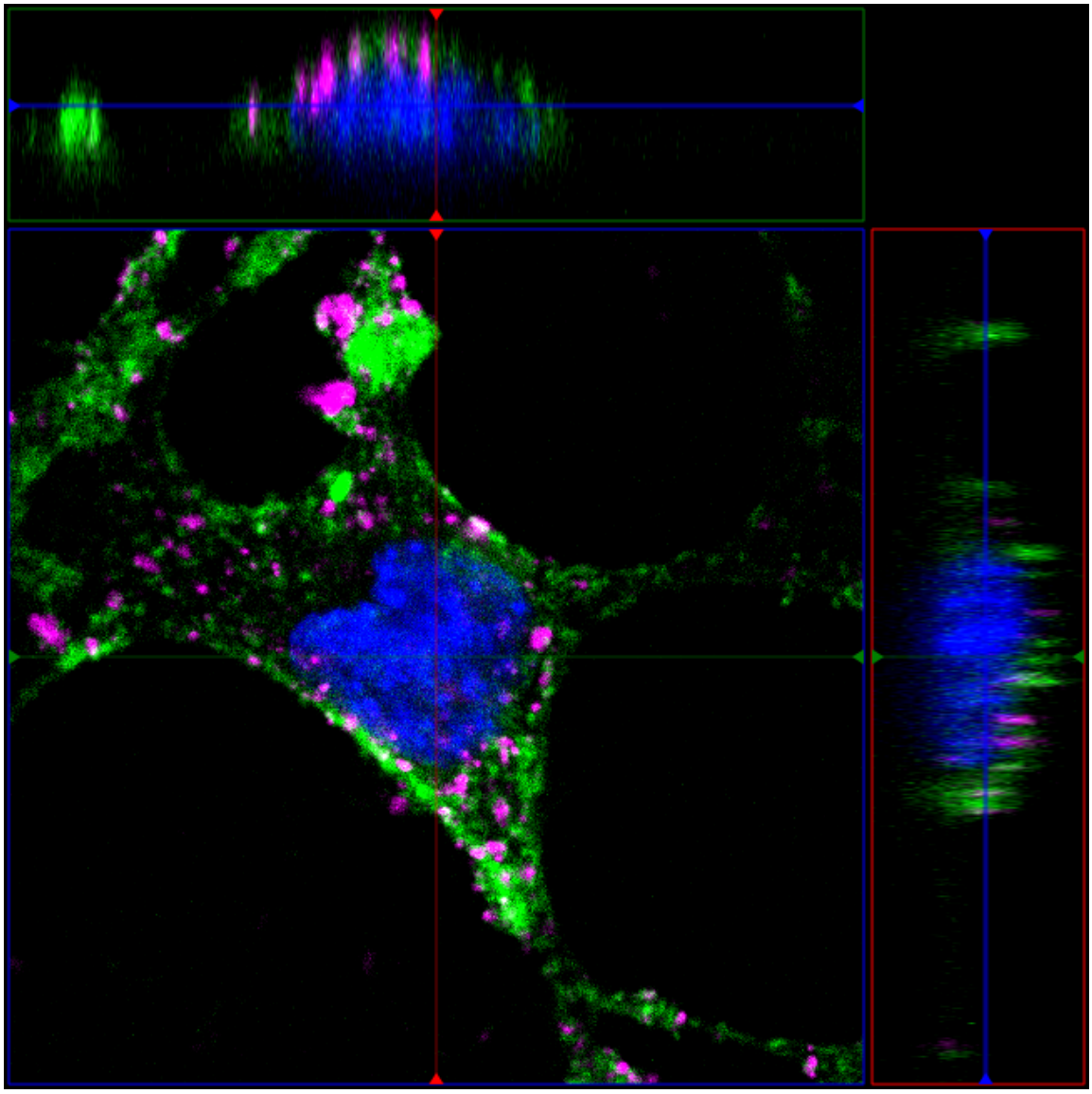

Figure 53. Maximum projections of confocal z-stacks of a cell from sample B of Figure 52.

4. DISCUSSION

The aim of this PhD project was to develop a new pH-sensitive liposomal carrier decorated with a cell penetration enhancer (CPE) for the site specific delivery of drugs to the cancer tissue. The liposomes are well known for their high biocompatibility and for their ability to load relatively high amounts of drugs both in their aqueous core and in their phospholipid bilayer. Furthermore, the liposomes may be administered parenterally, even if they show a nonspecific biodistribution and are rapidly removed from the bloodstream by the reticuloendothelial system (RES) with predominant accumulation in the liver and spleen. To limit the clearance process and to enhance the biodistribution to the tumor, one strategy is represented by the use the liposomal formulations provided with “stealth” characteristics to limit the clearance process and to improve biodistribution or the inclusion of functional components that provide surface properties that ensure responsiveness to local microenvironment for site selective targeting or local release. Liposomes can be thus designed in order to undergo sensitiveness to the environmental alterations of tissues affected by particular pathologies, such as solid tumors or local inflammation typical of arthritis. The tumor tissue possesses, in fact, peculiar features that can be leveraged for the selective targeting of macromolecular and colloidal systems that are aimed at accumulating and releasing the drug where morphological and functional alterations of the vascular, lymphatic system and microenvironment occur. Among the microenvironment alterations that differ the tumor tissue from healthy ones, the most relevant include: amplification of the enzymatic pool, overexpression of specific receptors, increase of the redox potential and temperature and lowering of the extracellular pH.

Conventional liposomes have shown limited efficacy in cancer therapy due to their short plasma half-life. The decoration of these liposomes with biocompatible hydrophilic and flexible polymers, first of all the polyethylene glycol, allows to generate liposomes defined as "stealth" systems in which the polymer is disposed on the carrier surface which reduces their processing and removal by the RES and thus they can persist in the human bloodstream up to 45 hours. Stealth liposomes are able to circulate freely in the bloodstream and, since blood vessels

in healthy tissues have fenestrations of about 5-10 nm, they do not distribute into these tissues by extravasation phenomena nor they are cleared by the kidneys. The tumor tissue, on the contrary, presents an incomplete and discontinuous vascular endothelium (fenestrations can reach 780 nm depending on the type of cancer) which allows the leakage of macromolecules and colloids. Notably, in many cases, the stealth liposome accumulation in the tumor tissue is not sufficient *per se* to ensure the therapeutic effect of the loaded drug which requires a timely release and access to the molecular intracellular target. One strategy to promote the intracellular access of the whole carrier and its drug payload is the decoration of liposome surface with targeting ligands that ensure the selective recognition of receptors overexpressed by cancer cells. However, also this strategy has limitations since the binding of the liposomes to the intended receptor does not always translate in the carrier endocytosis. Another possible strategy to promote the access of the liposomes to cytosol is to exploit the peculiar microenvironmental alterations of the tumor tissue, such as hypoxia, redox imbalances, increased temperature and decrease of pH to trigger the polymeric coating release and adsorption of adsorption of lipidic vesicles to the cell membrane to facilitate cell penetration and release of drugs. We aimed here to explore this strategy by coating the liposomes with a pH sensitive polymer that detach from liposomes surface thus revealing a cell penetration enhancer anchored on the lipid bilayer solely in the site of the tumor tissue.

At first, the thesis project was focused on the selection of a proper lipid mixture in order to generate stable “stealth” liposomes. Stealthiness is a result of the liposome composition and can be conferred to nanocarriers by a proper formulation design based on precise physicochemical determinants. The stealthiness and stability of liposomal carriers relay on the presence and organisation of flexible hydrophilic polymers on the particle surface. Density, thickness and association stability of the polymer are paramount to guarantee those features [95]. The selection of the lipidic mixtures to assemble liposomes was made by comparing the colloidal features of the resulting liposomes [59], as well as the data reported in the literature that are based on three major criteria: 1. in vivo stability, 2. pharmacokinetic profile [98], 3. low activation of the complement system.

All these considerations led to select HSPC, cholesterol and 5 kDa PEG-DSPE as components to assemble liposomes.

Once the lipidic composition had been selected, we focused on the designed and synthesis of the novel cell penetration enhancer (CPE) for the decoration of liposomes.

The design of the cell penetration enhancer was based on in silico simulation. The synthetic procedure to generate the G1 dendrimer scaffold was based on the use of 2,2-bis(hydroxyl-methyl)propionic Acid (bis-MPA) as core of the polyester dendrimer and 2,2-bis(amino-methyl)propionic Acid (bis-AMPA) as building blocks. The CPE function was provided by coupling multiple copies of peripheral arginines to the Dendron. This dendritic scaffold was chosen for its excellent biocompatibility, stability in physiological conditions and biodegradability, already investigated by Feliu et al., which make it suitable for clinical applications. Furthermore, Sheldon reported that cell penetrating peptides with dendritic architecture typically outperform their linear homologues in term of cellular uptake [179], [180] Since Wender demonstrated that the chirality of the backbone of TAT peptide is not crucial for cellular uptake[128], the stereochemistry of the resulting arginine-decorated Dendron was not considered in this thesis work. The Dendron was functionalized to its end with a diacyl glycerol (DAG) that mediate the association of the resulting penetration enhancer to liposomal membrane. The di-stearoyl derivative was selected to mimic a phospholipid but is devoid of free charges as for the phospholipid to avoid intra and intermolecular charge-to-charge interaction and solubility restrictions. The divergently synthetic strategy chosen to obtain the Dendron permits to provide multiple-arm derivatives up to generation (G) 5 with 4n external functionalities (where n = G). The natural TAT peptide possesses 6 arginines (sequence: GRKKRRQRRRPQ), thus the G1 and G2 bis-MPA/bis-AMPA Dendrons are the ones with the closest number of arginines. Notably, while the TAT peptide possesses 8 anionic charges, the G1 dendron we have designed, due to the presence of the both the guanidyl and free ammino groups of Arginines, possess 8 cationic charges at physiological pH. Thus, when comparing the charge number of the TAT peptide and dendrons, a G1 generation better comply the requirements for charge similarity. Furthermore, in order to

predict the theoretical charge density for the G1 and G2 arginine-decorated Dendrons, we calculated the average mutual distance of guanidinium carbons of arginines. This prediction showed that arginines are closer and less hindered in the G1 derivative. The higher hindrance in G2 implies the repulsion and lower charge density with respect to the 4 arginines of the G1 derivative. Moreover, the weight ratios between the polycationic dendritic block and the hydrophobic chains of DAG are 1:2.8 and 1:4.6 respectively for the 4-arginine and 8-arginine derivatives, confirming that the G1 Dendron would have better anchoring capacity to the liposome membrane due to a lower weight ratio of the dendritic block.

Furthermore, You-Rim et al. had already investigated the correlation between the number of arginines and CPE performance in vesicular systems, showing that despite multiple copies of arginines are beneficial to promote cell penetration enhancement, oligomers with three linear arginines, although short, are sufficient to promote efficient intracellular delivery. This was attributed to the cooperative effect that oligo-arginines may have when combined on a nanocarrier surface.[181] Therefore, taking into account the higher positive charge density, the better anchoring capacity, the number of cationic charges with respect to TAT peptide, we decided to synthetize the G1 Dendron bearing four arginines.

The synthesis of Arg_4-DAG was a quite long process that involved 13 steps, each of which included the purification by flash chromatography. The synthetic procedure included the generation of two separate blocks, which were separately synthetized and then combined: the distearolyl derivative terminating with an azide group (DAG), acting as anchor that mimics a phospholipid structure, and the polyester Dendron terminating on one side with a propargyl group. The hydroxyl groups of the bis-MPA monomers were at first converted into amines (bis-AMPA), in order to have a chemical anchor for the conjugation with the carboxyl group of arginine. The conjugation of the oligo-arginine Dendron to the diacyl moiety was achieved through an azide-alkyne Huisgen cycloaddition that is an orthogonal selective click reaction.

Generally speaking, CPPs possess no selectivity towards cellular targets. In fact, they promote a non-specific uptake by cells as consequence of a charge-to-charge electrostatic association to the proteoglycans on the cell membrane

surface. Thus, a polyanionic oligo-sulfadimethoxyl derivative was synthesized in order to be associated on the Arg_4-DAG decorated liposome surface as PEGylating agent and ensure the internalisation of liposomes in acidic micro-environmental conditions when it is induced to detach from liposomes. The oligo-sulfadimethoxyl block of the PEG based copolymer was designed in order to be deprotonated and anionic under physiological pH conditions (pH 7.4) in which condition it is capable of interacting electrostatically with the guanidyl cationic charges of oligo-arginine and shield the synthetic CPE with the pendant PEG chain. However, the oligo-sulfadimethoxyl block in slightly acidic pH result protonated and neutral thus dissociating from the oligo-arginines on the liposome surface. This causes the exposure of the CPE on the liposomal surface, and the interaction of the vesicular system with the anionic charges of the proteoglycans of the cancer cell cellular membranes and the internalization of the drug delivery system. Thus an intracellular and locally controlled drug delivery is expected with this “smart” nanocarrier.

A copolymeric of oligo-methacryloylsulfadimethoxine was synthesized starting from a 5 kDa amino-methoxy-polyethylene glycol. The synthesis of the derivative $mPEG_{5kDa}$-SDM_8 was realized by a radical polymerization of methacryloyl-sulfadimethoxine obtained by acylation reaction of the anilyl amine of sulfadimethoxine with methacryloyl chloride. The ATRP reaction was performed in water where the Cu catalyst remains in solution as chelated to TPMA. The Cu catalyst was added to the reaction mixture in the oxidized form Cu (II) and the reaction was initiated by the addition of ascorbic acid, which generates in situ the metal activator Cu (I). The monomer SDM was added in a molar ratio such as to obtain a maximum number of SDM residues per polymer chain up to twelve. Previous studies have shown that the $mPEG_{5kDa}$-SDM_n copolymer has appropriate responsive acid properties in pathological conditions when the degree of polymerization is between 7 and 12. Moreover, in silico studies performed by Ravazzolo[164] using elaboration of the chemical structure of a set of SDM derivatives showed that the pKa of the SDM bioconjugates increases as SDM units increases, plateauing at 7.3 with 9 SDM units. Therefore, to obtain a co-polymer that undergoes a phase transition in the physiopathological pH range of 6.9–7.2, the optimal number of SDM was calculated to be 7. The pKa of $mPEG_{5kDa}$-SDM_8

was in fact calculated to be 7.1 in the in silico simulation. This derivative was expected to display an overall negative charge at pH above 7.2, which bestows more hydrophilic character on the polySDM block and rapidly switches to the unionised hydrophobic form as the pH decreases.

After purification, the purity of the co-polymer obtained was determined by RP-HPLC analysis that showed no traces of unreacted SDM monomers. The degree of modification of the polymer was established by the iodine test and the UV-Vis analysis: the spectroscopic analysis (concentration of SDM and PEG in a solution of $mPEG_{5kDa}$-SDM_n) showed a molar ratio PEG/SDM of 1:8, which is in line with the desired conversion and the polymerization conditions adopted. This result was further confirmed by ^{1}H-NMR, in which the signal at 3.74 ppm relative to the aromatic ring of the methoxyl sulfadimethoxine integrated for 56 protons.

Finally, Arg_4-DAG decorated liposomes were prepared by thin layer evaporation technique. The results showed that liposomes of about 200 nm in size were obtained and that the post-extrusion decoration with the Arg_4-DAG does not alter significantly the size of the liposomes. On the other hand, the presence of the oligo-arginine lipid on the liposome bilayer was confirmed by the zeta potential that significantly increased upon decoration with Arg_4-DAG. Notably, the higher the density of Arg_4-DAG within the lipid bilayer the higher was found the absolute value of the zeta potential. In the preliminary formulative study, liposomes were decorated with increasing molar ratio of the CPE from 1 to 8% with respect to lipids. Zeta potential analysis showed that at CPE molar ratio higher than 4% the surface charge tends to a plateau. This percentage was thus selected for the further investigations, being in line with other cationic vesicle formulations decorated with TAT-like derivatives.

A dedicated study showed also that the zeta potential of the liposomes can be, at least in part, affected by the salt of the buffer used to disperse these cationic liposomes. As shown in Figure 38, all buffers induced a decrease of the zeta potential with respect to water which can be ascribed to charge shielding. In particular, the phosphate buffer caused a higher decrease with respect to HEPES. Sodium and mannitol behaved mostly similarly in term of charge shielding in the presence of phosphate as well in the presence of HEPES/MES.

According to the system design and the expected responsiveness, the shielding capacity of the pH-sensitive polymer was tested by incubating the cationic liposomes with increasing amounts of $mPEG_{5kDa}$-SDM_8, ranging from 0 to 1 molar ratio with respect to Arg_4-DAG at pH 7.4 and 6.5, mimicking physiological and cancer conditions respectively. It was observed that when the CPE and the polymer are at equimolar ratio in the liposomal formulations, the surface charge of the liposomes is screen at pH 7.4, while at pH 6.5 the zeta potential remains positive as a result of no charge-to-charge mediated interaction of the two functional components. Overall, the evidence showed that at pH 7.4, a 1:1 Arg4-DAG/mPEG-SDM molar ratio is required to fully shield the cationic charge of the liposomes when a 1:1 interaction between the 8 negative charges of the oligo-methacryloylsulfadimethoxine of the co-polymer and the 8 positive charges of the CPE (4 guadidinum + 4 amino groups) occurs. It has also been confirmed that the presence of serum proteins didn't alter the interaction between the pH responsive polymer and the CPE in the 1:1 CPE/pH sensitive polymer formulation which was then selected for SPR and biological studies. This information is crucial to ensure the exploitability of the drug delivery system in vivo.

The SPR study confirmed the association between the $mPEG_{5kDa}$-SDM_8 and the CPE under neutral conditions (pH 7.4) while the pH responsive polymer dissociate from the lipidic vesicles at pH 6.5 mimicking the tumor.

Liposomes were then loaded with calcein and fluorescently tagged albumin, which were chosen as model molecules as proxy for low and high molecular weight hydrophilic drugs. BSA was loaded using a protocol previously validated by the research team, which yielded a loading capacity of 25.2 µg per mg of lipids. Calcein was instead loaded according to a newly developed method that allowed to encapsulate 52 µg per mg of lipids. Both formulations were purified by dialysis in order to remove the non-encapsulated BSA and calcein, respectively. The release studies allowed to observe that the calcein wasn't released from the liposomes for at least 16 days, while BSA release was complete in 7 days. Notably, the pH conditions as well as the decoration with the CPE and the pH sensitive polymer were proved not to alter the release profiles.

The cell penetration capacity of liposomes labelled with rhodamine-DHPE and decorated with the synthetic CPE Arg_4-DAG was assessed by biological studies with HeLa cells. The results shown in Figure 47 of the cytofluorimetric study clearly indicate that the liposomes decorated with Arg_4-DAG associate with the cells with an efficiency that is about 30 times higher compared to that of liposomes used as a control. The efficiency of association very well correlated with the density of the oligocationic derivative Arg_4-DAG on the liposomes surface. The results confirmed that the synthetic CPE remains tightly associated to the liposome bilayer along the biological studies which can be ascribable to the weight ratio between the dendronic component and the dialkyl moiety on the Arg_4-DAG. Furthermore, the conformation of the oligo-arginyl dendronic moiety possess a suitable charge density that remote very efficiently the interaction of the cationic vesicles with the cell membrane associated proteoglycans.

The drug delivery efficiency of the CPE coated liposomes was then tested using the liposomal formulations loaded with albumin and calcein. The ability of the system to deliver the two molecules was confirmed, both by flow cytometry and by confocal microscopic investigation. Notably, very negligible BSA release occurs during incubation with cells, (only about 10% of the loaded BSA) which, however, does not affect the intracellular liposome mediated delivery of the biomolecule since BSA is not permeable to biological membranes as confirmed by incubation of cells with Rho-BSA. The results, therefore confirmed the delivery of the encapsulated protein to the Hela cells by the liposomal vehicle functionalized with CPE. Calcein was also efficiently delivered to the cells. Undecorated vesicles (no CPE coating) used as control couldn’t promote the delivery of the model molecules under the same conditions tested.

Finally, a cell study confirmed the pH controlled shielding of the pH-sensitive polymer and the resulting association of liposomes under acid conditions. Non loaded liposomes decorated with 4% of CPE and 4% of pH sensitive polymer were first tested with Hela cells, both at pH 7.4 and 6.5, which confirmed that the polymer, under physiological conditions, prevents the interaction of CPE engineered vesicle with the cells. Under tumor conditions, on the contrary, the charges of the sulfadimethoxine are protonated, according to the pKa, and the

mPEG-SDM polymer dissociates from the surface of the vesicles, whose cell penetration behaviour was restored. The association of the pH responsive liposomes with cells at pH 7.4 was mainly ascribable to a slightly capture of the liposomes by the testicular branches of the Hela cells. Confocal images showed clearly that under this condition the liposomes do not access the cytosol but remain adsorbed mostly on the outer cell membrane. On the contrary, massive intracellular fluorescent red spots occurred for cells incubated with pH responsive liposomes incubated at pH 6.5.

The pH controlled liposomes association to cells was confirmed when liposomes were loaded with calcein, confirming the potential of the liposomal system to be used for the delivery of drugs. The results confirmed that these liposomes provide for intracellular delivery of drugs that are impermeable to cell membranes and can do that selectively under pH environmental control.

5. CONCLUSIONS

This project was aimed at developing a novel liposomal carrier decorated with a synthetic CPE to facilitate the access to the cytosolic compartment of the nanocarrier and its drug payload. A pH-sensitive polymer that responds to pH physiopathological alterations was also synthesized to shield the CPE under physiological conditions(namely the blood stream) while revealing it at acid pH conditions of the tumor. Therefore, the sequential decoration of liposomes with the CPE and the masking agent allows the generation of “smart” vesicles for site-selective anticancer drug delivery.

This novel carrier is intended for the delivery of drugs to the tumor tissue. Actually, the environmentally controlled shielding and revealing capacity of $mPEG_{5kDa}$-SDM_8 can endow this family of PEGylated liposomes with enhanced site selectivity to the tumor by locally regulating the access of the liposomes to the cytosolic compartment and the loaded cargo delivery.

In vitro results have shown that the components ratios on the liposome surface must be properly selected in order to provide for colloidal stability and the pH responsiveness of the liposome formulation, which was proven to successfully vehiculate hydrophilic loaded molecules in the cytoplasmic compartment of cells selectively at tumor pH, whereas $mPEG_{5kDa}$-SDM_8 is able to prevent liposome cell internalization upon physiological conditions.

6. APPENDIX

Compound **1**: *Benzyl 3-hydroxy-2-(hydroxymethyl)-2-methylpropanoate*

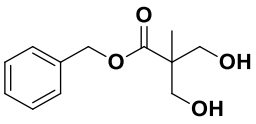

^{1}H-NMR (300 MHz) in $CDCl_3$

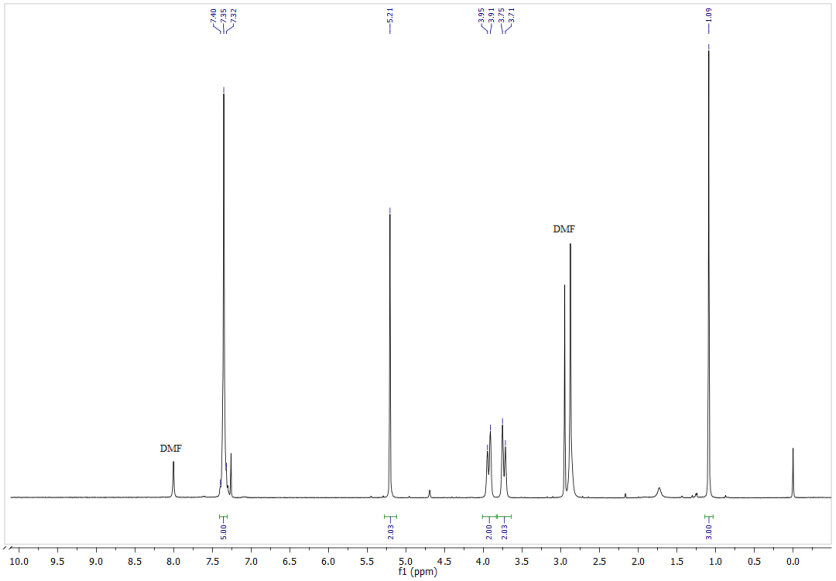

^{13}C-NMR (75 MHz) in $CDCl_3$

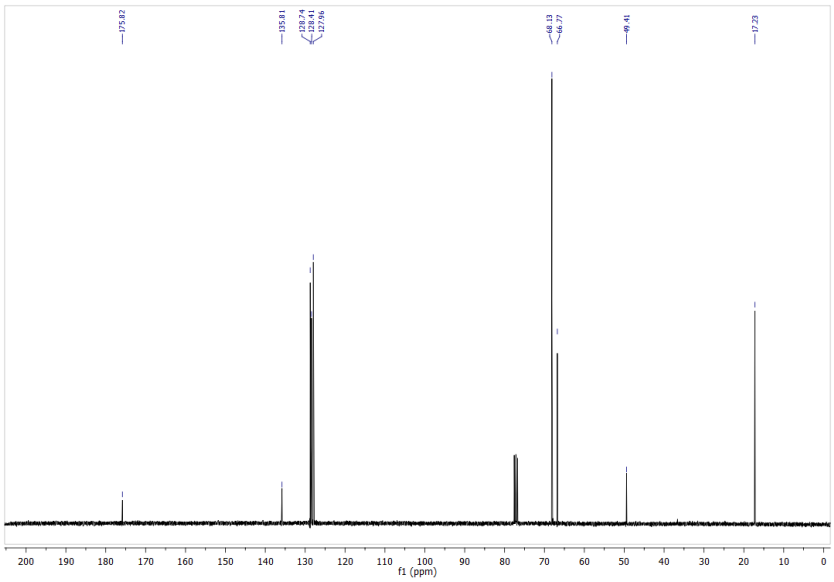

Compound **2**: *Benzyl 2-methyl-3-(tosyloxy)-2-((tosyloxy)methyl)propanoate*

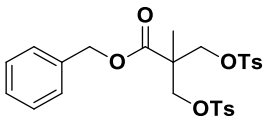

^{1}H-NMR (500 MHz) in CDCl3

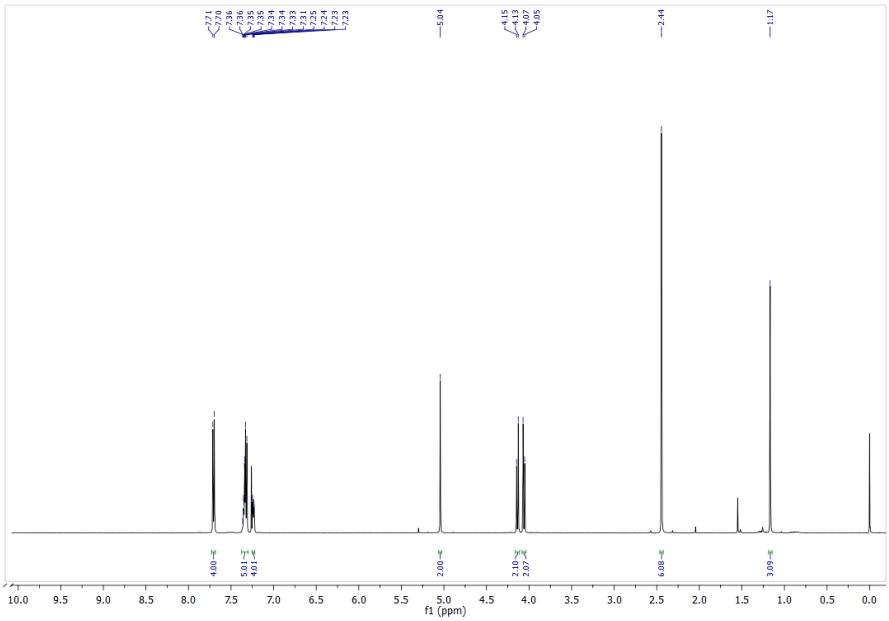

^{13}C-NMR (126 MHz) in $CDCl_3$

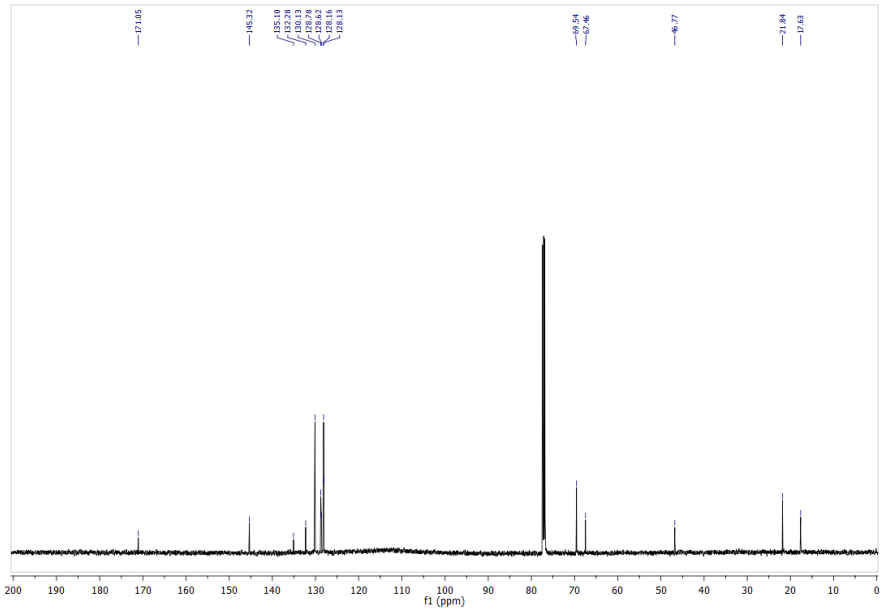

Compound **3**: *Benzyl 3-azido-2-(azidomethyl)-2-methylpropanoate*

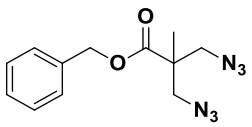

^{1}H-NMR (500 MHz) in $CDCl_3$

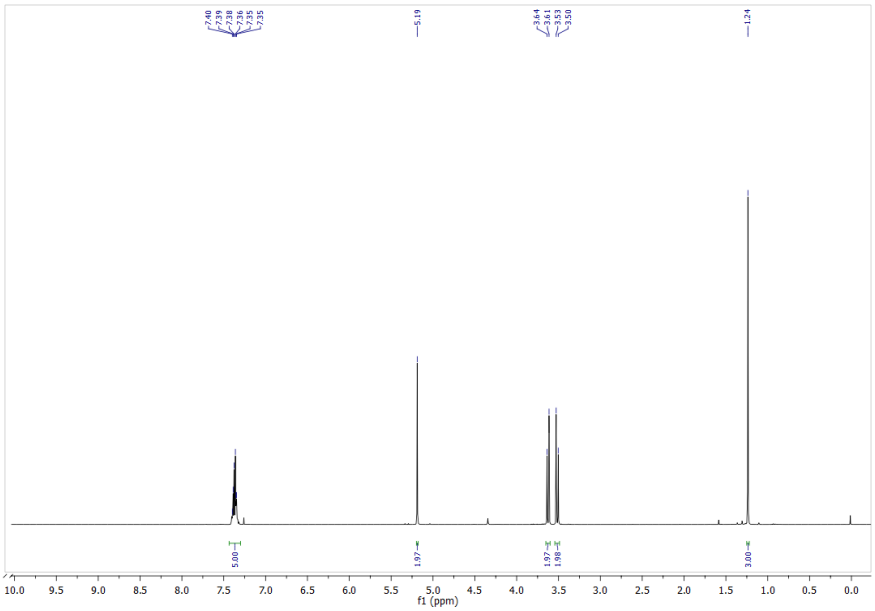

^{13}C-NMR (126 MHz) in $CDCl_3$

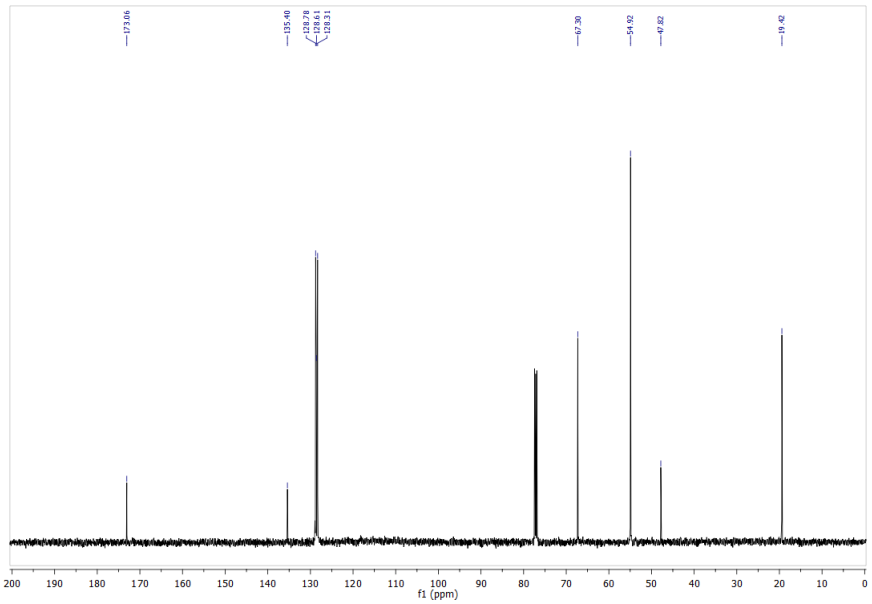

Compound **4**: *3-((tert-butoxycarbonyl)amino)-2-methyl-2-(pivalamidomethyl)propanoic acid*

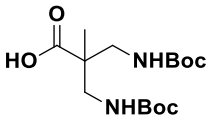

^{1}H-NMR (300 MHz) in $CDCl_3$

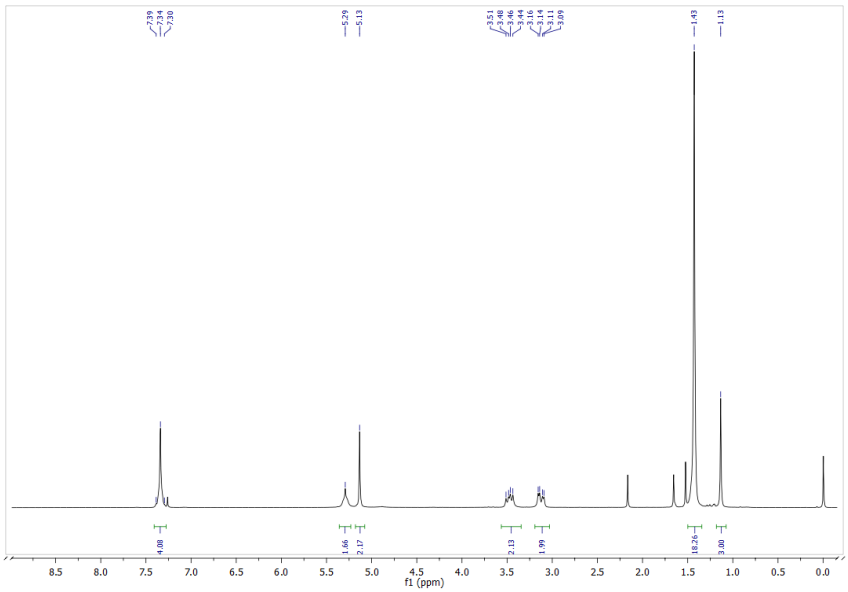

^{13}C-NMR (75 MHz) in $CDCl_3$

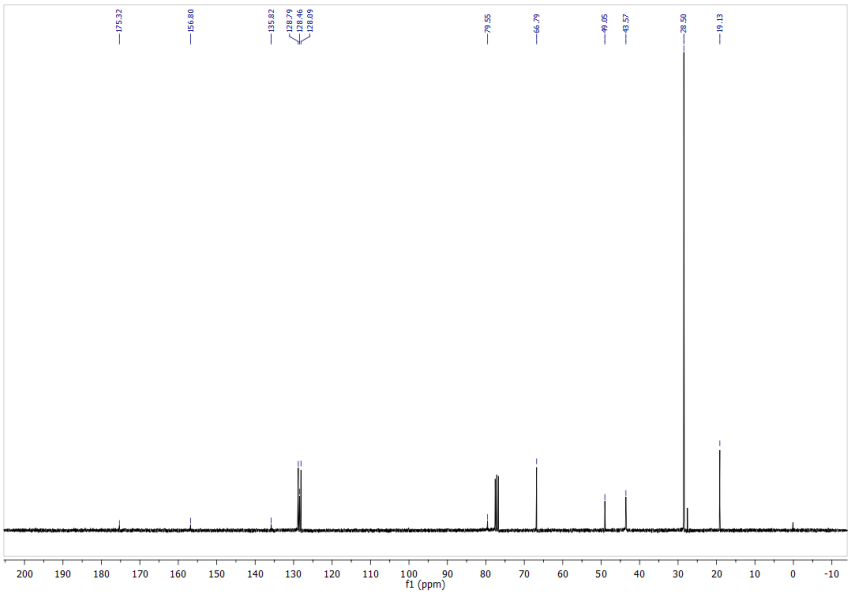

Compound **5**: *2,2,5-trimethyl-1,3-dioxane-5-carboxylic acid*

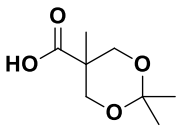

^{1}H-NMR (500 MHz) in $CDCl_3$

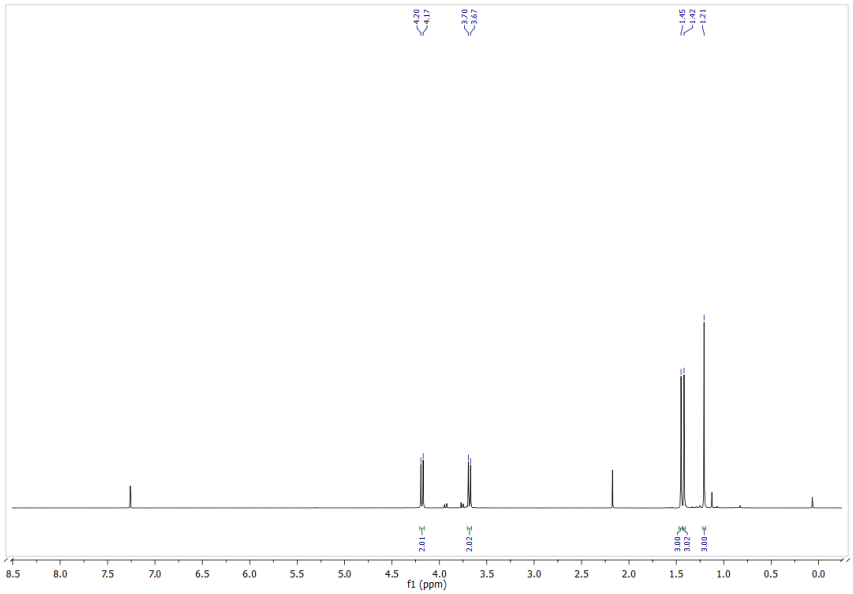

^{13}C-NMR (126 MHz) in $CDCl_3$

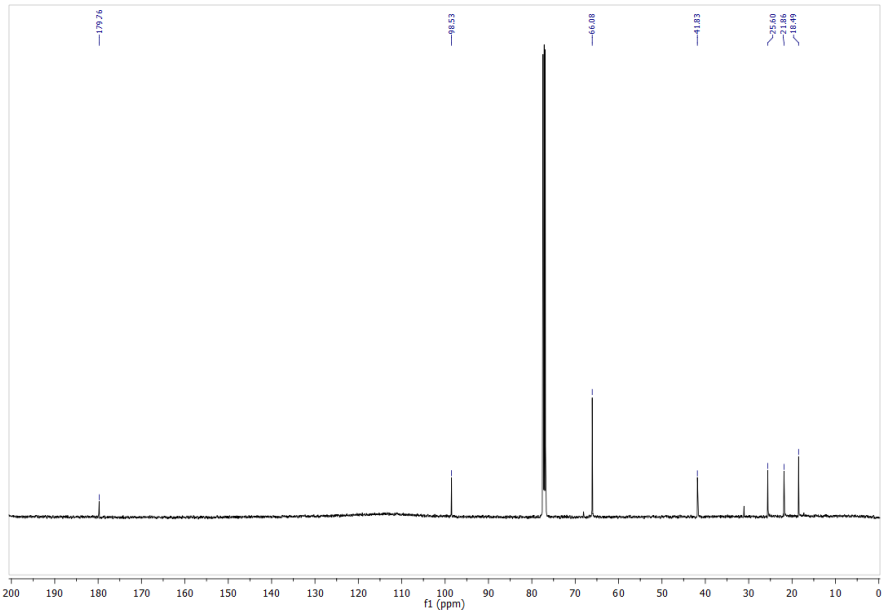

Compound **6**: *2,2,5-trimethyl-1,3-dioxane-5-carboxylic anhydride*

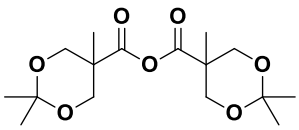

^{1}H-NMR (300 MHz) in $CDCl_3$

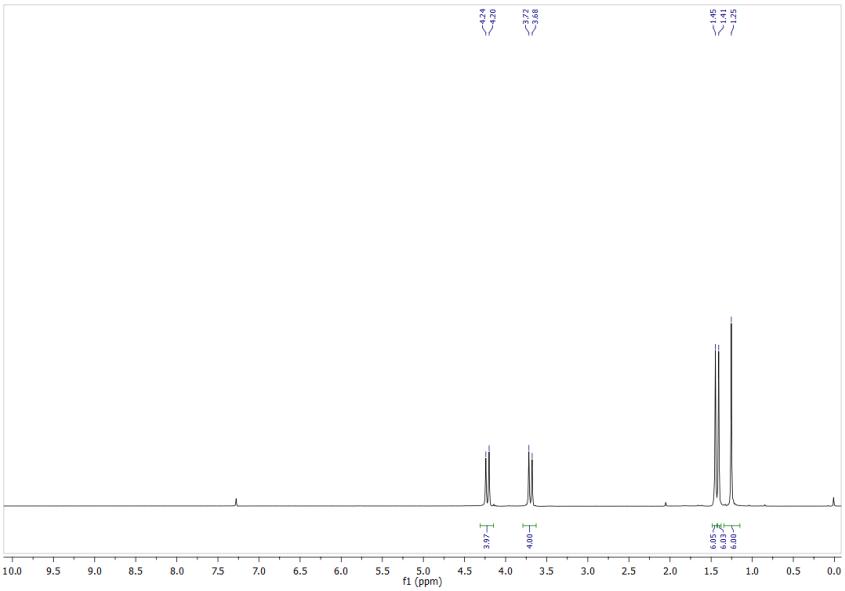

^{13}C-NMR (75 MHz) in $CDCl_3$

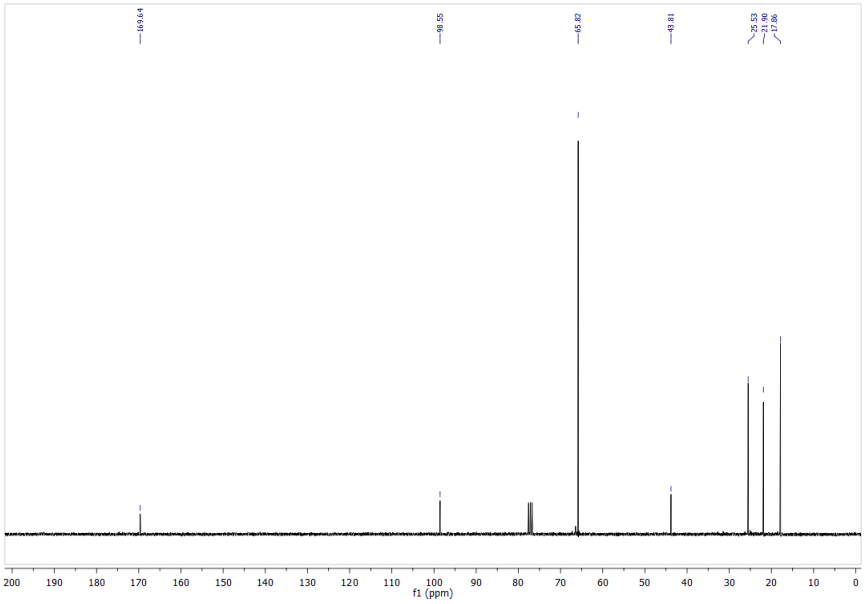

Compound **7**: *Prop-2-yn-1-yl 2,2,5-trimethyl-1,3-dioxane-5-carboxylate*

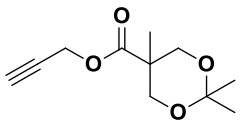

^{1}H-NMR (300 MHz) in $CDCl_3$

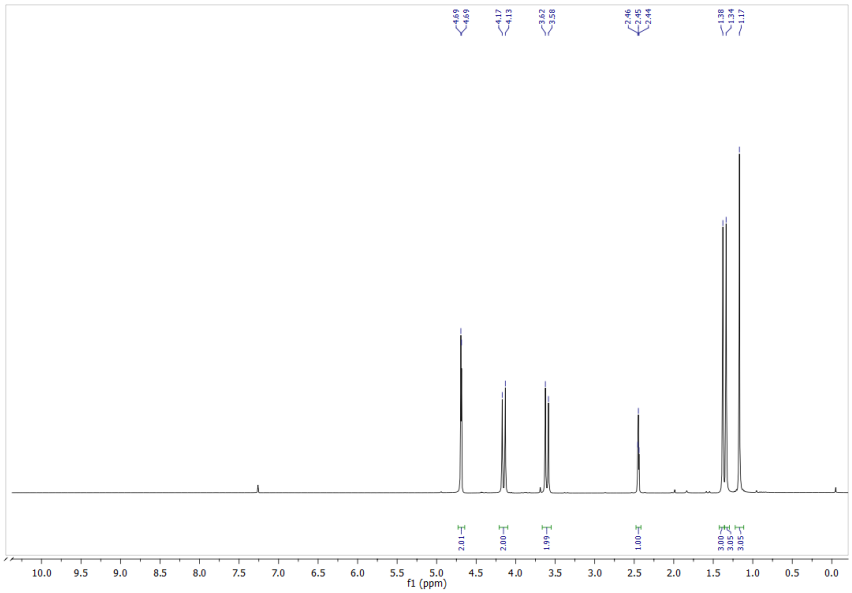

^{13}C-NMR (75 MHz) in $CDCl_3$

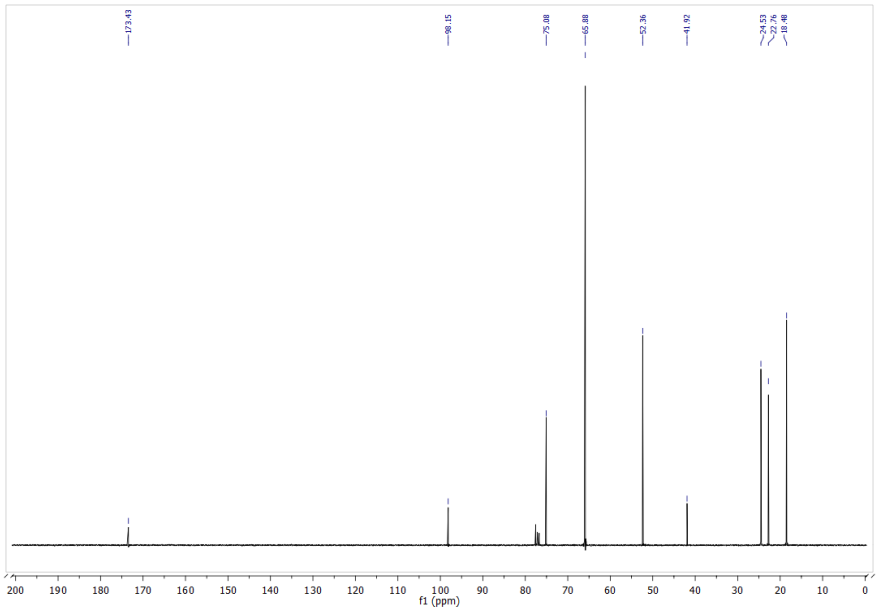

Compound **8**: *Prop-2-yn-1-yl 3-hydroxy-2-(hydroxymethyl)-2-methylpropanoate*

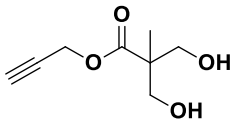

^{1}H-NMR (300 MHz) in $CDCl_3$

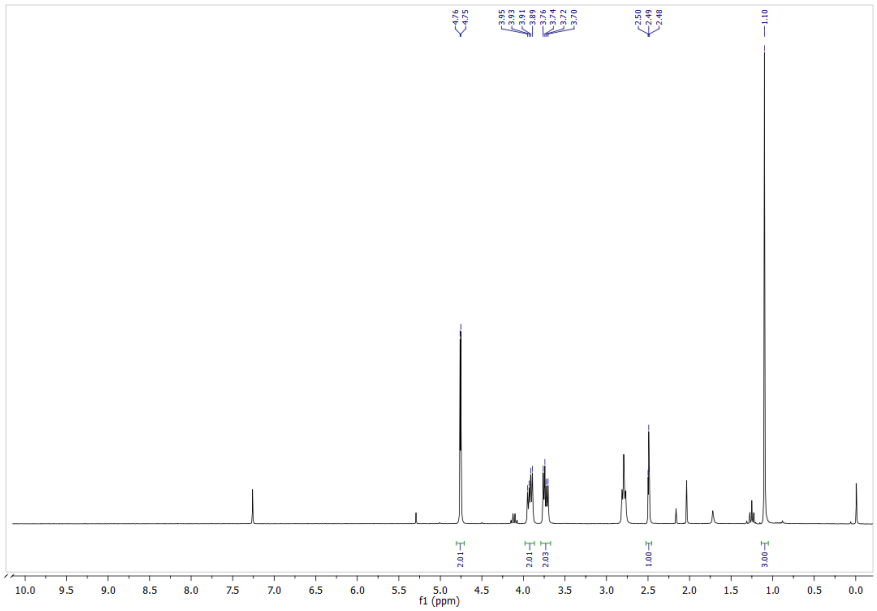

^{13}C-NMR (75 MHz) in $CDCl_3$

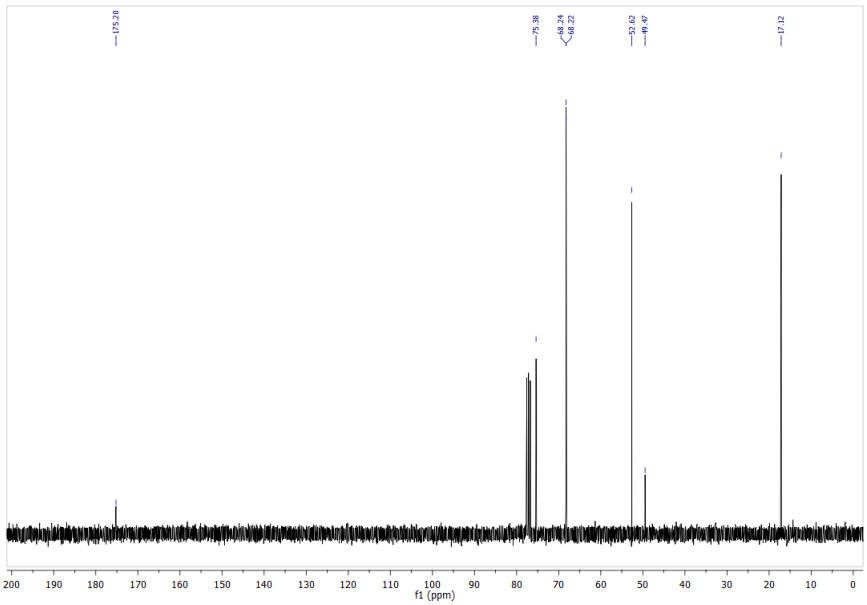

Compound **9**: *2-methyl-2-((prop-2-yn-1-yloxy)carbonyl)propane-1,3-diyl bis(3-((tert-butoxycarbonyl) amino)-2-(((tert-butoxycarbonyl)amino)methyl)-2-methylpropanoate)*

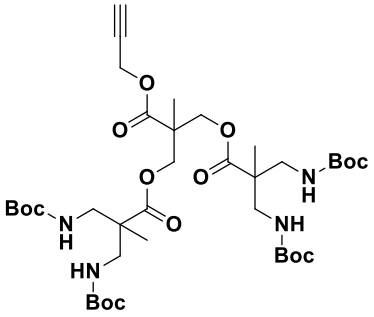

^{1}H-NMR (200 MHz) in $CDCl_3$

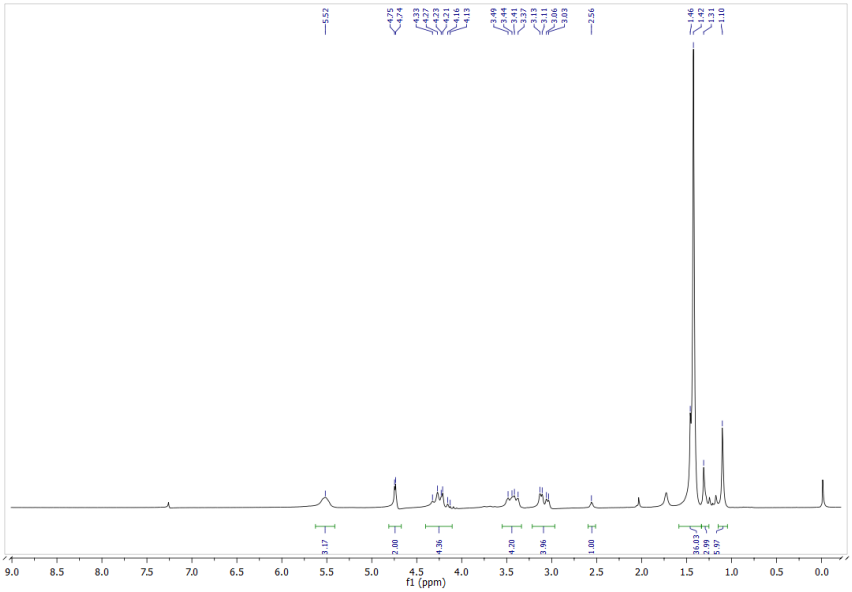

^{13}C-NMR (50 MHz) in $CDCl_3$

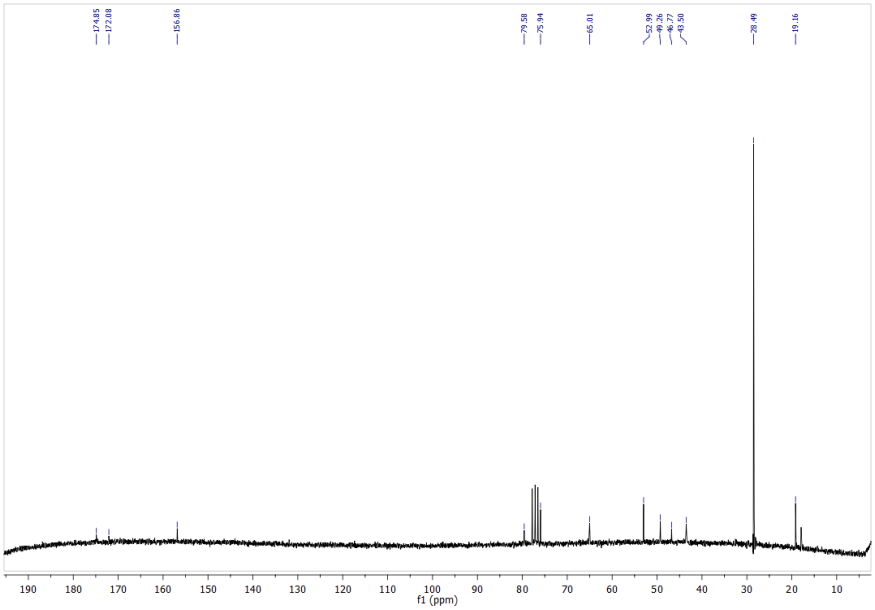

Compound **10**: *2-methyl-2-((prop-2-yn-1-yloxy)carbonyl)propane-1,3-diyl bis(3-(2-((tert-butoxycarbonyl)amino)-5- (3-((2,2,4,6,7-pentamethyl-2,3-dihydrobenzofuran-5-yl)sulfonyl)guanidino)pentanamido)-2-((2-((tert-butoxycarbonyl) amino)-5-(3-((2,2,4,6,7-pentamethyl-2,3-dihydrobenzofuran-5-yl)sulfonyl)guanidino)pentanamido)methyl)-2- methylpropanoate)*

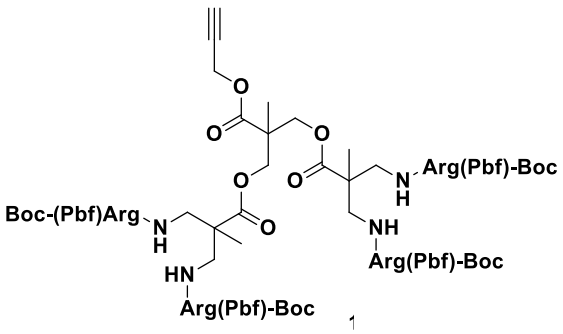

^{1}H-NMR (500 MHz) in $CDCl_3$

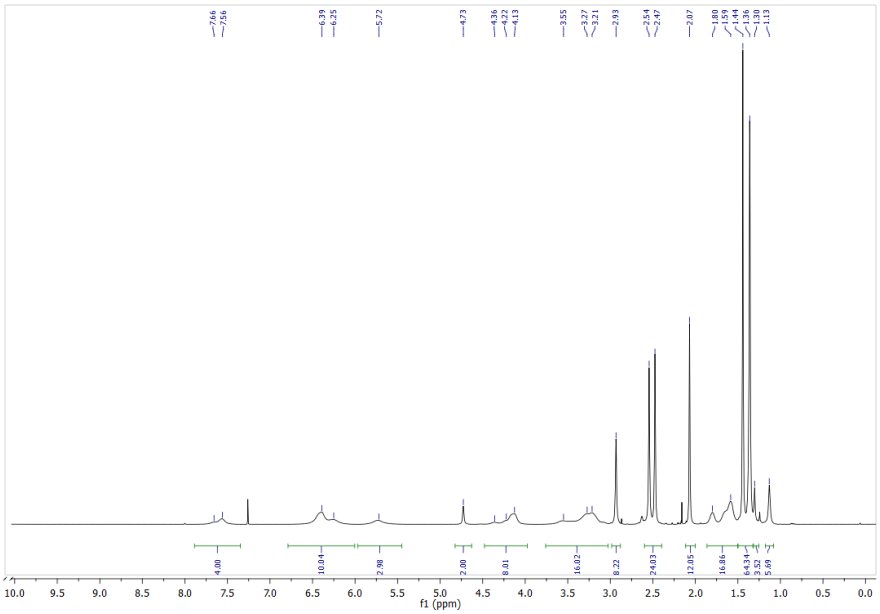

^{13}C-NMR (126 MHz) in $CDCl_3$

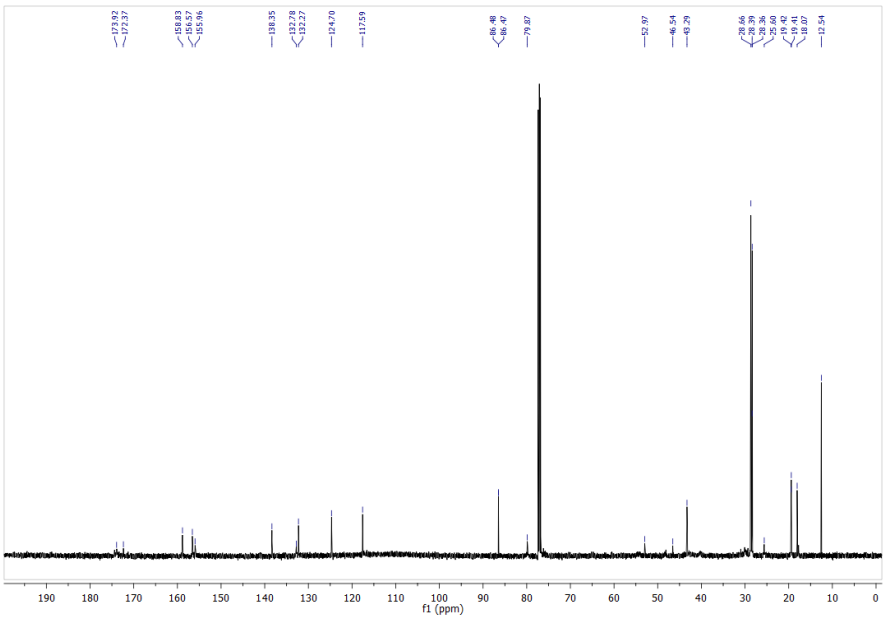

Compound **11**: *3-chloropropane-1,2-diyl distearate*

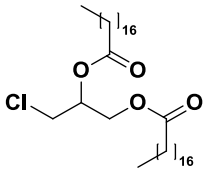

^{1}H-NMR (300 MHz) in $CDCl_3$

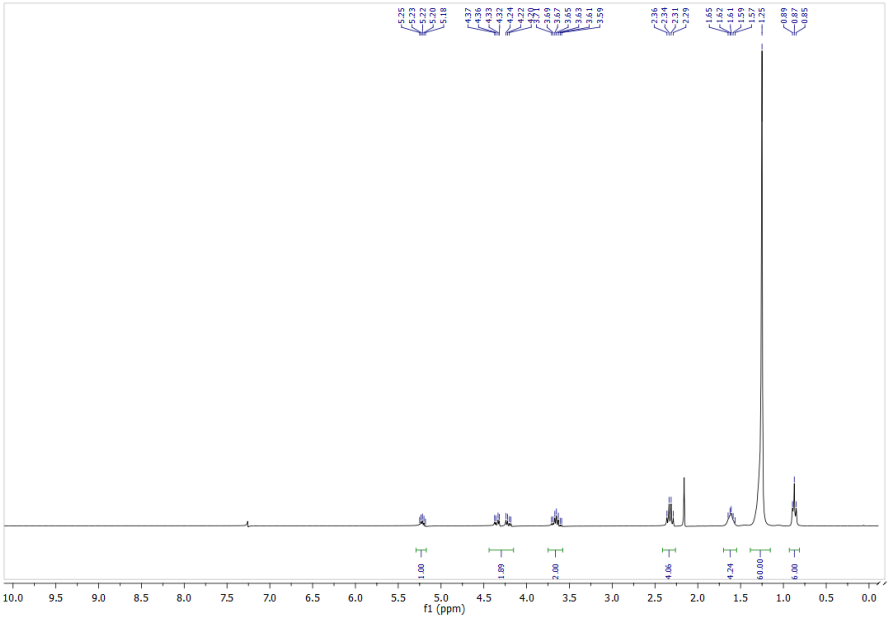

^{13}C-NMR (75 MHz) in $CDCl_3$

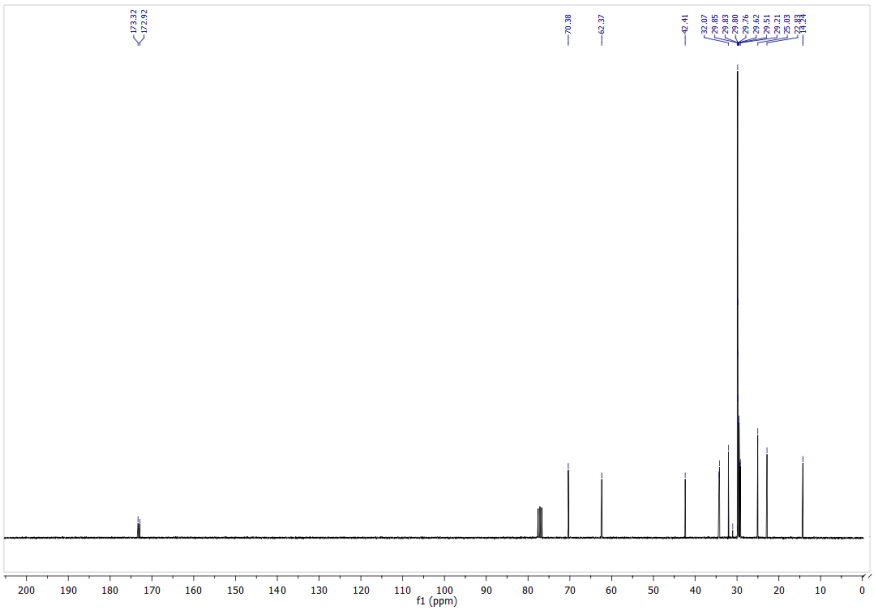

Compound **12**: *3-azidopropane-1,2-diyl distearate*

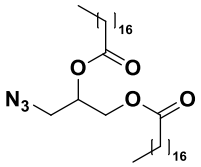

^{1}H-NMR (500 MHz) in $CDCl_3$

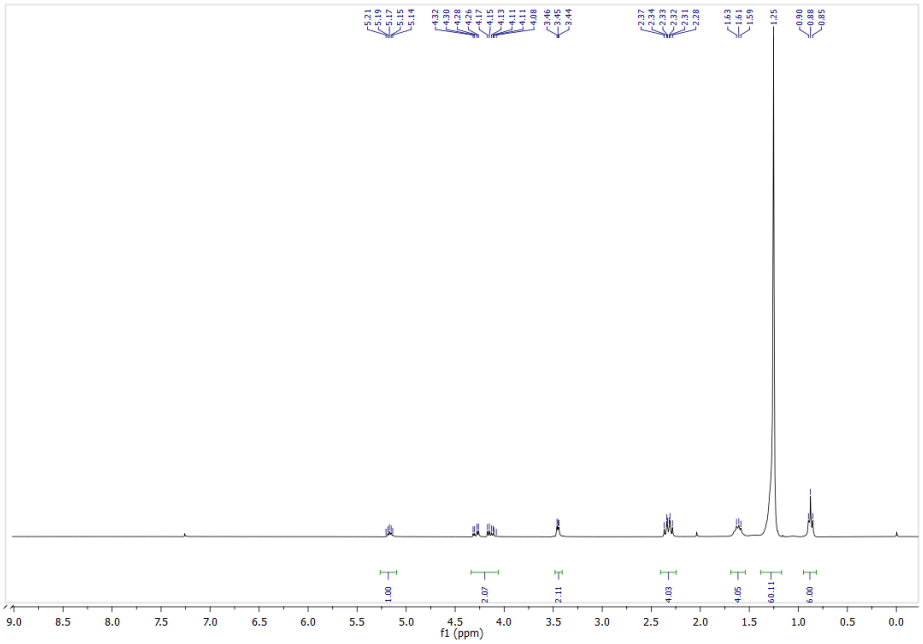

^{13}C-NMR (126 MHz) in $CDCl_3$

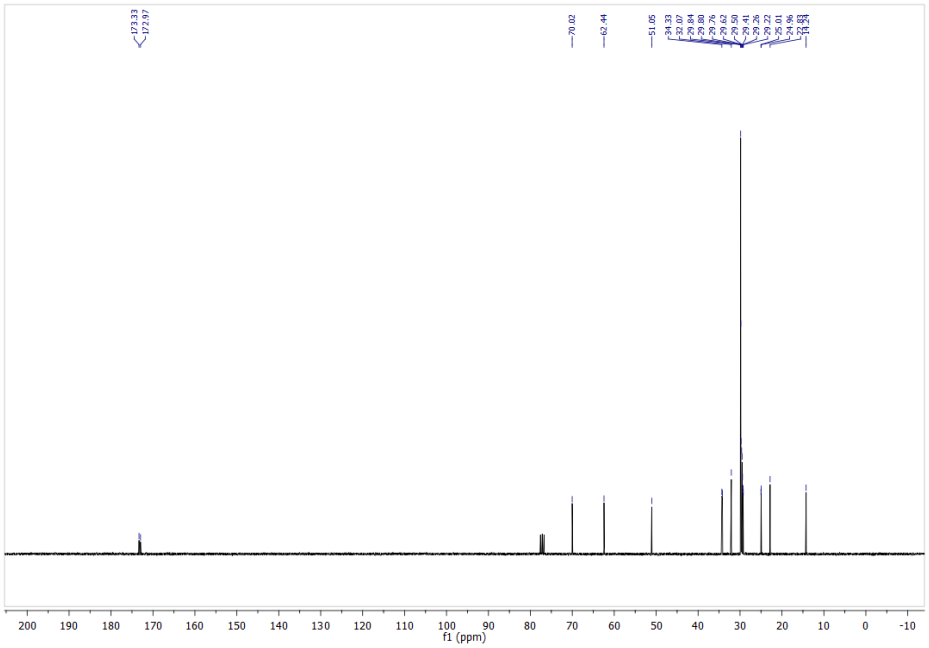

Compound **13**: *2-(((1-(2,3-distearoylpropyl)-1H-1,2,3-triazol-4-yl)methoxy)carbonyl)-2-methylpropane-1,3- diylbis(3-(2-((tert-butoxycarbonyl)amino)-5-(3-((2,2,4,6,7-pentamethyl-2,3-dihydrobenzofuran-5-yl) sulfonyl)guanidino) pentanamido)-2-((2-((tert-butoxycarbonyl)amino)-5-(3-((2,2,4,6,7-pentamethyl-2,3- dihydrobenzofuran-5-yl) sulfonyl)guanidino)pentanamido)methyl)-2-methylpropanoate)*

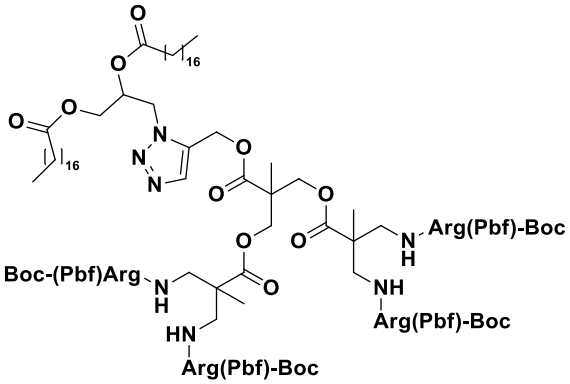

^{1}H-NMR (500 MHz) in $CDCl_3$

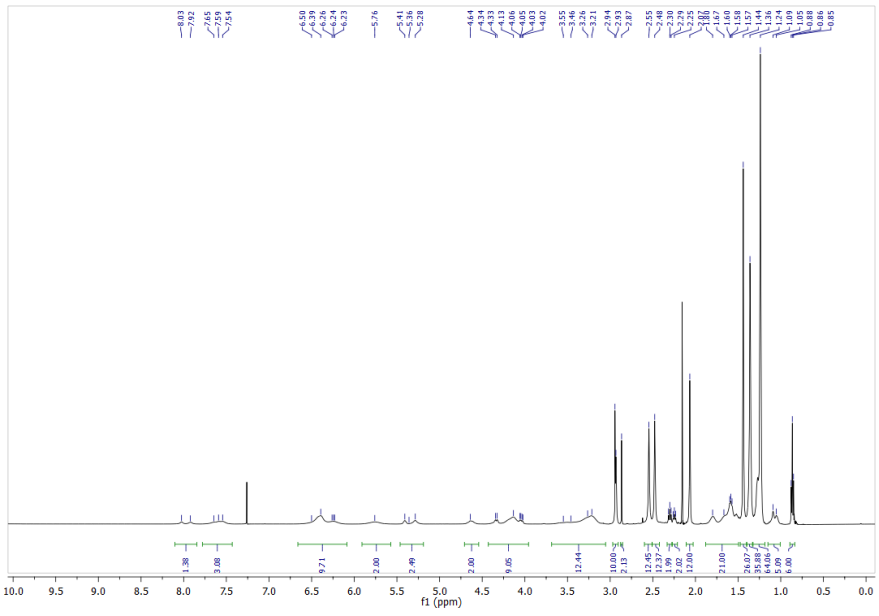

^{13}C-NMR (126 MHz) in $CDCl_3$

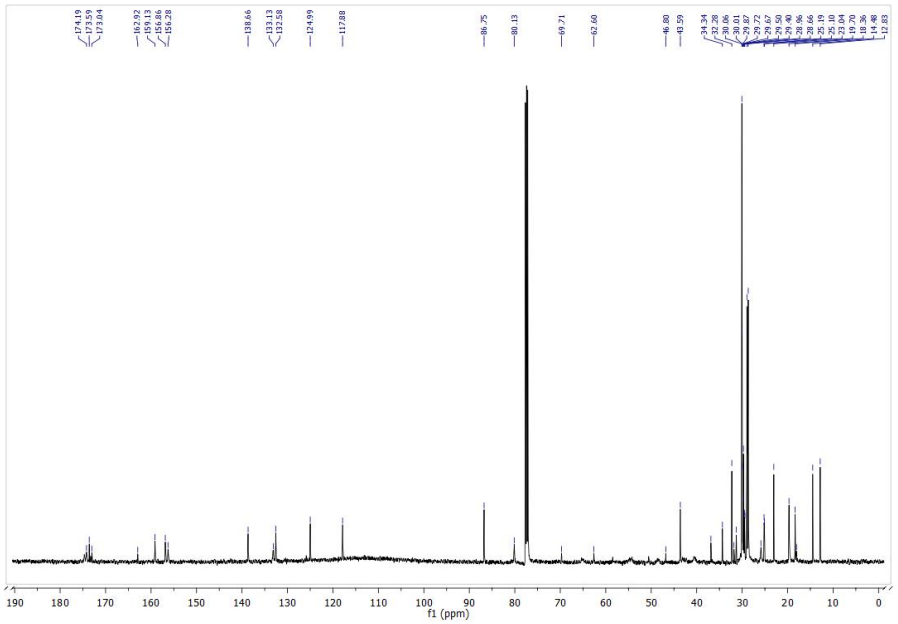

Compound **15**: *3-Methacryloyl sulfadimethoxine (SDM*)

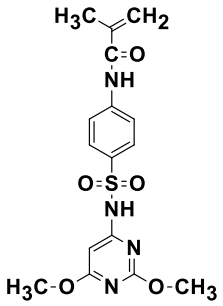

^{1}H-NMR (300 MHz) in DMSO-d6

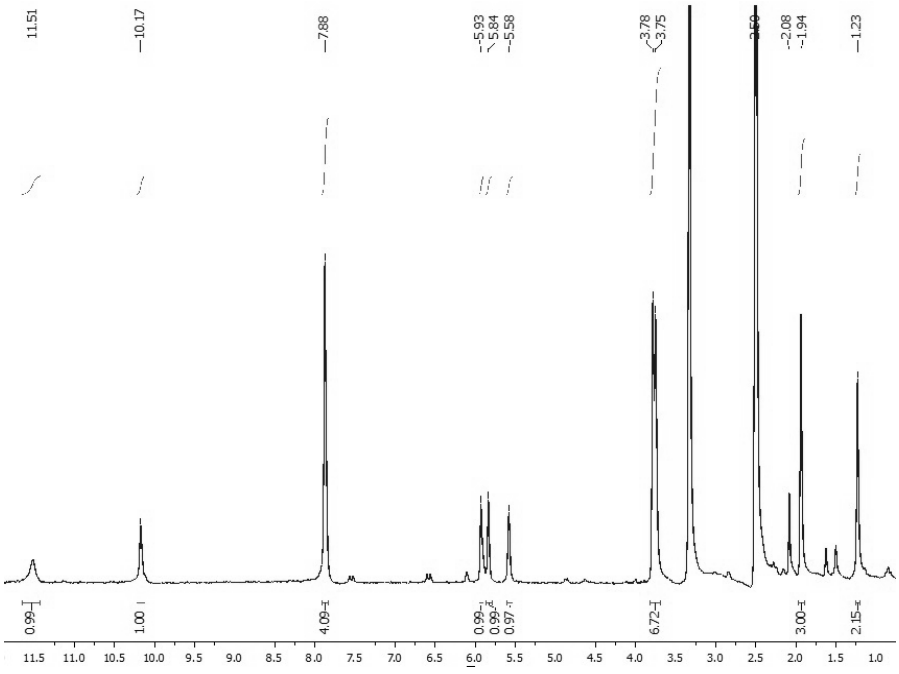

Compound **16**: *m-PEG-NH-CO-C-$(CH_3)_2$-Br (*mPEG-Br)

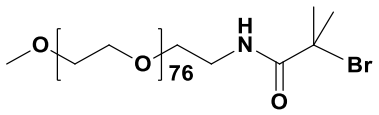

^{1}H-NMR (300 MHz) in $CDCl_3$

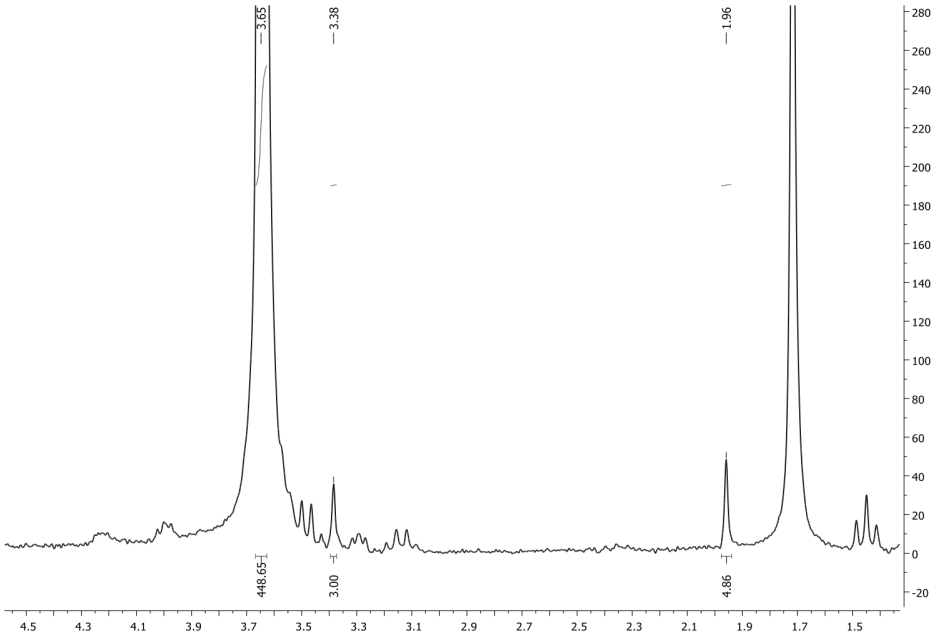

7. REFERENCES

1. Langer, R. *Nature* **1998***, 392*, 5-10.

2. Wike-Hooley, J.; Haveman, J.; Reinhold, H. *Radiotherapy and Oncology* **1984***, 2*, 343-366.

3. Tannock, I. F.; Rotin, D. *Cancer Res.* **1989***, 49*, 4373-4384.

4. Torchilin, V. *Adv. Drug Deliv. Rev.* **2011***, 63*, 131-135.

5. Duncan, R. *Curr. Opin. Biotechnol.* **2011***, 22*, 492-501.

6. Duncan, R. *Nature Reviews Cancer* **2006***, 6*, 688-701.

7. Wicki, A.; Witzigmann, D.; Balasubramanian, V.; Huwyler, J. *J. Controlled Release* **2015***, 200*, 138-157.

8. Lammers, T.; Subr, V.; Ulbrich, K.; Hennink, W. E.; Storm, G.; Kiessling, F. *Nano Today* **2010***, 5*, 197-212.

9. Beija, M.; Salvayre, R.; Lauth-de Viguerie, N.; Marty, J. *Trends Biotechnol.* **2012***, 30*, 485-496.

10. Martins, M.; Loureiro, A.; Azoia, N. G.; Silva, C.; Cavaco-Paulo, A. *Trends Biotechnol.* **2016***, 34*, 496-505.

11. Salmaso, S. F.; Bersani, S. F.; Semenzato, A. F.; Caliceti, P. *Journal of nanoscience and nanotechnology JID - 101088195* **1208**.

12. Pace, C. N.; Trevino, S.; Prabhakaran, E.; Scholtz, J. M. *Philos. Trans. R. Soc. Lond. B. Biol. Sci.* **2004***, 359*, 1225-34; discussion 1234-5.

13. Chang, B. S.; Hershenson, S. Practical approaches to protein formulation development. In *Rational Design of Stable Protein Formulations;* Springer: 2002; pp 1-25.

14. K. Lundstrom *Nanocarriesrs for the delivery of peptides and proteins;* 2009; , pp 193-205.

15. Salmaso, S.; Bersani, S.; Scomparin, A.; Mastrotto, F.; Caliceti, P. *Isr. J. Chem.* **2010***, 50*, 160-174.

16. Sugimura, T. *SCIENCE-NEW YORK THEN WASHINGTON-* **1992**, 603-603.

17. Hahn, W. C.; Weinberg, R. A. 1 - Cancer: A Genetic Disorder. In *The Molecular Basis of Cancer (Fourth Edition);* Mendelsohn, J., Gray, J. W., Howley, P. M., Israel, M. A. and Thompson, C. B., Eds.; Content Repository Only!: Philadelphia, 2015; pp 3-18.e1.

18. Keith, B.; Simon, M. C. 17 - Tumor Angiogenesis. In *The Molecular Basis of Cancer (Fourth Edition);* Mendelsohn, J., Gray, J. W., Howley, P. M., Israel, M. A. and Thompson, C. B., Eds.; Content Repository Only!: Philadelphia, 2015; pp 257-268.e2.

19. Folkman, J. *Adv. Cancer Res.* **1985***, 43*, 175-203.

20. Weis, S. M.; Cheresh, D. A. *Nat. Med.* **2011***, 17*, 1359-1370.

21. Makrilia, N.; Lappa, T.; Xyla, V.; Nikolaidis, I.; Syrigos, K. *Eur. J. Intern. Med.* **2009***, 20*, 663-671.

22. Maeda, H.; Bharate, G. Y.; Daruwalla, J. *European Journal of Pharmaceutics and Biopharmaceutics* **2009***, 71*, 409-419.

23. Hait, W. N.; Rubin, E.; Bertino, J. R. 46 - Cancer Therapeutics. In *The Molecular Basis of Cancer (Fourth Edition);* Mendelsohn, J., Gray, J. W., Howley, P. M., Israel, M. A. and Thompson, C. B., Eds.; Content Repository Only!: Philadelphia, 2015; pp 635-650.e1.

24. Hellman, S.; Rosenberg, S. A.; DeVita, V. T. *Cancer: principles & practice of oncology;* Lippincott-Raven: 1997; Vol. 2.

25. Casanovas, O. *Nature* **2012***, 484*, 44-46.

26. Bertram, J. S. *Mol. Aspects Med.* **2000***, 21*, 167-223.

27. Coates, A.; Abraham, S.; Kaye, S. B.; Sowerbutts, T.; Frewin, C.; Fox, R.; Tattersall, M. *European Journal of Cancer and Clinical Oncology* **1983***, 19*, 203-208.

28. de Boer-Dennert, M.; de Wit, R.; Schmitz, P. I.; Djontono, J.; v Beurden, V.; Stoter, G.; Verweij, J. *Br. J. Cancer* **1997***, 76*, 1055-1061.

29. Berardi, R.; Caramanti, M.; Savini, A.; Chiorrini, S.; Pierantoni, C.; Onofri, A.; Ballatore, Z.; De Lisa, M.; Mazzanti, P.; Cascinu, S. *Crit. Rev. Oncol.* **2013***, 88*, 75-86.

30. Brannon-Peppas, L.; Blanchette, J. O. *Adv. Drug Deliv. Rev.* **2012***, 64*, 206-212.

31. Sievers, E. L.; Senter, P. D. *Annu. Rev. Med.* **2013***, 64*, 15-29.

32. Wang, A. Z.; Langer, R.; Farokhzad, O. C. *Annu. Rev. Med.* **2012***, 63*, 185-198.

33. Chabner, B. A.; Fine, R. L.; Allegra, C. J.; Yeh, G. W.; Curt, G. A. *Cancer* **1984***, 54*, 2599-2608.

34. Holohan, C.; Van Schaeybroeck, S.; Longley, D. B.; Johnston, P. G. *Nature Reviews Cancer* **2013***, 13*, 714-726.

35. Lam, K. S. *Anticancer Drug Des.* **1997***, 12*, 145-167.

36. Oliff, A.; Gibbs, J. B.; McCormick, F. *Sci. Am.* **1996***, 275*, 144-149.

37. Devi, G. *Cancer Gene Ther.* **2006***, 13*, 819-829.

38. Li, J.; Chen, F.; Cona, M. M.; Feng, Y.; Himmelreich, U.; Oyen, R.; Verbruggen, A.; Ni, Y. *Targeted oncology* **2012***, 7*, 69-85.

39. Vermeulen, K.; Van Bockstaele, D. R.; Berneman, Z. N. *Cell Prolif.* **2003***, 36*, 131-149.

40. Tiwari, G.; Tiwari, R.; Sriwastawa, B.; Bhati, L.; Pandey, S.; Pandey, P.; Bannerjee, S. K. *International journal of pharmaceutical investigation* **2012***, 2*, 2.

41. Torchilin, V. P. *Adv. Drug Deliv. Rev.* **2012***, 64*, 302-315.

42. L von Ranke, N.; M Fierro, I.; MS Antunes, A. *Recent patents on anti-cancer drug discovery* **2016***, 11*, 112-120.

43. Stolnik, S. F.; Shakesheff, K. *Biotechnology letters JID - 8008051* **1205**.

44. FAU, P. D.; FAU, K. M.; Balu-Iyer, S. V. *Journal of pharmaceutical sciences JID - 2985195R* **0713**.

45. Ambrosio, E.; Barattin, M.; Bersani, S.; Shubber, S.; Uddin, S.; van der Walle, C. F.; Caliceti, P.; Salmaso, S. *J. Controlled Release* **2016***, 226*, 35-46.

46. Dorsett, Y.; Tuschl, T. *Nature Reviews Drug Discovery* **2004***, 3*, 318-329.

47. Oh, Y.; Park, T. G. *Adv. Drug Deliv. Rev.* **2009***, 61*, 850-862.

48. Jansson, M. D.; Lund, A. H. *Molecular Oncology* **2012***, 6*, 590-610.

49. zur Hausen, H. *International Journal of Cancer* **2008***, 122*, ix-ix.

50. Zhang, X.; McIntosh, T. J.; Grinstaff, M. W. *Biochimie* **2012***, 94*, 42-58.

51. Dreaden, E. C.; Austin, L. A.; Mackey, M. A.; El-Sayed, M. A. *Therapeutic delivery* **2012***, 3*, 457-478.

52. Aires, A.; Ocampo, S. M.; Simões, B. M.; Rodríguez, M. J.; Cadenas, J. F.; Couleaud, P.; Spence, K.; Latorre, A.; Miranda, R.; Somoza, Á *Nanotechnology* **2016***, 27*, 065103.

53. Haag, R. *Angewandte Chemie International Edition* **2004***, 43*, 278-282.

54. Hoffman, A. S.; Stayton, P. S.; Bulmus, V.; Chen, G.; Chen, J.; Cheung, C.; Chilkoti, A.; Ding, Z.; Dong, L.; Fong, R.; Lackey, C. A.; Long, C. J.; Miura, M.; Morris, J. E.; Murthy, N.; Nabeshima, Y.; Park, T. G.; Press, O. W.; Shimoboji, T.; Shoemaker, S.; Yang, H. J.; Monji, N.; Nowinski, R. C.; Cole, C. A.; Priest, J. H.; Harris, J. M.; Nakamae, K.; Nishino, T.; Miyata, T. *J. Biomed. Mater. Res.* **2000***, 52*, 577-586.

55. Croy, S. R.; Kwon, G. S. *Curr. Pharm. Des.* **2006***, 12*, 4669-4684.

56. Yu, B.; Okano, T.; Kataoka, K.; Kwon, G. *J. Controlled Release* **1998***, 53*, 131-136.

57. Yoncheva, K.; Calleja, P.; Agüeros, M.; Petrov, P.; Miladinova, I.; Tsvetanov, C.; Irache, J. M. *Int. J. Pharm.* **2012***, 436*, 258-264.

58. Salmaso, S.; Bersani, S.; Pirazzini, M.; Caliceti, P. *J. Drug Target.* **2011***, 19*, 303-313.

59. Chang, H. I.; Yeh, M. K. *Int. J. Nanomedicine* **2012***, 7*, 49-60.

60. Cosco, D.; Paolino, D.; Cilurzo, F.; Casale, F.; Fresta, M. *Int. J. Pharm.* **2012***, 422*, 229-237.

61. Lee, J. S.; Feijen, J. *J. Controlled Release* **2012***, 161*, 473-483.

62. Christian, D. A.; Cai, S.; Bowen, D. M.; Kim, Y.; Pajerowski, J. D.; Discher, D. E. *European Journal of Pharmaceutics and Biopharmaceutics* **2009***, 71*, 463-474.

63. Mora-Huertas, C. E.; Fessi, H.; Elaissari, A. *Int. J. Pharm.* **2010***, 385*, 113-142.

64. Chow, E. K.; Ho, D. *Sci. Transl. Med.* **2013***, 5*, 216rv4.

65. Larson, N.; Ghandehari, H. *Chemistry of Materials* **2012***, 24*, 840-853.

66. Bozzuto, G.; Molinari, A. *International journal of nanomedicine* **2015***, 10*, 975.

67. Martin, F. J. Chapter 8.2 - Clinical pharmacology and antitumor efficacy of DOXIL (pegylated liposomal doxorubicin). In *Medical Applications of Liposomes;* D.D. Lasic, D. Papahadjopoulos, Eds.; Elsevier Science B.V.: Amsterdam, 1998; pp 635-688.

68. Uster, P. S.; Working, P. K.; Vaage, J. *Int. J. Pharm.* **1998***, 162*, 77-86.

69. Jain, S.; Hirst, D.; O'sullivan, J. *Br. J. Radiol.* **2014**.

70. Vigderman, L.; Zubarev, E. R. *Adv. Drug Deliv. Rev.* **2013***, 65*, 663-676.

71. Kumar, P.; Roy, I. *International Journal of Pharmacy and Pharmaceutical Sciences* **2016***, 8*.

72. Yildiz, I.; Shukla, S.; Steinmetz, N. F. *Curr. Opin. Biotechnol.* **2011***, 22*, 901-908.

73. Franzen, S.; Lommel, S. A. *Nanomedicine* **2009***, 4*, 575-588.

74. Steinmetz, N. F. *Molecular pharmaceutics* **2013***, 10*, 1-2.

75. Maeda, H. *Adv. Enzyme Regul.* **2001***, 41*, 189-207.

76. Wu, N. Z.; Da, D.; Rudoll, T. L.; Needham, D.; Whorton, A. R.; Dewhirst, M. W. *Cancer Res.* **1993***, 53*, 3765-3770.

77. Torchilin, V. P. Passive and active drug targeting: drug delivery to tumors as an example. In *Drug delivery;* Springer: 2010; pp 3-53.

78. Leamon, C. P.; Low, P. S. *Proc. Natl. Acad. Sci. U. S. A.* **1991***, 88*, 5572-5576.

79. Szakács, G.; Paterson, J. K.; Ludwig, J. A.; Booth-Genthe, C.; Gottesman, M. M. *Nature reviews Drug discovery* **2006***, 5*, 219-234.

80. Kunjachan, S.; Pola, R.; Gremse, F.; Theek, B.; Ehling, J.; Moeckel, D.; Hermanns-Sachweh, B.; Pechar, M.; Ulbrich, K.; Hennink, W. E. *Nano letters* **2014***, 14*, 972-981.

81. Lammers, T.; Kiessling, F.; Hennink, W. E.; Storm, G. *J. Controlled Release* **2012***, 161*, 175-187.

82. Gottesman, M. M.; Pastan, I. H. *J. Natl. Cancer Inst.* **2015***, 107*, 10.1093/jnci/djv222. Print 2015 Sep.

83. Ughachukwu, P.; Unekwe, P. *Annals of medical and health sciences research* **2012***, 2*, 191-198.

84. Stoorvogel, W.; Strous, G. J.; Geuze, H. J.; Oorschot, V.; Schwartzt, A. L. *Cell* **1991***, 65*, 417-427.

85. Bangham, A.; Standish, M. M.; Watkins, J. *J. Mol. Biol.* **1965***, 13*, 238-IN27.

86. Abraham, S. A.; Waterhouse, D. N.; Mayer, L. D.; Cullis, P. R.; Madden, T. D.; Bally, M. B. *Meth. Enzymol.* **2005***, 391*, 71-97.

87. Moreira, J. N.; Ishida, T.; Gaspar, R.; Allen, T. M. *Pharm. Res.* **2002***, 19*, 265-269.

88. Nag, O. K.; Awasthi, V. *Pharmaceutics* **2013***, 5*, 542-569.

89. Woodle, M. C.; Engbers, C. M.; Zalipsky, S. *Bioconjug. Chem.* **1994***, 5*, 493-496.

90. Bersani, S.; Vila-Caballer, M.; Brazzale, C.; Barattin, M.; Salmaso, S. *European Journal of Pharmaceutics and Biopharmaceutics* **2014***, 88*, 670-682.

91. Shehata, T.; Ogawara, K.; Higaki, K.; Kimura, T. *Int. J. Pharm.* **2008***, 359*, 272-279.

92. Monteiro, N.; Martins, A.; Reis, R. L.; Neves, N. M. *J. R. Soc. Interface* **2014***, 11*, 20140459.

93. Akbarzadeh, A.; Rezaei-Sadabady, R.; Davaran, S.; Joo, S. W.; Zarghami, N.; Hanifehpour, Y.; Samiei, M.; Kouhi, M.; Nejati-Koshki, K. *Nanoscale research letters* **2013***, 8*, 1.

94. Banerjee, R.; Tyagi, P.; Li, S.; Huang, L. *International journal of cancer* **2004***, 112*, 693-700.

95. Salmaso, S.; Caliceti, P. *Journal of drug delivery* **2013***, 2013*.

96. Moghimi, S.; Szebeni, J. *Prog. Lipid Res.* **2003***, 42*, 463-478.

97. Van Blitterswijk, W. J.; Van der Meer, B Wieb; Hilkmann, H. *Biochemistry* **1987***, 26*, 1746-1756.

98. Gabizon, A.; Shmeeda, H.; Barenholz, Y. *Clin. Pharmacokinet.* **2003***, 42*, 419-436.

99. Koynova, R.; Caffrey, M. *Biochimica et Biophysica Acta (BBA)-Reviews on Biomembranes* **1998***, 1376*, 91-145.

100. Gill, P. S.; Espina, B. M.; Muggia, F.; Cabriales, S.; Tulpule, A.; Esplin, J. A.; Liebman, H. A.; Forssen, E.; Ross, M. E.; Levine, A. M. *J. Clin. Oncol.* **1995***, 13*, 996-1003.

101. Shearer, W. T.; Atkinson, J. P.; Frank, M. M.; Parker, C. W. *J. Exp. Med.* **1975***, 141*, 736-752.

102. Moghimi, S. M.; Farhangrazi, Z. S. *Nanomedicine: Nanotechnology, Biology and Medicine* **2013***, 9*, 458-460.

103. Pio, R.; Ajona, D.; Lambris, J. D. In *In Complement inhibition in cancer therapy;* Seminars in immunology; Elsevier: 2013; Vol. 25, pp 54-64.

104. Szebeni, J.; Muggia, F.; Gabizon, A.; Barenholz, Y. *Adv. Drug Deliv. Rev.* **2011***, 63*, 1020-1030.

105. Markiewski, M. M.; Lambris, J. D. *Trends Immunol.* **2009***, 30*, 286-292.

106. Semple, S. C.; Chonn, A.; Cullis, P. R. *Adv. Drug Deliv. Rev.* **1998***, 32*, 3-17.

107. Allen, T.; Hansen, C.; Martin, F.; Redemann, C.; Yau-Young, A. *Biochimica et Biophysica Acta (BBA)-Biomembranes* **1991***, 1066*, 29-36.

108. Derksen, J.; Morselt, H.; Kalicharan, D.; Hulstaert, C.; Scherphof, G. *Exp. Cell Res.* **1987***, 168*, 105-115.

109. Nilsson, U.; Storm, K.; Elwing, H.; Nilsson, B. *Mol. Immunol.* **1993***, 30*, 211-219.

110. Yuan, F.; Dellian, M.; Fukumura, D.; Leunig, M.; Berk, D. A.; Torchilin, V. P.; Jain, R. K. *Cancer Res.* **1995***, 55*, 3752-3756.

111. Hobbs, S. K.; Monsky, W. L.; Yuan, F.; Roberts, W. G.; Griffith, L.; Torchilin, V. P.; Jain, R. K. *Proc. Natl. Acad. Sci. U. S. A.* **1998***, 95*, 4607-4612.

112. Moreira, J. N.; Gaspar, R.; Allen, T. M. *Biochimica et Biophysica Acta (BBA)-Biomembranes* **2001***, 1515*, 167-176.

113. Vemuri, S.; Rhodes, C. *Pharm. Acta Helv.* **1995***, 70*, 95-111.

114. Bangham, A. *Chem. Phys. Lipids* **1993***, 64*, 275-285.

115. Castile, J. D.; Taylor, K. M. G. *Int. J. Pharm.* **1999***, 188*, 87-95.

116. Babai, I.; Samira, S.; Barenholz, Y.; Zakay-Rones, Z.; Kedar, E. *Vaccine* **1999***, 17*, 1223-1238.

117. Baselga, J.; Metselaar, J. *Principles and Practice of Biological Therapy of Cancer* **2000**, 475-489.

118. Farkhani, S. M.; Valizadeh, A.; Karami, H.; Mohammadi, S.; Sohrabi, N.; Badrzadeh, F. *Peptides* **2014***, 57*, 78-94.

119. Sawant, R. R.; Patel, N. R.; Torchilin, V. P. *European Journal of Nanomedicine* **2013***, 5*, 141-158.

120. Madani, F.; Lindberg, S.; Langel, U.; Futaki, S.; Graslund, A. *J. Biophys.* **2011***, 2011*, 414729.

121. Schmidt, N.; Mishra, A.; Lai, G. H.; Wong, G. C. L. *FEBS Lett.* **2010***, 584*, 1806-1813.

122. Torchilin, V. P. *Peptide Science* **2008***, 90*, 604-610.

123. Gupta, B.; Levchenko, T. S.; Torchilin, V. P. *Adv. Drug Deliv. Rev.* **2005***, 57*, 637-651.

124. Lindgren, M.; Hällbrink, M.; Prochiantz, A.; Langel, Ü *Trends Pharmacol. Sci.* **2000***, 21*, 99-103.

125. Green, M.; Loewenstein, P. M. *Cell* **1988***, 55*, 1179-1188.

126. Frankel, A. D.; Pabo, C. O. *Cell* **1988***, 55*, 1189-1193.

127. Fawell, S.; Seery, J.; Daikh, Y.; Moore, C.; Chen, L. L.; Pepinsky, B.; Barsoum, J. *Proc. Natl. Acad. Sci. U. S. A.* **1994***, 91*, 664-668.

128. Wender, P. A.; Mitchell, D. J.; Pattabiraman, K.; Pelkey, E. T.; Steinman, L.; Rothbard, J. B. *Proc. Natl. Acad. Sci. U. S. A.* **2000***, 97*, 13003-13008.

129. Rothbard, J. B.; Jessop, T. C.; Lewis, R. S.; Murray, B. A.; Wender, P. A. *J. Am. Chem. Soc.* **2004***, 126*, 9506-9507.

130. Nakase, I.; Takeuchi, T.; Tanaka, G.; Futaki, S. *Adv. Drug Deliv. Rev.* **2008***, 60*, 598-607.

131. Koren, E.; Torchilin, V. P. *Trends Mol. Med.* **2012***, 18*, 385-393.

132. Su, Y.; Waring, A. J.; Ruchala, P.; Hong, M. *Biochemistry* **2010***, 49*, 6009-6020.

133. Verdurmen, W. P. R.; Wallbrecher, R.; Schmidt, S.; Eilander, J.; Bovee-Geurts, P.; Fanghänel, S.; Bürck, J.; Wadhwani, P.; Ulrich, A. S.; Brock, R. *J. Controlled Release* **2013***, 170*, 83-91.

134. Wallbrecher, R.; Verdurmen, W. P.; Schmidt, S.; Bovee-Geurts, P. H.; Broecker, F.; Reinhardt, A.; van Kuppevelt, T. H.; Seeberger, P. H.; Brock, R. *Cellular and Molecular Life Sciences* **2013**, 1-13.

135. Zorko, M.; Langel, Ü *Adv. Drug Deliv. Rev.* **2005***, 57*, 529-545.

136. Zaro, J. L.; Shen, W. *Biochem. Biophys. Res. Commun.* **2003***, 307*, 241-247.

137. Richard, J. P.; Melikov, K.; Brooks, H.; Prevot, P.; Lebleu, B.; Chernomordik, L. V. *J. Biol. Chem.* **2005***, 280*, 15300-15306.

138. Stewart, K. M.; Horton, K. L.; Kelley, S. O. *Organic & biomolecular chemistry* **2008***, 6*, 2242-2255.

139. Torchilin, V. P.; Rammohan, R.; Weissig, V.; Levchenko, T. S. *Proc. Natl. Acad. Sci. U. S. A.* **2001***, 98*, 8786-8791.

140. Levchenko, T. S.; Rammohan, R.; Volodina, N.; Torchilin, V. P. *Meth. Enzymol.* **2003***, 372*, 339-349.

141. Tseng, Y. L.; Liu, J. J.; Hong, R. L. *Mol. Pharmacol.* **2002***, 62*, 864-872.

142. Tréhin, R.; Merkle, H. P. *European journal of pharmaceutics and biopharmaceutics* **2004***, 58*, 209-223.

143. Sarko, D.; Beijer, B.; Boy, R. G.; Nothelfer, E.; Leotta, K.; Eisenhut, M.; Altmann, A.; Haberkorn, U.; Mier, W. *Molecular pharmaceutics* **2010***, 7*, 2224-2231.

144. Jiang, T.; Olson, E. S.; Nguyen, Q. T.; Roy, M.; Jennings, P. A.; Tsien, R. Y. *Proc. Natl. Acad. Sci. U. S. A.* **2004***, 101*, 17867-17872.

145. Daily, A.; Nath, A.; Hersh, L. B. *J. Neurovirol.* **2006***, 12*, 153-160.

146. Vives, E.; Brodin, P.; Lebleu, B. *J. Biol. Chem.* **1997***, 272*, 16010-16017.

147. Shahana, S.; Kampf, C.; Roomans, G. M. *Mediators Inflamm.* **2002***, 11*, 141-148.

148. Webster, O.; Hertler, W.; Sogah, D.; Farnham, W.; RajanBabu, T. V. *J. Am. Chem. Soc.* **1983***, 105*, 5706-5708.

149. Matyjaszewski, K.; Xia, J. *Chem. Rev.* **2001***, 101*, 2921-2990.

150. Hawker, C. J.; Bosman, A. W.; Harth, E. *Chem. Rev.* **2001***, 101*, 3661-3688.

151. Chiefari, J.; Chong, Y.; Ercole, F.; Krstina, J.; Jeffery, J.; Le, T. P.; Mayadunne, R. T.; Meijs, G. F.; Moad, C. L.; Moad, G. *Macromolecules* **1998***, 31*, 5559-5562.

152. Arslan, H. *Edited by Ailton De Souza Gomes* **2012**, 279.

153. Jakubowski, W.; Matyjaszewski, K. *Macromolecules* **2005***, 38*, 4139-4146.

154. Becer, C. R.; Hoogenboom, R.; Fournier, D.; Schubert, U. S. *Macromolecular rapid communications* **2007***, 28*, 1161-1166.

155. Xia, J.; Zhang, X.; Matyjaszewski, K. The effect of ligands on copper-mediated atom transfer radical polymerization. In 2000; .

156. Braunecker, W. A.; Matyjaszewski, K. *Progress in Polymer Science* **2007***, 32*, 93-146.

157. Chiefari, J.; Chong, Y.; Ercole, F.; Krstina, J.; Jeffery, J. *Macromolecules* **1998***, 31*, 5559-5562.

158. Moad, G.; Chiefari, J.; Krstina, J.; Mayadunne, R. T. A.; Postma, A.; Rizzardo, E.; Thang, S. H. *Polym. Int.* **2000***, 49*, 993-1001.

159. Moad, G.; Rizzardo, E.; Thang, S. H. *Aust. J. Chem.* **2005***, 58*, 379-410.

160. Zalipsky, S. *Bioconjug. Chem.* **1995***, 6*, 150-165.

161. Yamaoka, T.; Tabata, Y.; Ikada, Y. *J. Pharm. Sci.* **1994***, 83*, 601-606.

162. Veronese, F. M.; Pasut, G. *Drug Discov. Today* **2005***, 10*, 1451-1458.

163. Kang, S. I.; Bae, Y. H. *J. Controlled Release* **2002***, 80*, 145-155.

164. Ravazzolo, E.; Salmaso, S.; Mastrotto, F.; Bersani, S.; Gallon, E.; Caliceti, P. *European Journal of Pharmaceutics and Biopharmaceutics* **2013***, 83*, 346-357.

165. Shimanouchi, T.; Ishii, H.; Yoshimoto, N.; Umakoshi, H.; Kuboi, R. *Colloids and Surfaces B: Biointerfaces* **2009***, 73*, 156-160.

166. Sims, G. E. C.; Snape, T. J. *Anal. Biochem.* **1980***, 107*, 60-63.

167. Marvin, L. F.; Roberts, M. A.; Fay, L. B. *Clinica chimica acta* **2003***, 337*, 11-21.

168. Granqvist, N.; Yliperttula, M.; Välimäki, S.; Pulkkinen, P.; Tenhu, H.; Viitala, T. *Langmuir* **2014***, 30*, 2799-2809.

169. Löfås, S.; Johnsson, B. *Journal of the Chemical Society, Chemical Communications* **1990**, 1526-1528.

170. Torres, A. G.; Milflores-Flores, L.; Garcia-Gallegos, J. G.; Patel, S. D.; Best, A.; La Ragione, R. M.; Martinez-Laguna, Y.; Woodward, M. J. *International Journal of Medical Microbiology* **2007***, 297*, 177-185.

171. Barnard, A.; Posocco, P.; Pricl, S.; Calderon, M.; Haag, R.; Hwang, M. E.; Shum, V. W.; Pack, D. W.; Smith, D. K. *J. Am. Chem. Soc.* **2011***, 133*, 20288-20300.

172. Kim, M. S.; Lee, D. S.; Choi, E.; Park, H.; Kim, J. *Macromolecular Research* **2005***, 13*, 147-151.

173. Sethuraman, V. A.; Na, K.; Bae, Y. H. *Biomacromolecules* **2006***, 7*, 64-70.

174. Ishida, T.; Iden, D. L.; Allen, T. M. *FEBS Lett.* **1999***, 460*, 129-133.

175. Iden, D. L.; Allen, T. M. *Biochimica et Biophysica Acta (BBA) - Biomembranes* **2001***, 1513*, 207-216.

176. Pappalardo, J. S.; Langellotti, C. A.; Di Giacomo, S.; Olivera, V.; Quattrocchi, V.; Zamorano, P. I.; Hartner, W. C.; Levchenko, T. S.; Torchilin, V. P. *International journal of nanomedicine* **2014***, 9*, 963.

177. Koren, E.; Apte, A.; Jani, A.; Torchilin, V. P. *J. Controlled Release* **2012***, 160*, 264-273.

178. Vila-Caballer, M.; Codolo, G.; Munari, F.; Malfanti, A.; Fassan, M.; Rugge, M.; Balasso, A.; de Bernard, M.; Salmaso, S. *J. Controlled Release* **2016***, 238*, 31-42.

179. Sheldon, K.; Liu, D.; Ferguson, J.; Gariepy, J. *Proc. Natl. Acad. Sci. U. S. A.* **1995***, 92*, 2056-2060.

180. Sung, M.; Poon, G. M. K.; Gariépy, J. *Biochimica et Biophysica Acta (BBA) - Biomembranes* **2006***, 1758*, 355-363.

181. Yoon, Y.; Lim, Y.; Lee, E.; Lee, M. *Chemical Communications* **2008**, 1892-1894.